

**Proceedings of the
X-Ray FEL Theory and Simulation Codes Workshop
Stanford Linear Accelerator Center
Stanford University
September 23 and 24, 1999**

Organization and Program
H.-D. Nuhn ^a, C. Pellegrini ^b

^a *Stanford Linear Accelerator Center
Stanford Synchrotron Radiation Laboratory
P.O. Box 4349, Bin 69
Stanford CA 94309-0210*

^b *University of California Los Angeles
Physics Department
405 Hilgard Ave.
Los Angeles, CA 90095-1547*

Working Group Organization and Summary
W.B. Colson ^c, W.M. Fawley ^d, K.-J. Kim ^e

^c *Naval Postgraduate School
Physics Department
833 Dyer Road
Monterey, Stanford CA 93943*

^d *Lawrence Berkeley National Laboratory
Accelerator Fusion Research Division
1 Cyclotron Road, MS 71J
Berkeley, CA 94720*

^e *Argonne National Laboratory
ASD Department
9700 S. Cass Avenue, MS 401
Argonne, IL 60439*

TABLE OF CONTENTS

<i>INTRODUCTION</i> _____	7
I. Background _____	7
REFERENCES _____	9
II. Workshop Objective _____	9
III. Workshop Organizers _____	9
<i>EXECUTIVE SUMMARY</i> _____	10
<i>SUMMARY OF WORKING GROUP I</i> _____	12
I. Report Outline _____	12
II. Status of FEL Physics R&D for LCLS _____	13
Introduction _____	13
Present status of FEL physics _____	13
Short wavelength related questions _____	14
Questions related to the electron beam _____	14
Methods and scenarios to control the X-ray pulse characteristics _____	14
Commissioning scenarios _____	15
III. SASE Fluctuation, Quantum Corrections and Undulator Errors _____	16
SASE Fluctuation _____	16
Quantum Effects _____	16
Undulator Errors _____	17
References _____	17
IV. High-Gain, Higher-Harmonic Theory _____	17
V. Status of the 3D FEL Theory _____	18
VI. 3D Nonlinear Harmonics _____	20
References _____	21
VII. Discussion _____	21
VIII. Impedance Effects _____	22
IX. Schemes for Improving the SASE Performances: _____	22
Two-stage undulator for a narrow spectrum _____	22
Pulse compression _____	22
Circular polarization _____	23
References _____	23
X. LCLS Saturation Theory _____	23
XI. LCLS Diagnostics _____	24

<i>SUMMARY OF WORKING GROUP II</i>	25
I. Introduction	25
II. Undulator modeling and beam transport issues	25
III. Harmonics	27
IV. Code Interface and Communication	27
V. Radiation Transport beyond the Undulator	28
VI. Numerical Issues and Need for Additional Physics	29
<i>LIST OF PRESENTATIONS</i>	32
X-ray FEL Physics Overview	33
Simulation Code Overview	47
Remarks on SASE Fluctuations and Undulator Errors	77
3D Analysis of Nonlinear Harmonic Generation	97
Exact and Variational Solutions of 3D Eigenmodes for High Gain FELs	109
High-Gain, Higher-Harmonic Theory	125
Particle Transport	139
Interfacing Multiple Simulation Codes	143
The High-Gain Harmonic Generation Experiment	147
<i>APPENDIX A. Synopses of several FEL Simulation Codes</i>	155
MEDUSA Simulation Code, Version 2.0	156
Electron Beam/Magnetostatic Fields:	156
The Radiation Field	157
Numerical Algorithm	157
Diagnostics	157
FELEX - LANL version	159
References	160
FELEXN, Boeing simulation code, version B08	161
GENESIS 1.3 Simulation Code	162
The Electron Beam	162
The Radiation Field	162
Diagnostics	162
Input	163
Additional Options	163
Description of the time-dependent GINGER FEL Simulation Code	165
Overview	165

Time-dependent Formulation _____	165
Interaction Equations, Radiation Field Description, Gridding and Spatial BC ____	166
Macroparticle Loading and Particle Mover _____	166
Wiggler and Focusing Description _____	167
Additional Capabilities _____	167
Input/Output _____	167
Possible Future Upgrades _____	168
<i>APPENDIX B: List of Attendees</i> _____	169

INTRODUCTION

This is a report on a workshop held at SLAC on September 23 and 24, 1999 to aid the detailing of the LCLS FEL Physics R&D for the FY2000 to FY2002 period.

This report consists of an Executive Summary and Summaries by the speakers of each of the two working groups. The workshop program and copies of most of the viewgraphs that were shown are attached. Also included are summary descriptions of the five major FEL simulation codes. The summaries are written by the code authors.

I. Background

The Stanford Linear Accelerator Center (SLAC) is leading the effort to build a Free-Electron-Laser (FEL) operating in the wavelength range 1.5-15 Å. This X-ray FEL called "Linac Coherent Light Source" (LCLS) utilizes the last third of the SLAC Linac and is characterized by extremely high peak brightness, sub-picosecond long pulses and a fully transversely coherent radiation pulse.

The LCLS is based on the high gain Self-Amplified Spontaneous Emission (SASE) FEL, as proposed in the 1980's. The SASE-FEL theory has been verified in experiments performed in the 1990's, experiments which have also provided a foundation for the key technologies involved in such a system.

A Design Study started in June 1996 and was completed and published in April 1998 [1]. The Design Study was supported by the original LCLS collaborating institutions (Stanford Linear Accelerator Center (SLAC), Los Alamos National Laboratory (LANL), Lawrence Livermore National Laboratory (LLNL) and the University California at Los Angeles (UCLA)). Additional help was provided by members from other laboratories (Deutsches Elektronen-Synchrotron (DESY), European Synchrotron Radiation Laboratory (ESRF), Lawrence Berkeley National Laboratory (LBNL), University of Milan, University of Rochester). A panel of experts chaired by Dr. Joe Bisognano (Thomas Jefferson National Accelerator Laboratory) reviewed the design in November 1997. The report of the Review Committee finds no "show-stoppers" in meeting the design specifications and states that "the design presented establishes the feasibility of such a project".

The properties of the LCLS as a novel and unique radiation source in the X-ray region were also discussed in several workshop on X-ray driven science, leading to a growing interest in this new system, and the definition of a 4th Generation synchrotron radiation source.

Two more panels organized by DOE to review the status of synchrotron radiation sources in the US, the Birgenau-Shen Panel in 1997 [2] and the Leone Panel in 1999 [3], recognized the unique role that LCLS can play in this field.

The Birgenau-Shen Report recognizes that "fourth generation x-ray sources ... will in all likelihood be based on the free electron laser concepts. If successful, this technology could yield improvements in brightness by many orders of magnitude". The Birgenau-Shen Panel also assigned the highest priority to the R&D of 4th generation x-ray sources. The Leone Panel states

that "Given current available knowledge and limited funding resources, the hard X-ray region (8-20 keV or higher) is identified as the most exciting potential area for innovative science. DOE should pursue the development of coherent light source technology in the hard X-ray region as a priority. This technology will most likely take the form of a linac-based free electron laser device using self amplified stimulated emission ... ". The Leone report also recommends R&D funding be made available to determine the feasibility and design of such a linac-based free-electron laser source.

The following is a brief description of the facility. A photoinjector will be used to generate a bright electron beam. Bunches of electrons (one bunch at the repetition rate of 120 Hz) are accelerated and magnetically compressed from an initial length of 10 psec FWHM to a final one of 280 fsec FWHM. After acceleration to 150 GeV, the beam is transported to a 112-m long undulator arrangement, where the FEL radiation is generated and channeled to an experimental area. The transport system and the undulator area use an existing tunnel that presently houses the Final Focus Test Beam (FFTB).

The LCLS undulator will produce a wide spectrum of conventional spontaneous radiation in sub-picosecond long pulses, four orders of magnitude above existing synchrotron radiation sources. In addition to the wide bandwidth spontaneous radiation there is the small bandwidth FEL radiation line, with a projected peak brightness ten orders of magnitude greater than presently operating synchrotron radiation sources. This leap in performance is possible because of the FEL amplification of the spontaneous radiation, and of major advances in the physics and technology of FELs and high brightness electron beams. Important elements contributing to these advances are the development of rf photo-injectors, the acceleration of very high-brightness electron beams in linear colliders, and the progress in undulator design and their error control. In the LCLS, all these technologies converge to produce a scientific tool of extraordinary performance.

Although the design of the LCLS is based on a consistent and feasible set of parameters and hardware specifications, it is recognized (as was pointed out by the Bisognano Technical Review Committee) that some components require research and development in order to guarantee the performance and to optimize parameters and cost. The major focus of the R&D is in the areas of generating the dense electron beam (i.e. RF photo-injectors and bunch compression), improving the understanding the FEL/SASE process (undulator design, SASE saturation and extension to lower wavelengths), and developing the X-ray optics that can sustain the high LCLS peak power. In addition, a Conceptual Design Report will be written using the LCLS Design Study Report as a basis to fill in engineering details for the project.

The LCLS FEL Physics R&D program is part of a four year LCLS R&D program, which has been approved in April 1999 by the Department of Energy. This R&D program will cover the various subsystems, including photo-injector, linac, undulator, X-ray optics and FEL theory research. Important tools of the latter are FEL computer simulations. The workshop discussed the present status of X-ray FEL theory and simulations, and the program to be carried out as part of the LCLS project R&D.

REFERENCES

- [1] LCLS Technical Design Review Report, SLAC, SLAC-R-521, April 1998, (Revised December 1998).
- [2] Report of the Basic Energy Sciences Advisory Committee, Synchrotron Radiation Light Source Working Group, Birgenau-Shen Report, October 1997.
(URL: <http://www.er.doe.gov/production/bes/BESAC/syncpanel.pdf>)
- [3] Report of the Leone Subcommittee of the Basic Energy Sciences Advisory Committee on Novel Coherent Light Sources, Leone Panel Report, February 1999.
(URL: http://www.er.doe.gov/production/bes/BESAC/NCLS_rep.PDF)

II. Workshop Objective

- Survey the present theoretical status of X-ray FELs.
- Identify physics issues to be investigated for the LCLS, a 1.5 Å X-Ray FEL.
- Characterize existing FEL simulation codes, and identify capabilities that are missing in one or more of the existing simulation codes.
- Discuss the means of upgrading existing codes or producing a new code.

III. Workshop Organizers

The workshop was organized by Heinz-Dieter Nuhn (SLAC) and Claudio Pellegrini (UCLA). William B. Colson (NPGS), William M. Fawley (LBNL) and K.-J. Kim (APS) were chairmen of the working groups. Dorothy Antwine is thanked for the organization of the logistical aspects of the workshop. Dave Dungan and Suzanne Barrett provided invaluable on guidance on workshop organization.

EXECUTIVE SUMMARY

A meeting to review the present status of the FEL theory and of simulation codes for the LCLS project was held at SLAC on September 23 and 24, 1999. The fields of FEL theory and FEL simulations were covered by two working groups.

The main conclusion from the discussions of the FEL theory group is that the agreement obtained in the early SASE-FEL experiments between theory and experimental results, in particular on the value of the gain length and its dependence on beam parameters, give us confidence that we understand the basic features of a SASE-FEL well enough to design the LCLS. Another important conclusion reached at the workshop is that we cannot find at present any reason to believe that the same theory will not work in the Angstrom region as it does in the infrared to visible region where it has been tested so far.

There are however a number of points where the experimental demonstration of the theory is missing and where further work is needed. Principal among these is the saturation level and the intensity fluctuations at saturation. Other points are the intensity of harmonics, the details of the spectral and frequency distribution and the effect of projected versus slice emittance on the gain. We expect that the LEUTL, VISA and TESLA SASE experiments will give us the needed information during the year 2000.

Other points where additional theoretical work will be needed is in the area of optimizing the beam properties in the electron gun-linac-compressor-undulator system to create the most favorable conditions for a successful commissioning and operation of the LCLS, and for controlling the X-ray beam output power, line width and pulse duration. An example of this type of work is the seeded FEL with harmonic generation. We expect that work in these directions will continue in the near future with the participation of scientists from all the collaborating institutions.

The discussions of the FEL simulations group focused on undulator modeling, beam transport issues, radiation harmonics, code-to-code communication and interface issues, as well as radiation transport beyond the undulator. Also discussed were issues such as inclusion of additional physics (*e.g.* wake fields) and numerical accuracy requirements (*e.g.* particle statistics) in SASE-relevant simulation codes. Among the topics discussed and the conclusions reached are the following:

More analytical and simulation work on the sensitivity of the 3rd and 5th harmonic power as a diagnostic of electron beam and wiggler quality could be useful. For example, the effects of "real" wiggler errors (as determined by wiggler field mapping) upon the predicted growth rates of harmonics should be examined.

The working group agreed that the SDDS data format developed at APS should be adopted by as many FEL codes as possible to assist with exchange of data both, with other FEL codes and with linac codes.

Descriptions of the temporal and transverse structure of the radiation field as a function of fundamental wavelength for the first and third harmonics need to be provided to the X-ray optics group.

Losses from wakefields associated with surface roughness of the beam tube and any radial interruptions will vary from the beam head to the tail and can cause a chirping of the output spectrum for SASE FELs. Here, the energy loss can lead to a detuning effect that cannot be corrected with microtapering (due to its dependence on the position within the electron bunch). Some studies have been done with both the GENESIS and GINGER codes but more work is needed. Moreover, the group felt that additional theoretical work is required to increase our confidence in the actual loss formulae.

The question of whether any important physics is being missed by adoption of the wiggler-averaged (KMR) FEL interaction equations was discussed. The working group felt that it would be highly useful for the MEDUSA code (a non-wiggler-averaged code) to have a wiggler-averaging option in order to permit examination of what differences in performance prediction would arise between the two formulations in the context of the LCLS and longer wavelength SASE FELs.

There was a consensus that the SASE FEL simulation codes currently provide reasonable predictions for X-ray FEL performance. However, there are a number of physics phenomena, relevant for the LCLS design, that need to be implemented into the codes.

SUMMARY OF WORKING GROUP I

FEL Theory

Working Group Members:

Ilan Ben-Zvi (BNL), Vinod Bharadwaj (SLAC), Bruce Carlsten (LANL), Jym Clendenin (SLAC), Bill Colson (NPGS), Max Cornachia (SLAC), Zhirong Huang (ANL), Kwang-Je Kim (ANL), Lowell Klaisner (SLAC), Patrick Krejcik (SLAC), Claudio Pellegrini (UCLA), Hai Jiang (UCLA), Claudio Pellegrini (UCLA), Carl Schroeder (LBL), Ming Xie (LBL), Li-Hua Yu (BNL)

I. Report Outline

The two-day workshop began with several introductory talks. Claudio Pellegrini gave an introduction talk, which is summarized below. Several theory topics were mentioned early in the meeting to stimulate discussion. They are listed below:

- Startup from Noise, classical and quantum effects
- Harmonic Generation
- Error Sensitivity along Undulator
- Vacuum Pipe Impedance
- Beta-function Modulation
- Separations between undulator sections
- Total Radiation Spectrum
- Coherent Radiation at Wavelength beyond the Bunch Length
- Diagnostics
- Improvement to Temporal and Spectral Properties
- Monochromatization
- Bunch Compression
- X-ray Radiation Modes
- Radiation Transport outside the Undulator

Comments are made on these topics throughout the report. Following the introductory remarks, there were four short talks of about 15 minutes each during the first discussion period. These informal talks are intended to review status and stimulate discussion on a variety of theory topics relevant to the LCLS.

- "Shot noise, fluctuations, & undulator errors" by Kwang-Je Kim
- "3D Nonlinear Harmonics" by Zhirong Huang
- "Status of 3D FEL Theory" by Ming Xie

- "High-Gain, Higher-Harmonic Theory" by Li Hua Yu

In the discussion section, individual topics were evaluated as to their relative maturity.

II. Status of FEL Physics R&D for LCLS

by Claudio Pellegrini

Introduction

The LCLS is now in the initial R&D phase, and a second, more detailed, conceptual design report must be prepared by the end of the year 2000, to be presented soon after to DOE. The Workshop on FEL physics is being held to discuss the work needed to advance the LCLS to its next development stage, and will be followed by more workshops next year. The present workshop has the following goals:

- Discuss what are the most important physics issues that should be addressed during the next year.
- Make the LCLS project more likely to be a success.
- Establish priorities, and how to make good use of the manpower present in the LCLS collaboration.
- Organize an R&D plan.

Present status of FEL physics

The experiments on SASE-FELs in the infrared have given data in agreement with our theoretical model on: gain, and its dependence on the electron beam 6-D phase-space density; line width and mode of the amplified radiation; intensity fluctuations due to start-up from noise.

We still have no experimental data on:

- Saturation and its characteristics.
- Complete radiation mode structure.
- Gain and other characteristics of harmonics, and their dependence on electron beam parameters.

The experiments now in the initial state of data taking, VISA, LEUTL, TESLA, HGHG, will hopefully provide the additional information that we need. One important task for the LCLS physics section is to understand and analyze the data produced by these experiments, and examine any possible implication for the LCLS. However, while these experiments can provide additional missing data on FEL physics they cannot extend the wavelength to the 0.1 nm region. This will be done by the LCLS, itself. What are the most important questions we should try to answer in preparation for the LCLS and to optimize the design of the experiment? They can be divided in four areas:

- A) Short wavelength related questions
- B) Beam related questions
- C) X-ray pulse manipulation questions
- D) Scenarios for commissioning and demonstrating FEL gain.

In what follows we will make a list of possible questions to be answered for each one of these four areas, with some short comments on initial results from the workshop.

Short wavelength related questions

The key question in this group can be asked as: is there any effect in the FEL physics model that we use, which is important at 0.1 nm while it is negligible at 1000 nm? Issues related to this might be: start-up noise; effects of coherent and incoherent radiation emission in the undulator or wakefield effects in a long undulator and for a high energy, multi-GeV, electron beam; quantum effects.

This question was discussed at the workshop, and the main conclusion reached is that to the best of our present knowledge there is no effect that will prevent the LCLS to operate as predicted by our theoretical models. Quantum effects should be negligible for the LCLS beam parameters. Long wavelength coherent radiation and wakefields will however continue to be studied in order to control any possible effect on the beam six-dimensional phase-space, which might influence the FEL gain.

Questions related to the electron beam

Examples of these are,

- choice of initial LCLS operating parameters, like use of a 1nC or 0.5 nC electron bunch charge;
- beam manipulation to optimize the FEL gain, like emittance compensation schemes, or like low emittance, low charge operation to reduce wakefield effects;
- control of the peak power of the X-ray pulse by changing the beam charge and emittance.

The last question can also be reformulated to see if there is a way to cut the beam 6-D phase space keeping the FEL gain constant while reducing the FEL peak power.

Much work can be done in this area to continue to optimize the LCLS, and extend the range of operating parameters beyond that of the original LCLS design report.

Methods and scenarios to control the X-ray pulse characteristics

The main issues in this group are the studies of methods to manipulate the LCLS X-ray pulse to optimize its characteristics from the point of the view of the particular experiment one is doing with the X-ray pulses. It is important to point out that the LCLS is a flexible system, and we should be able to control its output pulse characteristics, similarly to what is done with visible lasers. From this point of view some of the issues are:

- control of line-width and fluctuations by seeding and harmonic generation;
- control of line-width and fluctuations by filtering a small band-width with a monochromator, and amplification of the filtered radiation;
- pulse compression using the wide gain bandwidth of the FEL.

Much work is needed in all these areas to develop practical schemes to manipulate the X-ray pulse.

Commissioning scenarios

The LCLS is, at least initially, a SASE-FEL experiment. The main goal of this experiment is to show that there is FEL gain at 0.15 nm, and that the gain agrees with the theoretical FEL model. It is important to prepare to achieve this goal in the shortest possible time, so that we can then proceed to the other stages of the LCLS. Some of the questions relevant to this end are:

What are the scenarios for initial measurements of LCLS radiation characteristics? Measurement of intensity vs. charge at undulator exit? Measurement of intensity along the undulator? Others?

What is the minimum set of measurements and the minimum set of diagnostic and instrumentation necessary to establish the gain and measure its dependence on the electron beam parameters?

What is the required level of beam control in photoinjector and linac, and what is the required level of the instrumentation needed to reduce the intensity fluctuation to the value determined by the initial start-up noise? If this reduction of the intensity fluctuation is not possible can we use pulse selection techniques to reduce the fluctuation level? How do we do it? Although some initial work has been done, much more detailed work is needed to prepare for commissioning of the LCLS.

III. SASE Fluctuation, Quantum Corrections and Undulator Errors

By Kwang-Je Kim

SASE Fluctuation

Statistical properties of SASE light are completely determined from the fact that the amplitude E_ω is proportional to the sum of a large numbers of random phase factors. Light with these properties, such as the sunlight or the spontaneous undulator radiation, is referred to as “chaotic”. The topic has been extensively discussed, for example by Goodman [1]. In the context of SASE it was thoroughly discussed by Saldin, Schneidmiller, and Yurkov [2]. A simple review can be found in reference [3]. The probability distribution of the field amplitude, E_ω , of a chaotic light is Gaussian, as a straightforward application of the central limit theorem. Equivalently, the intensity at a given frequency $I_\omega = |E_\omega|^2$ has an exponential probability distribution in which the variance is equal to the average intensity. The fluctuation is therefore 100%. In general, we consider a partial flux ΔW as the flux within a phase space volume $\Delta\Omega$. The probability distribution of ΔW is given by the “gamma” probability distribution [1]. In the gamma distribution, the fluctuation is reduced by a factor \sqrt{M} , where the mode number M is the number of coherent modes in $\Delta\Omega$. We can write $M = M_T M_L$, where M_T and M_L are, respectively, the transverse and the longitudinal mode numbers. For an electron beam of length cT generating a radiation pulse of bandwidth $\Delta\omega$, the longitudinal mode number is given by $M_L = T\Delta\omega$.

We can now compare the fluctuation in SASE from the LCLS and in undulator radiation from typical third generation light sources at X-ray wavelengths. For the former, $M_T = 1$ (full transverse coherence), $\Delta\omega \approx \rho\omega$, $\rho \approx 10^{-3}$, T is about 100 fs, while for the latter $M_T \gg 1$, $\Delta\omega \approx 0.01\omega$, and T is about 100 ps. Therefore the fluctuation in SASE is larger by at least two orders of magnitudes than that in the undulator radiation.

Quantum Effects

There are several quantum corrections to the SASE properties. However, these effects are all negligible in the case of X-ray SASE as discussed below:

First, the quantum correction to the classical gain formula is small if the recoil energy is small compared to the gain bandwidth, or the photon energy is smaller than the electron energy spread. This condition is well satisfied for the X-ray SASE parameters.

Second, the effective noise signal needs to be modified when more than one electron occupies the quantum mechanical unit cell of volume, $(\lambda_C)^3$, where λ_C is the electron’s Compton wavelength. This is far from the case in the X-ray SASE.

Third, the mode number, M , becomes, after taking the quantum effect into account, $M/(1+1/\delta)$, where δ , known as the degeneracy number, is the number of photons per mode. This correction is also negligible in the X-ray SASE since $\delta \gg 1$.

Undulator Errors

The errors in undulator magnets are most conveniently characterized by the phase error. For a long undulator such as needed by a SASE FEL, the errors could be controlled by steering corrections at regular intervals. In this case, the errors in the derivative of the phase with respect to the distance along the undulator can be regarded as uniformly distributed along the undulator. The degrading effect of the undulator errors on SASE performance was most completely analyzed for this type of error [4], which may be referred to as the random kick error (RKE). However, there could be another type of error. Indeed, for well-optimized undulators, corrected by suitably placed shims, the phase error itself rather than its derivative should be regarded as distributed uniformly along the undulator. This type of error may be referred to as the random phase error (RPE). Effects of the RKE and RPE on the performance of spontaneous emission and high-gain FEL have been studied in reference [5]

References

- [1] J. Goodman, "Statistical Optics" (John Wiley & Sons, New York, 1985).
- [2] E.L. Saldin, E.A. Schneidmiller, and M.V. Yurkov, DESY preprint TESLA-FEL97-02 (April 1997)
- [3] K.-J. Kim, in Proceedings of the Workshop on Single Pass High Gain FELs from Noise, Aiming at Coherent X-rays, Lake Garda, Italy, June 2-7, 1997.
- [4] L.H. Yu, S.Krinsky, R.Gluckstern, van Zeijt, Phys. Rev. A45 (1992) 1163.
- [5] K.-J. Kim, 1999 FEL conference

IV. High-Gain, Higher-Harmonic Theory

By Li Hua Yu

Recent results from the High Gain Harmonic Generation (HG HG) experiment at BNL show that it is possible to use longer wavelength laser light as a subharmonic seed for an FEL to achieve saturation by exponential growth at shorter wavelength. The output radiation from HG HG is very stable and has Fourier-transform-limited bandwidth. The experiment agrees with the theory.

A theoretical study recently showed that the HG HG process can be cascaded by several stages starting from 288-Angstroms radiation (available from conventional laser sources) to reach 1.5 Å. Preliminary simulations showed that to achieve the same output power as the LCLS (10 GW) the required total length of the undulators including those for longer wavelengths is the same as the total undulator length (about 100 m) for the LCLS using the same set of electron beam parameters.

The parameters used in this calculation are not optimized, so far. With optimization, it is expected that the total undulator length can be reduced. In particular, the undulator section for the 1.5-Angstrom radiation is already shorter than half the total length of the present design when using the present parameters without optimization. This may help reduce the effect due to the surface roughness of the vacuum chamber wall since the undulator sections for longer wavelengths have larger periods and hence can use larger undulator gaps.

This cascading HGHG scheme needs five electron bunches, and hence a study about different methods to generate e-beams with several bunches is needed in the future. During the group discussion it was also suggested to study the parameter sensitivity of the system performances to synchronization errors and other beam parameters. It was also suggested to study the transition between different stages of the HGHG cascade, for example the optical transport between stages.

V. Status of the 3D FEL Theory

By Ming Xie

There are three major developments that have made linac-based, single pass FELs the approach of choice to reach short wavelength:

- first, technological advances in the generation, acceleration and preservation of high brightness electron beams,
- second, theoretical advances in the understanding of high gain FEL physics, leading to confident prediction, optimization, and scaling of FEL system performance to short wavelength, and
- third, an enthusiastic support from the light source user community. Of the theoretical advances the most significant and impressive achievement is the development of high gain 3D FEL theory over the past fifteen years.

There are two milestone achievements in the development of 3D FEL theory, which have laid the theoretical foundation for a great leap forward toward short wavelength. The first one is the discovery in 1984 and subsequent elucidation of optical guiding. With optical guiding, the diffraction problem is solved, thus FEL amplification can be extended indefinitely in a long wiggler to reach power saturation in a single pass. The next question is, of course, how long a wiggler does it take for this to happen? In other words, how does the FEL growth rate depend on electron beam and other system parameters? Furthermore, how does this dependence scale to short wavelengths? To answer these questions, the most important and difficult task is the understanding of the effects of emittance and associated betatron focusing. The solutions to this problem therefore constitute the second milestone achievement in 3D FEL theory. Today, the state-of-the-art analytical 3D theory has reached such a sophisticated stage that in several crucial aspects of physics it can simultaneously treat the effects due to energy spread, emittance and betatron focusing of electron beams, as well as diffraction and optical guiding of the laser field with high accuracy. Yet, there is still a lot to be desired of this theory and its full potential is far

from being reached. Solutions to a number of important problems can be expected in the near future.

The main objective of the 3D FEL theory is the determination of initiation, growth, saturation, and coherence characteristics of the laser field, as well as the evolution of the electron beam associated in the process. In the case of single pass FELs, it is fortunate that most of these tasks can be carried out in the framework of linear theory, therefore through analytical approach. In a nutshell, the 3D theory is about the solutions of two problems: the eigenvalue problem and the initial value problem.

The solution to the eigenvalue problem has been the most successful part in 3D FEL theory, in terms of both, an efficient numerical technique for the exact solution and an effective method for an approximate solution. Based on these solutions, growth rate and mode properties of the laser field can be calculated with high accuracy. The solution has been mapped out in the entire parameter space and interpolated into simple formulas to facilitate system design and optimization. In addition, the solution to higher order FEL eigenmodes has led to a quantitative analysis of transverse coherence of SASE. Of the two models considered for electron beam distribution in transverse phase space: waterbag and Gaussian, only an approximate solution is available for the former.

On the other hand, the initial value problem has been solved only in the case of a parallel electron beam without angular spread. Thus the effects of emittance and betatron focusing are not included in the solution. As a result, our predictions of SASE noise power, saturation length, and degree of transverse coherence of SASE are less accurate. The initial value problem, including effects of emittance and betatron focusing, is one of the most important outstanding issues.

Most of the 3D solutions obtained so far assume constant gradient for betatron focusing. One extension is available to model alternating gradient focusing, however, the model is valid under restricted conditions of a smooth approximation. In order to study the effects of beam envelope modulations due to alternating gradient focusing, the theory has to be further extended.

Harmonic generation in the high gain regime is an attractive and promising approach to reach short wavelengths. To further distinguish between different types of harmonic generation, let's introduce some new terminology: parasitic harmonic generation and cascade harmonic generation. Parasitic harmonic generation, by definition, exists in all FELs under all circumstances. A 3D analysis is available for this process. It would be interesting to know if the power in the harmonics could be optimized and how. Cascade harmonic generation, known as high gain harmonic generation (HG), is a very important alternative approach to SASE in reaching short wavelength. The analytical theory on this process is essentially 1D. An important issue of this approach is the possibility of scaling the scheme to very high harmonics in order to reach hard X-rays. Due to the involvement of multiple wigglers of quite different specifications and the large possibility in the variation of the scheme, a 3D analytical theory is a necessary complement to simulation for a system optimization.

The analysis on wiggler errors still remains 1D. This 1D analysis is expected to be reasonably good if the optical mode size is much larger than the electron beam size. However, for the LCLS case, the optical mode size is slightly smaller than the beam size.

Finally, the radiation field profile from the SASE process, although determined completely before saturation by the linear theory, can be modified by the nonlinear process at saturation. It is important to know about this effect, as it is the modified field that is delivered to the users through the X-ray optics beamline. Also, our estimation of saturation power is still based on either a simple model or an empirical formula, and its region of validity has not been extensively tested. Improvement might be possible by employing either a quasi-linear theory or a scaling law in the nonlinear regime, coupled with simulation

VI. 3D Nonlinear Harmonics

By Zhirong Huang

In a high-gain FEL based on a planar wiggler, strong bunching at the fundamental wavelength can drive substantial harmonic bunching and sizable power levels at the first few odd harmonic frequencies. Unlike a subharmonically seeded high-gain harmonic generation (HG) FEL [1] that employs two wigglers with the second wiggler resonant to one of the harmonics of the first and a dispersion section between the wigglers to maximize the spatial bunching at the fundamental of the second wiggler, this nonlinear harmonic generation occurs naturally in one long planar wiggler for a SASE FEL with an initially uniform bunch, as well as for the second stage of an HG FEL using a density-modulated bunch. Thus, such a natural harmonics generation mechanism may be utilized to reach shorter radiation wavelengths or to relax some stringent requirements on the electron beam quality for x-ray free-electron lasers.

A three-dimensional theory of the nonlinear harmonic generation is presented [2] in this workshop, using the coupled Maxwell-Vlasov equations that include the effects due to energy spread, emittance, and betatron focusing of the electron beams, as well as the diffraction and optical guiding of the radiation field. Each harmonic field is the sum of a self-amplified term and a term driven by nonlinear harmonic interactions. In the exponential gain regime, the growth rate of the dominant nonlinear term is much faster than that of the self-amplified harmonic field. As a result, the gain length, the bandwidth and the transverse profile of the first few harmonics are completely determined by those of the fundamental. For example, the third nonlinear harmonic grows three times faster than the fundamental, has a narrower gain bandwidth (by a factor of $1/\sqrt{3}$), is transversely coherent (with a smaller spot size), and has a power level on the percentage of the fundamental with the current LEUTL FEL and LCLS design parameters.

During the workshop, several key issues regarding nonlinear harmonic generation are discussed. The present theory has been compared with the 3D MEDUSA simulation code that tracks the nonlinear harmonic evolution up to the ninth harmonic [3]. Good agreement is found on the power level of the third harmonic radiation using the LEUTL FEL parameters. However, the simulation indicates the beam sizes of all the harmonics diverge, while the theory predicts constant beam sizes for these nonlinear harmonics generated by the transversely coherent fundamental radiation. It is emphasized that the nonlinear harmonic generation comes from the non-sinusoidal electron trajectory in a planar wiggler (the figure-eight motion in the electron's co-moving frame), not from the non-sinusoidal magnetic field distribution. It is also pointed out

that the higher harmonic radiation is more sensitive to magnetic field errors and gaps between separate wiggler sections due to the phase decoherence. These effects have yet to be studied.

References

- [1] L.H. Yu, Phys. Rev. A 44, 5178 (1989).
- [2] Z. Huang, K.-J. Kim, Three-Dimensional Analysis of Harmonic Generation in Self Amplified Spontaneous Emission, to be published in the FEL99 proceedings, Hamburg, 1999.
- [3] H. Freund et al., Nonlinear Harmonic Generation and Proposed Experimental Verification in SASE FELs, to be published in the FEL99 proceedings, Hamburg, 1999.

VII. Discussion

Throughout the workshop, the Theory Working Group was seeking to identify topics that were less mature and thus worthy of more attention. Most importantly, the group was looking for possible new effects that might jeopardize the LCLS project at 1 Å. Particularly treacherous would be an effect that would be undetectable at longer wavelengths (e.g. 1 μm), but harmful at short 1-Angstrom wavelengths. At the conclusion of the workshop, there was no such effect identified.

Several theory topics that were considered to be relatively mature are

- Classical and quantum start-up from noise,
- Undulator error sensitivity,
- Betatron function modulation, and
- Undulator section separations.

Less mature theory topics that may require more attention are

- Vacuum pipe impedance effects, see Kwang-Je Kim's talk below,
- New schemes, see Li Hua Yu's talk,
- Harmonics, see Zhirong Huang's talk,
- Saturation, see Bill Colson below, and
- Diagnostics, what to measure and how accurately, see Bill Colson below.

Other topics that for consideration were

- The total radiation spectrum,
- Coherent radiation beyond 1-Angstrom wavelength,
- Improved temporal and spatial properties, and
- Monochromatization.

VIII. Impedance Effects

By Kwang-Je Kim

The total radiation intensity from an electron beam passing through an undulator consists of the incoherent part proportional to the number of electrons, N_e , and the coherent part proportional to N_e^2 . The reaction of both of these parts on the electron beam could lead to degradation of the electron beam limiting the performance of SASE. Thus an obvious effect is the reduction in electron beam energy (deceleration) which must be within the gain bandwidth. The effect of the incoherent part on the electron beam energy spread was analyzed by the DESY group. The effect of the coherent part (most of which is in the form of SASE radiation) is basically an impedance effect, which was studied in old references (for example, by Y.H. Chin). This impedance may need another look, including a literature search.

The “normal” impedance effect due to the surface roughness of the narrow bore of the vacuum chamber was studied by G. Stupakov leading to a stringent specification of the surface roughness.

IX. Schemes for Improving the SASE Performances:

By Kwang-Je Kim

Two-stage undulator for a narrow spectrum

The scheme was proposed by the DESY group as a promising way to achieve a spectral width much narrower than the natural SASE bandwidth $\Delta\omega/\omega \approx \rho$ [1]. It consists of undulator U1, a monochromator, and undulator U2. In U1, SASE grows well above the noise level in the exponential gain regime. The signal is spectrally filtered in the monochromator, and is amplified to the saturation in U2. In order to reduce the fluctuation, the length of U2 is chosen to be sufficiently long so that it is operating well into the non-linear saturation regime. The scheme has been analyzed within 1-D theory. However, 3-D effects could be important, as the transverse mode profile in the saturation regime will be, in general, different from that in the exponential gain regime.

Pulse compression

The length of a SASE pulse, $c\tau$, is normally determined by the electron beam, which is about 100 fs. However, it consists of x-ray wavelets each about ρ^{-1} periods, where $\rho \approx 10^{-3}$ is the FEL scaling parameter. Therefore it should be possible to compress the SASE pulse to a length $\tau_{min} \approx \lambda/c\rho$, which is about 1 fs for $\lambda = 1 \text{ \AA}$ [2]. The compression is accomplished by introducing an energy slew in the electron beam leading to the frequency chirp (frequency shift per unit length). The maximum chirp consistent with the FEL gain is given by $(\Delta\omega/\omega)_{max}/c\tau = \rho/(\lambda/\rho) = \rho^2/\lambda$. The chirped pulse can then be compressed with a grating pair. The minimum pulse length achievable is $c\tau_{min} = \rho c\tau/(\Delta\omega/\omega)_{max} = \lambda/\rho$. The technique for pulse compression has been extensively developed for high-power solid state lasers at visible

wavelengths. For the X-ray SASE pulse, a major research project will be to demonstrate that the required optical elements exist.

Circular polarization

Recently, a crossed undulator configuration was proposed for a high-gain free electron laser for versatile polarization control [3]. It consists of a long (saturation length) planar undulator, a dispersive section, and a short (a few gain lengths) planar undulator oriented perpendicular to the first one. In the first undulator, a radiation component linearly polarized in the x-direction is amplified to saturation. In the second undulator, the x-polarized component propagates freely, while a new component polarized in the y-direction is generated and reaches saturation in a few gain lengths. By adjusting the strength of the dispersive section, the relative phase of two radiation components can be adjusted to obtain a suitable polarization, including the circular polarization, for the total radiation field. The operating principle of the high-gain crossed undulator, which is quite different from that of the crossed undulator for spontaneous radiation, was studied in 1-D FEL theory in the exponential gain regime. However, the analysis did not take the fluctuation effect into account, which will be important especially near saturation.

References

- [1] J. Feldhaus, E.L. Saldin, J.R Schneider, E.A. Schneidmiller, M.V. Yurkov, DESY preprint TESLA-FEL 96-10
- [2] C. Pellegrini
- [3] K.-J. Kim

X. LCLS Saturation Theory

By Bill Colson

Almost all of the hundreds of FELs that have been operated over the last 20 years have reached saturation in strong optical fields. In the high gain regime, the LLNL ELF experiments reached saturation many years ago and the results are well understood. But ELF operated at 1-cm wavelength and the radiation mode was confined to a waveguide with an electron beam that was smaller than the cross-section of the radiation mode. The LCLS FEL is expected to have high gain comparable to ELF, but the X-ray radiation mode is freely propagating without a waveguide.

It can be expected that the one-dimensional aspects of saturation without diffraction can be determined by the same theory and simulation codes that successfully described ELF. These

simulations and theories predict fluctuations in the LCLS X-ray radiation field before and after saturation. The radiation fluctuations at saturation were not measured in detail for ELF.

Current high-gain SASE experiments will provide a better confirmation of our understanding of fluctuations at saturation. Since the X-ray radiation spectrum is an important aspect of the LCLS, an improved understanding of saturation should be directed towards developing techniques or modes of operation to reduce fluctuations at saturation.

The three-dimensional aspects of LCLS saturation are more likely to lead to new effects not observed in ELF or any other FEL experiment. The shot noise from the tenuous electron beam at the out edges of the x-ray radiation mode is a new feature that may alter fluctuation results. It was felt that there are opportunities for new theory research in this area.

XI. LCLS Diagnostics

By Bill Colson

An important contribution from theory will be to make a statement about what should be measured in the LCLS experiment and how accurately it should be measured. This contribution is not to be made here, but the workshop theory group acknowledges that this is an area for further work.

One result of the diagnostic study will be the finding that many variables affect the growth rate and coherence of the X-ray beam. The most significant effects from the six-dimensional electron beam phase-space can be summarized by converting their contributions to the electron phase velocity, or z-velocity distribution function. There was extensive use of this reduced distribution function during the development and analysis of the LLNL ELF FEL experiments. Coupling between the electron beam and X-ray radiation is primarily determined by the electron phase distribution within each x-ray wavelength. It is the electron phase velocity distribution that determines the electron phase distribution during the interaction along the 100-m undulator length. It is therefore recommended that the electron beam's phase velocity distribution be used as a method of summarizing the parametric effects of the many variables that can influence LCLS performance.

SUMMARY OF WORKING GROUP II

Code Status, Development Plans and Options

Working Group Members:

Sandra Biedron (ANL), Michael Borland (ANL), Roger Dejus (ANL), Paul Emma (SLAC), William Fawley (BNL), Henry Freund (SAIC), Massimo Ferrario (INFN-LNF), John Goldstein (LANL), Heinz-Dieter Nuhn (SLAC), Claudio Parazzoli (Boeing), Roman Tatchyn (SLAC), Richard Binonta (LLNL)

I. Introduction

Working Group II was comprised of approximately one dozen individuals who met for approximately six hours spread over 1-1/2 days to discuss simulation code issues relevant to XUV and X-ray SASE FELs. In order to make efficient use of our very limited time, we had agreed before meeting upon a format of several different topic areas together with one or more individuals tasked to make a short status presentation in each area. In order of discussion together with their respective presenters, these areas were (a) Undulator modeling and transport issues (H. Freund) (b) Harmonics (S. Biedron) (c) Code communication and interface issues (M. Borland) (d) Radiation transport beyond the undulator (R. Bionta). We also discussed issues such as inclusion of additional physics (*e.g.* wake fields) and numerical accuracy requirements (*e.g.* particle statistics) in SASE-relevant simulation codes.

This report summarizes our findings and conclusions, if any, in each of these various areas together with indications of where the group felt additional work should be applied over the next 12-18 months. This short time scale is dictated by the present schedule of the LCLS project which plans to present a design proposal to DOE by late spring 2001 for which simulation information will be needed by December 2000. Appendix A gives an extended synopsis of a number of FEL codes presently in use for modeling short wavelength SASE FEL's. All in all, the working group felt we had a productive session, especially given the short available time and the persistent (but humorous) interruptions by the SLAC aerobics Mafia.

II. Undulator modeling and beam transport issues

All of the proposed XUV and shorter wavelength SASE FEL devices employ undulators with hundreds-to-thousands of wiggler periods. These great lengths together with the relatively low gain of these devices dictate that the undulator must be of high quality (*i.e.* good field quality and alignment) and similarly that the code transport models and algorithms must also be of high accuracy.

Much of the discussion in this area centered upon the issue of whether any important physics is being missed by adoption of the wiggler-averaged (KMR) FEL interaction equations. With the exception of the MEDUSA code, nearly all simulation codes in the SASE area employ

wiggler-averaging. Although the KMR formulation has significant advantages due to its simplicity, it requires assumptions in areas such as radiation emission in the first few wiggler periods following a drift and the coupling to higher harmonics (*i.e.* the [JJ] term). A non-wiggler averaging algorithm, in theory at least, can treat the "exact", imperfect wiggler field at each point in space. However, it intrinsically requires longitudinal step sizes that are much smaller than a wiggler period whereas other longitudinal scale lengths (*e.g.* radiation gain length, Rayleigh range, synchrotron oscillation wavelength) might be much larger than a period and for which the wiggler averaging approach might be far more efficient computationally. There also remain (among certain workers in the FEL simulation field) some questions of self-consistency in the decomposition of the local source terms between those, which couple to the radiation "far field" and those, which might be evanescent and/or propagating at large angles compared to $1/\gamma$. This issue is probably of most concern at much lower energies than the LCLS and it would be surprising if the two approaches gave significantly different results. Hence, the working group felt it would be highly useful for MEDUSA's author (H. Freund) to implement a wiggler-averaging option in order to permit examination of what prediction differences (*e.g.* output power) would arise between the two formulations in the context of LCLS- and LEUTL-like parameters.

Another area of discussion concerned magnetic field models and the implementation of external focusing and wiggler errors into simulation codes. Many codes have the ability to read in tables of wiggler errors; MEDUSA can read in a detailed 3D field map (which even for 100-m long wigglers as in the case of the LCLS only requires a couple of minutes or less on a workstation). H. Freund mentioned that R. Jackson, while at NRL in the 1980's, put together a computational package to determine higher order off-axis derivatives of the wiggler fields, which might be of use to those who want to include such terms in their particle movers. Given the presence of external quadrupoles and the existence of periodic drift sections (which are normally used for diagnostic access) in both the LEUTL and proposed LCLS wiggler lattices, Working Group II believed it was important that all of the simulation codes be able to treat both types of elements.

Wiggler "errors" come in a variety of forms. The most important are probably amplitude errors in pole-to-pole excitation which, in general, will lead to transverse kicks and offsets. This type of error can also lead to a longitudinal phase error in the coupling between the radiation and the electron beam. Another type of detuning error exists when the average of a_w (averaged locally over one or more periods) deviates by an amount on the order of ρ from the wanted value. However, for all but the shortest wavelength/low gain FEL's, this detuning is normally not important. Most of the existing "3D" codes, *e.g.* FELEX, MEDUSA, GENESIS; and some 2D ones such as RON already include the transverse kicks due to wiggler errors and can also model steering corrections by appropriately placed dipoles. The details of wiggler error treatment undoubtedly vary from one code to the next. Therefore, R. Dejus of ANL offered to make freely available in a standard format such as SDDS the results of detailed measurements of the first five LEUTL undulator sections (and proposed dipole steering corrections) for each author to use in their respective code in order to determine effects upon the predicted LEUTL performance. During a joint meeting with the FEL Theory working group, a short talk by L.-H. Yu (BNL) suggested that wiggler errors would in general more seriously degrade power at higher

harmonics. This prediction could be studied with some of the existing simulation codes (see Sec. **III**).

There was a group consensus that further wiggler error tolerance studies needed to be made for the LCLS. Probably the great majority of this study can be done with a monochromatic formulation. Paul Emma (SLAC) suggested a need for a quick running code, which could examine the efficacy of different optimization strategies for electron beam trajectory control. Many of the existing codes have the ability to run a "reduced" problem in which the electron beam evolves independent of any background radiation field. It may also be useful for two or more of the codes to be able to accept a trajectory control (i.e. steering magnet setting) algorithm "module" from the "outside". To some extent, such module interchangeability falls within the code "interface" issues discussed in section **IV**.

III. Harmonics

It is well known that there will be extensive radiation at odd harmonics of the fundamental for SASE FELs with linearly polarized wigglers. S. Biedron presented predictions by the MEDUSA code for the output power and coherent spontaneous "gain" lengths of harmonics in LEUTL and in the High-Gain Harmonic Generation (HG HG) experiment at BNL. Despite the quite short gain lengths (which are a factor of n shorter for the n^{th} harmonic than the fundamental), the power in each harmonic remains relatively small until within a couple gain lengths of fundamental saturation. The HG HG experiment will test many of these principles, in addition to investigating the 2nd harmonic bunching performance of an optical klystron section for a high gain, single-pass amplifier.

During the discussion of Working Group II, there was interest in using 3rd and 5th harmonic power as a diagnostic of beam and wiggler quality. More analytical and simulation work on the sensitivity could be useful. For example, the effects of "real" wiggler errors (as determined by wiggler field mapping) upon the predicted growth rates of harmonics should be examined. The question of differences between wiggler- and non-wiggler-averaged codes arose again and it was suggested that harmonics be included in the comparison studies suggested in Section **II**. The LEUTL experiment at ANL could be a very useful test bed in the area of harmonic growth from noise. Unfortunately, the short fundamental wavelength $\lambda=532$ nm together with the open-air transport from the wiggler exit to the diagnostic station will cause severe absorption losses at the 3rd and higher harmonics. It may be possible for LEUTL to "back off" sufficiently in wavelength (e.g. by increasing a_w or decreasing E_{beam}) so that the 3rd harmonic enters the blue region of the spectrum.

IV. Code Interface and Communication

M. Borland (ANL) discussed the advantages of and the need for one (or possibly two) standard data formats with which FEL and accelerator (e.g. tracking) codes could exchange data. One distinct advantage of using an externally defined format is that it frees individual codes from being "locked" to each other. One such format, the Self-Describing Data Set (SDDS), is in wide use at ANL and some other DOE accelerator labs. In addition to providing I/O capabilities, the SDDS package also has some analysis and scientific visualization features, which have proven

quite useful for various tasks such as parameter sensitivity studies. As an alternative to embedding the SDDS or other format package in a given FEL or accelerator code, Borland suggested a different approach of writing simple adapter programs to "repackage" the output. Such was done with the GINGER code at ANL a couple years ago. This approach may also be desirable for simulation codes written in Fortran because the SDDS package is heavily oriented toward C/C++ routines at present. The ANL group has offered to write such adapter programs for individual codes so long as a sufficiently clear specification is provided. The working group quickly agreed that the SDDS format should be adopted by as many FEL codes as possible to assist with exchange of data both to other FEL codes and to outside codes.

A related issue to code interfacing is that of "start-to-end" modeling of FEL performance. C. Parazzoli (Boeing) presented some of the studies he has done with the FELEX code to examine output power sensitivities to input particle distributions provided by the PARMELA-TRACE3D package. In many cases, realistic distributions gave quite different results from simple Gaussian distributions and he stressed that similar interfacing would probably be needed for the LCLS. One issue that arose during the discussion of interfacing tracking codes to FEL codes was the great temporal "mismatch" between the FEL codes and tracking codes. FEL codes typically use thousands of macro-particles per sub-femtosecond slice, as compared with most tracking codes, which typically use a couple of thousand or fewer macroparticles to model the entire picosecond duration of the electron beam pulse. It may be necessary to modify one or more of the tracking codes to make them capable of providing a greater sampling density of 6D phase space in discrete sections of the pulse and/or both formulate and write a clever algorithm to interpolate from the sparsely populated tracking results to the required high density needed by polychromatic FEL codes.

V. Radiation Transport beyond the Undulator

R. Bionta discussed some aspects of the LLNL group's work on modeling transport of the FEL radiation pulse after the wiggler and the development of detectors for beam diagnostics as well as the optical components for transport. One important area is plasma formation and hydrodynamic phenomena associated with the interaction of the intense EM pulse with the attenuator, bending mirrors, crystals, diffraction gratings and sensors placed in the beam. Successful development of diagnostics and optical components requires reasonable models of both the FEL beam and the spontaneous radiation emissions. These models must cover the significant FEL harmonics and electron beam energies (especially if the 3rd harmonic will be used at reduced beam energy.)

At present, it is believed that valid preliminary assessments of LCLS radiation-matter interactions can be started with the simplified descriptions of the LCLS radiation given in the LCLS Design Study Report supplemented with further 3D FEL simulation runs. For the purposes of designing sensors and optics, the FEL beam will be modeled using Gaussian wave packets in space and time for each micropulse. In addition to a central frequency, the Gaussian wave packet has essentially 4 other parameters: transverse beam size, w ; phase curvature, R ; peak amplitude, A ; and micropulse duration, τ . The central frequency of the fundamental and all other modes can be obtained at all values of beam energy from the well-known formula in the LCLS Design Study Report. The transverse beam size, w , and phase curvature, R , are also given explicitly in

the report for the minimum and maximum beam energies and can be found at other beam energies and other modes by a linear interpolation.

Values for the peak amplitude, A , and micropulse duration, τ , are more difficult to obtain. The Design Study Report gives data and formulae for calculating the saturated power of the FEL fundamental at all beam energies. To convert saturated power to peak amplitude requires knowledge of the number and duration of the micropulses, as well as statistics on the distribution of energy amongst the micropulses. A simplifying assumption, good for many of the situations under consideration, is to model the micropulses as a series of wave packets with equal duration at a given repetition rate with the energy divided equally among the packets. With this assumption, the amplitude of the wave packets can be calculated from the saturated power, the repetition rate, and the duration. H. -D. Nuhn has produced a 12-fs simulation showing the time structure of the FEL fundamental at full beam energy from which the average pulse duration and repetition rate can be measured as well as some limited statistics on the individual micropulse intensities.

The radiation time structure at other beam energies is not yet available. It can probably be crudely estimated from H.-D. Nuhn's result through some sort of scaling of the slippage and cooperation lengths at different energies. Since the LCLS could start up at lower than maximum beam energies, it is important to clarify the time structures at all beam energies and have explicit simulations at the energy chosen for start up.

Finally the power levels of the higher harmonics are not given in the LCLS Design Study Report. Since there is interest in utilizing higher harmonics in initial operations of the LCLS at lower beam energies, it is important to model (either theoretically or numerically) the expected intensities.

It is anticipated that more refined studies, as well as certain classes of LCLS experiments (e.g., single-shot imaging and diffraction) would benefit from a detailed knowledge of the photon distributions along each of the phase space dimensions associated with the individual slippage regions of the bunch. A similar level of simulational accuracy would also benefit the design of optical instrumentation for characterizing the lasing performance of the LCLS, as well as for transporting the radiation to experiments. A desirable goal would be to relate the required descriptions of the radiation to the specific phase space structure of a single electron bunch, from which bunch-to-bunch variations in the photon phase space distributions could be deduced. In general, while the nominal goal of the LCLS diagnostics is to characterize each of these distributions - either statistically or on a single shot basis - it is anticipated that direct temporal profiling of the radiation's longitudinal structure will be the most difficult to achieve. Such information would be of particular interest during the commissioning phase to help determine which portions of the electron beam pulse are lasing and which are not. In this regard, maximally realistic and accurate 3D simulations could be critical in assessing or developing techniques to perform such a measurement.

VI. Numerical Issues and Need for Additional Physics

Working Group II had a brief interchange concerning the numerical/statistical accuracies of the various FEL codes represented in the group. In general we agreed that 1000-4000 macroparticles/slice give good results, with the larger number needed when there is a significant

instantaneous energy spread. For fully gridded 3D codes, Cartesian geometries normally require more than 64×64 zones as compared with 32–64 radial zones for 2D codes. For an r - θ code such as FRED3D, 2–4 azimuthal zones per radial zone are sufficient for most problems. For a code such as MEDUSA, which uses a Gauss-Hermite spatial mode decomposition, 3–24 independent modes are normally adequate. In time-dependent (polychromatic) simulations, ~ 128 temporal slices give appropriate resolutions for LCLS-type problems with periodic boundary conditions in time.

Regarding the need for additional physics effects in the existing codes, there were two particular areas of concern. The first was the incoherent energy loss, both in terms of a time-averaged loss (which can require microtapering of the wiggler strength with z) and statistical fluctuations, which can increase the instantaneous energy spread. The GENESIS code already includes this loss and there was a consensus that other codes such as GINGER, MEDUSA, and RON should also implement it.

A second loss term is due to wakefields associated with surface roughness of the beam tube and any radial interruptions (*e.g.*, pumping and/or diagnostic ports) of the wiggler beam tube. These losses will temporally vary from the beam head to the tail and can cause a chirping of the output spectrum for SASE devices. Here, the energy loss can lead to a detuning effect that cannot be corrected with microtapering (due to the time-dependence). Some studies have been done with both the GENESIS and GINGER codes but more work is probably needed. Moreover, the group felt that additional theoretical work is required to increase our confidence in the actual loss formulae.

WORKSHOP PROGRAM

- **Thursday September 23, 1999**
 - **8:30-9:00 Continental Breakfast**
 - **9:00-9:10 Introduction, M. Cornacchia**
 - **9:10-9:50 X-ray FEL Physics Overview, C. Pellegrini**
 - **9:50-10:30 Simulation Code Overview, H.-D. Nuhn**
 - **10:30-11:00 Coffee Break**
 - **11:00-12:30 Working Group Discussion**
 - **12:30-13:30 Lunch Break**
 - **13:30-15:30 Working Group Discussion (Combined)**
 - **15:30-16:00 Coffee Break**
 - **16:00-18:00 Working Group Discussion**
 - **18:00-18:10 Short Summary of Working Group I**
 - **18:10-18:20 Short Summary of Working Group II**
 - **18:30 Workshop Dinner**
- **Friday September 24, 1999**
 - **8:30-9:00 Continental Breakfast**
 - **9:00-10:30 Working Group Report Generation**
 - **10:30-11:00 Coffee Break**
 - **11:00-11:45 Report of Working Group I**
 - **11:45-12:30 Report of Working Group II**
 - **12:30 Adjourn**

LIST OF PRESENTATIONS

C. Pellegrini	X-ray FEL Physics Overview
H.-D. Nuhn	Simulation Code Overview
K.-J. Kim	Remarks on SASE Fluctuations and Undulator Errors
Z. Huang	3D Analysis of Nonlinear Harmonic Generation
M. Xie	Exact and Variational Solutions of 3D Eigenmodes for High Gain FELs
L.-H. Yu	High-Gain, Higher-Harmonic Theory
H. Freund	Particle Transport
M. Borland	Interfacing Multiple Simulation Codes
S. Biedron	The High-Gain Harmonic Generation Experiment

WORKSHOP PRESENTATIONS I

X-ray FEL Physics Overview

By C. Pellegrini

FEL Physics R&D for LCLS

- The LCLS is now in the R&D phase, and a second, and more detailed, conceptual design report must be prepared by the end of the Y2K, to be presented soon after to DOE.
- The goal of this workshop is to prepare an R&D plan, to help decide what are the issues that should be addressed to make the LCLS project more likely to be a success, what are the priorities, and how to make good use of the manpower present in the LCLS collaboration.

***FEL Physics R&D for
LCLS***

Present status of FEL physics

1. The experiments on SASE-FELs in the infrared have given data in agreement with our theoretical model on:
 - 1.1 Gain, and its dependence on the electron beam 6-D phase-space density
 - 1.2 Line width and mode of the amplified radiation
 - 1.3 Intensity fluctuations due to start-up from noise

***FEL Physics R&D for
LCLS***

2. We still have no experimental data on:
 - 2.1 Saturation and its characteristics
 - 2.2 Complete radiation mode structure
 - 2.3 Gain and other characteristics of harmonics, and the dependence on electron beam parameters.

FEL Physics R&D for LCLS

The experiments now in the initial state of data taking, - VISA, LEUTLE, TESLA- will hopefully provide the additional information that we need.

One important task for the LCLS physics section is to understand and analyze the data produced by these experiments, and examine any possible implication for LCLS.

FEL Physics R&D for LCLS

While these experiments can provide additional missing data on FEL physics they cannot extend the wavelength to the 0.1nm region. This will be done by LCLS, and this is the primary goal of the LCLS experiment.

What are the most important questions can we should try to answer in preparation for LCLS and to optimize the design of the experiment?

- A) short wavelength related questions
- B) beam related questions
- C) X-ray pulse manipulation questions
- D) scenario for commissioning and demonstrating FEL gain

***FEL Physics R&D for
LCLS***

A) The main question in group A is:
is there any effect in the FEL physics model that we use,
which is important at 0.1 nm while it is negligible at 1000
nm?

Issues related to this might be:

- A1) start-up noise
- A2) effects of coherent and incoherent radiation
emission or wakefield effects in a long undulator and
for a high energy -multi GeV- electron beam
- A3) quantum effects

***FEL Physics R&D for
LCLS***

B) questions related to the electron beam are:

B1) choice of initial LCLS operating parameters, like use of a 1nC or 0.5 nC electron bunch

B2) beam manipulation to optimize the FEL gain, like emittance compensation

B3) control of the radiation power changing the beam charge and emittance; can we cut the beam 6-D phase space to keep the gain constant while reducing the FEL peak power?

***FEL Physics R&D for
LCLS***

C) The main issues in this group are the studies of methods and scenarios to control the X-ray pulse characteristics:

C1) control of line-width and fluctuations by seeding and harmonic generation

C2) control of line-width and fluctuations by filtering a small band-width with a monochromator, and amplification of the filtered radiation

C3) pulse compression using the wide gain bandwidth of the FEL

FEL Physics R&D for LCLS

D) Commissioning scenarios. The LCLS is at least initially a SASE-FEL experiment. The main goal of this experiment is to show that there is FEL gain at 0.1nm, and that the gain agrees with the theoretical FEL model.

D1) What are the scenarios for initial measurements of LCLS? Measure the intensity vs charge at undulator exit? Measure intensity along the undulator? Others?

D2) What is the minimum set of measurements and the minimum set of diagnostic and instrumentation to establish the gain and measure its dependence on the electron beam parameters?

*FEL Physics R&D for
LCLS*

D3) what is the required level of beam control in the photoinjector and linac, and the instrumentation needed to reduce the intensity fluctuation to the value determined by the initial start-up noise? If this is not possible can we use pulse selection techniques to reduce the fluctuation level? How do we do it?

FEL Physics R&D for LCLS

Conclusions

What I have discussed is only a preliminary list of issues, with no priorities between them.

I hope that by the end of the workshop we will have a more complete list, and an understanding of where our effort should be oriented during the R&D phase of LCLS.

WORKSHOP PRESENTATIONS II

Simulation Code Overview

H.-D. Nuhn

Simulation Codes Overview

SLAC, September 23, 1999
Heinz-Dieter Nuhn, SLAC / SSRL

LCLS Design Report

Experiments

FEL Simulation Codes

Simulation Task

Workshop Organization

X-Ray FEL Simulations

- **Gun**
- **Linac**
- **Bunch Compressor**
- **Undulator**
- **X-Ray Optics**

Focus of Present Workshop

- **Undulator**
- **Linac Undulator Interface**
- **X-Ray Beam Characterization**

→ **Next Simulation Workshop to Include Full Scope**

Workshop Objective

- **Survey the present theoretical status of X-ray FELs.**
- **Identify physics issues to be investigated for LCLS, a 1.5 Å X-Ray FEL.**
- **Characterize existing FEL simulation codes, and identify capabilities that are missing in one or more of the existing simulation codes.**
- **Discuss the means of upgrading existing codes or producing a new code.**

LCLS Schedule

April 1998	LCLS Design Report
April 1999	DOE Funding for 4 year R&D program and CDR (FY1999-2002)
June 1999	First Funding for FY99 arrives
December 2000	CDR Draft completed
May 2001	CDR completed
June 2001	Lehman Review
FY2003	Start of LCLS construction phase
FY2005	First beam through the undulator

LCLS Design Report

- 1 -

- **General Parameter Optimization**
Operational Range 5 - 15 GeV (15 - 1.5 Å)
- **FODO Lattice Design**
10 cm long quadrupoles spaced 2 m apart. Integrated gradient 5.6 T.
- **Effects of β -Function Modulations**
Modulation amplitudes of 23 % at 1.5 Å (70 % at 15 Å) appear acceptable
- **Magnet Error Tolerances**
0.1 % rms acceptable, larger tolerance with special magnet sorting conceivable
- **Beam Position Control**
Requirement: RMS deviation from straight line 2 - 5 μm

LCLS Design Report

- 2 -

- **Alignment Tolerances**
Established tolerances based on estimates and simulations.
- **Effect of Section Separations**
Analytical and simulation study indicate low sensitivity.
- **Sensitivity to Parameter Fluctuations**
Based on 3D theory.
- **Effect of Initial Phase Space Distribution**
Model distributions studied with 3D code.

LCLS Design Report

- 3 -

- **Effects of Spontaneous Radiation**

Estimate of effects of energy spread and emittance increase to be small. Energy Loss of .15 % will require micro-tapering.

- **Effects of Wall Roughness and Resistive Wall Impedance.**

Simulation of energy-change dependence on position within a bunch with modified GINGER code. Tolerance .1% over 100 m undulator at 15 GeV. Average change to be corrected with additional micro-tapering.

- **Output Power Control**

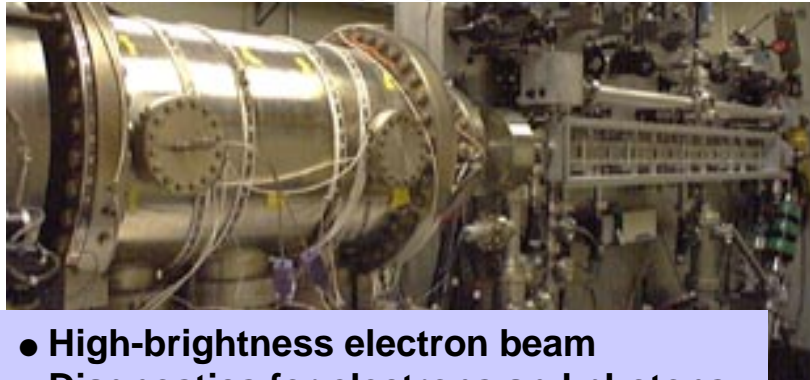
Based on GINGER simulations. Operation in exponential gain regime leads to unacceptable fluctuations.

Experimental SASE Data for Code Tests

- **VISA (Visible to Infrared SASE Amplifier)**
 - BNL-LANL-LLNL-SLAC-UCLA collaboration
 - Undulator built and installed in ATF at NSLS (4 m long, strong focusing)
 - SASE saturation experiment at 0.8-0.6 μm in 1999
- **LEUTL at ANL**
 - Uses part of the APS Linac
 - 0.53 μm (218 MeV) in 1999, eventually down to 0.12 μm (440 MeV)
- **Mid-Infrared Saturated Amplifier (MISA) at LANL**
 - Capitalizes on availability of existing hardware at AFEL
 - 19 μm in 1999
- **TTF-FEL at DESY**
 - Phase 1: 390 MeV, 420 \AA , under commissioning, first operation 1999
 - Phase 2: 1000 MeV, 60 \AA , start commissioning in March, 2002
- **Source Development Laboratory (SDL) at NSLS**
 - 210 MeV linac, SASE demonstration at 300 nm in 2000-2001
- **X-ray FEL study under way at KEK**

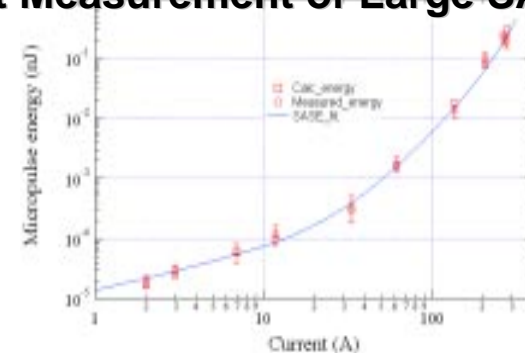
Gain of 3×10^5 at $12 \mu\text{m}$ Los Alamos Experiment

Test-stand for High-gain SASE Expts.



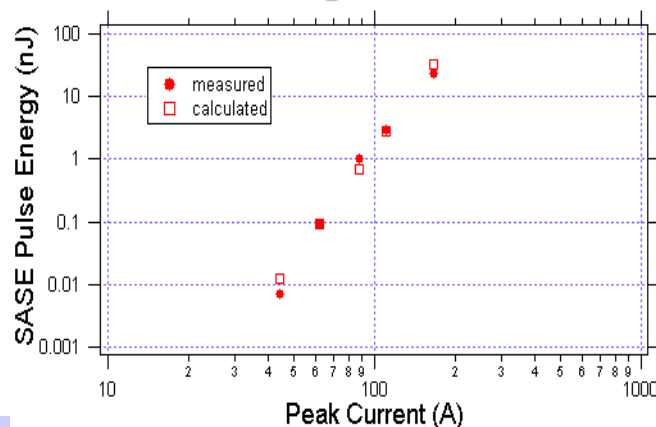
- High-brightness electron beam
- Diagnostics for electrons and photons

First Measurement of Large SASE Gain



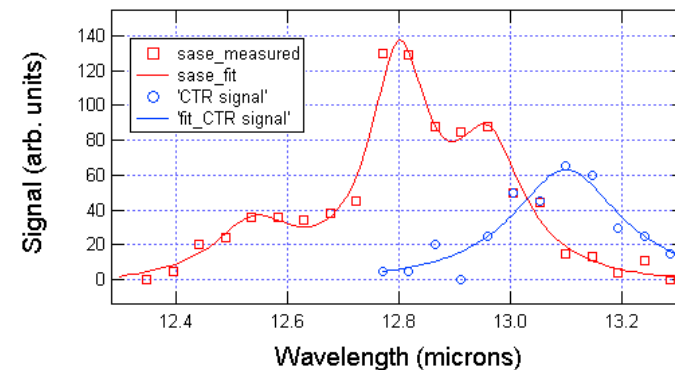
- Gain = 300 for the one-meter undulator

Measurement of Largest SASE Gain



- Gain = 10^5 for the two-meter undulator

Observation of SASE-induced bunching



- Observation of coherent transition radiation
- Results corroborate SASE measurements

SASE Codes Timeline

1982 -1985	First publications of SASE principle
1986-1989	FEL Simulation Codes FRED, NUTMEG, FRED3D, GINGER, FELEX, TDA3D
1986	First SASE experiments ELF, PALADIN
1992	Start of the LCLS design
... -1998	FEL Simulation Code MEDUSA
1993	Quadrupole focusing addition to TDA3D
1993-1995	Theory temporal structure (SARAH)
1994	Start of the DESY TTF design
1996	FEL Simulation Code RON
1997-1998	FEL Simulation Codes FAST, FS1T
1997-1998	UCLA/LANL high gain experiment
1998	FEL Simulation Code GENESIS 1.3
1999	Expected results from SASE experiments: TTF FEL, LEUTL, VISA...
2003	Construction start for LCLS
2009	Possible construction start for TESLA

Amplifier FEL Codes and Authors

FAST	E.L. Saldin, E.A. Schneidmiller, M.V. Yurkov
FELEX	C.J. Elliott, J.C. Goldstein, B.D. McVey, M.J. Schmitt
FELOS	Z. Weng, Y. Shi
FRED3D	E. T Scharlemann
FS1T	E.L. Saldin, E.A. Schneidmiller, M.V. Yurkov
GENESIS 1.3	S. Reiche
GINGER	W.M. Fawley, E.T. Scharlemann
MEDUSA	H.P. Freund, S. Biedron, S.V.Milton
NUTMEG	E.T. Scharlemann
RON	R.J. Dejus, O. Chevchenko, N.A. Vinokurov
SARAH	P. Pierini
TDA3D	B. Faatz, S. Reiche, P. Pierini, T.M. Trans, G.A. Travish, J.S. Wurtele

Code Classification

- **2D harmonics**
NUTMEG
- **1D polychromatic**
FS1T*, SARAH*
- **3D-Particles/2D-Field polychromatic**
GINGER*
- **3D-Particles/3D-Field monochromatic**
FRED3D, TDA3D
- **3D-Particles/3D-Field harmonics**
MEDUSA
- **3D-Particles/3D-Field polychromatic**
FAST*, FELEX (*), FELOS(*), GENESIS 1.3*, RON*

* simulates SASE startup from shot-noise.

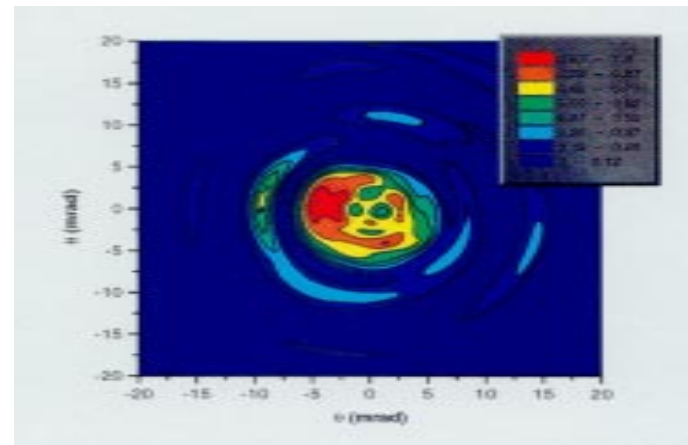
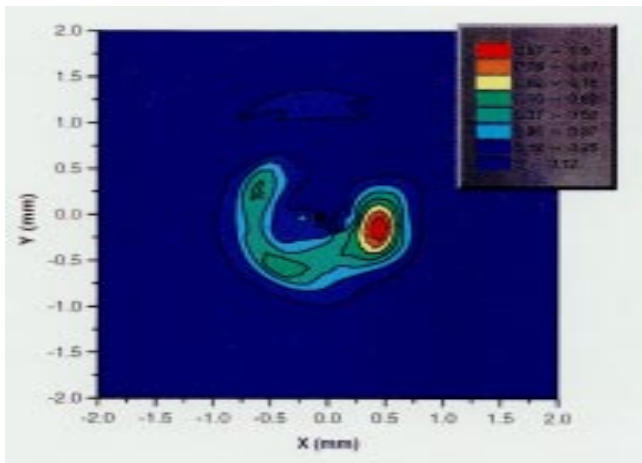
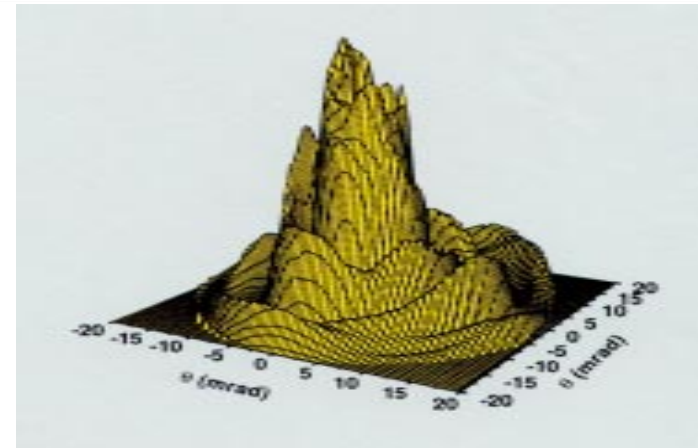
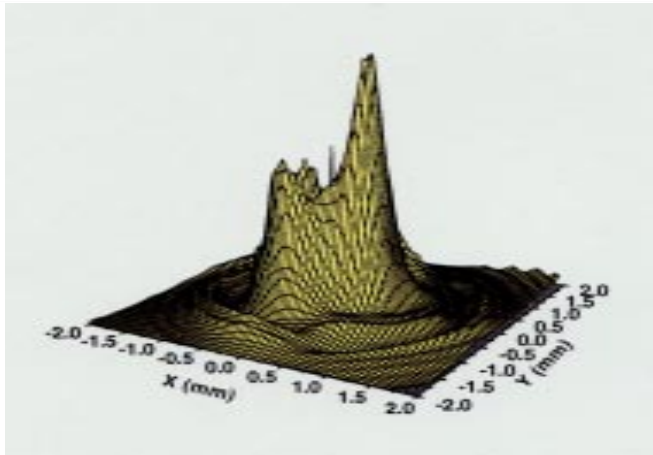
Linear Simulation Codes

- **Fully 3D Time-Dependent Simulation Codes based on macro-particles are CPU-Time intensive.**
- **Alternative approach based on kinetic equations describing the evolution of the distribution function of the electron beam.**
- **Examples: RON, Linear version of FAST.**
- **Approach capable of answering all questions not related to saturation.**
- **CPU time requirements are two order of magnitude less than for macro-particle-based codes.**
- **Full statistical analysis possible.**

SASE Startup from Noise.

- Generally a method of **Quiet Loading** is used to load macro-particle phases.
- **GINGER, SARAH, RON, FAST, F1ST** and **GENESIS 1.3** simulate the SASE startup from shot-noise.
- For simulation of startup from noise, a **phase increment or decrement is added** to each particle phase.
- Phase increment or decrement chosen from a **uniform distribution** related to the square root of the number of macro-particles.

SASE Startup Studies



Transverse power distribution for the UCLA experiment predicted by FAST
in the low gain regime. **Courtesy of Mikhail Yurkov, DESY.**

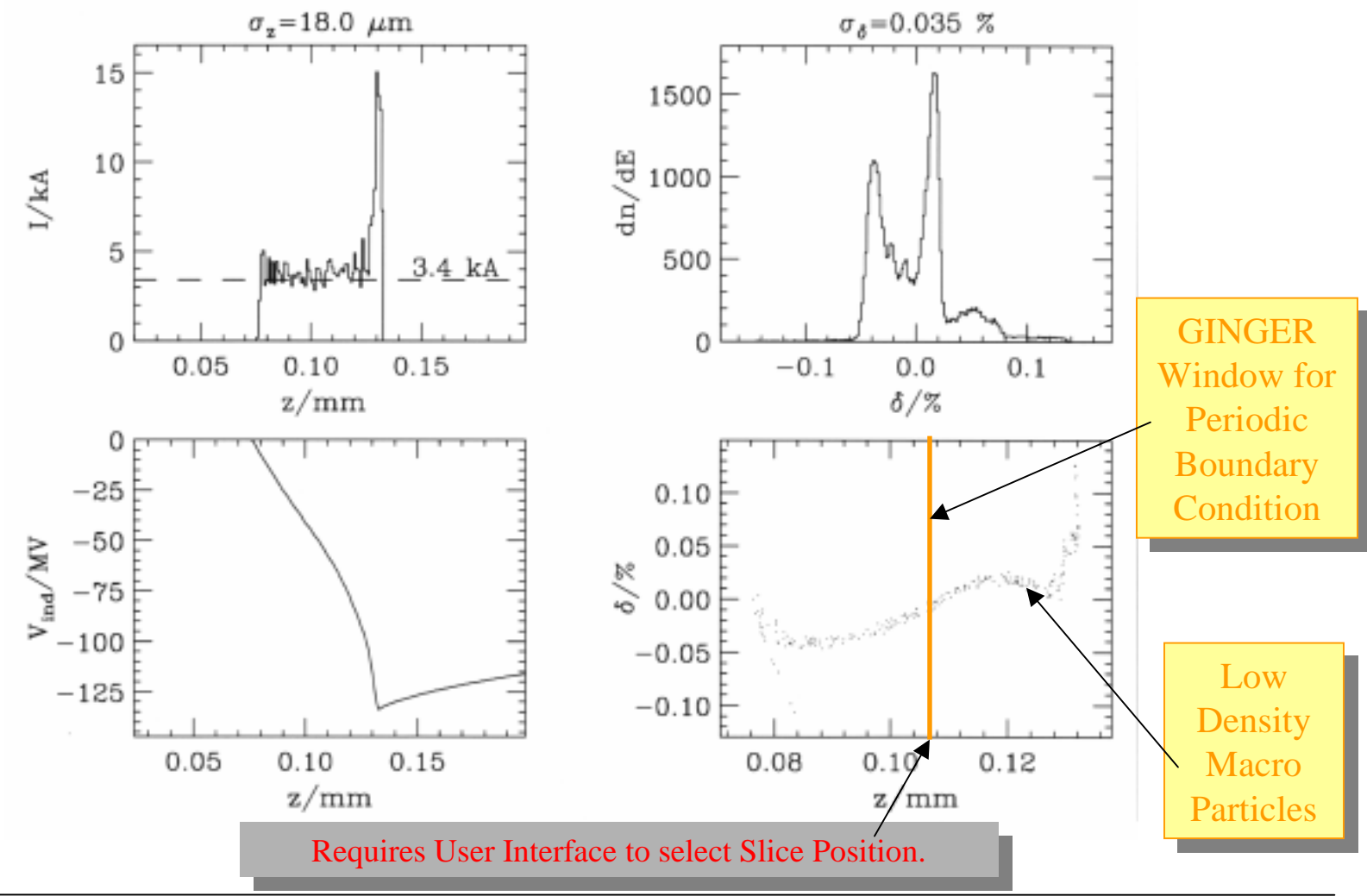
Statistical Analysis

- **Simulation results are dependent on seeding of particle and field distributions.**
- **Limited information obtainable from single run.**
- **Distribution of simulation results relevant.**
- **Many simulation runs required to answer each problem.**
- **Not accessible yet for macro-particle codes due to CPU time requirements.**
- **Can be done with linear codes.**
- **Multiprocessor Farms could be suitable:
 Different seeding on each processor.**

Non-Uniform Particle Seeding

- **Codes generally provide seeding capability for standard distributions:**
 - Gaussian
 - Flat-Top
 - Parabolic (4D Paraboloid)
- **Actual distributions expected to deviate from ideal shapes.**
- **Option for user-provided distributions useful:**
 - Non axis-symmetric beam distributions.
 - Model distributions using combinations of ideal shapes.
 - **Distributions from gun/linac simulations. (Start-to-End Simulations)**

LCLS LINAC Phase Space Distribution



Particle Distributions used in GINGER for LCLS

Macro Particles per Electron Slice:

512 – 4096

Electron Slices per Slippage Length:

128

Mirror Particles for Quiet Start:

÷ 8

Periodic Boundary Condition:

Slice-independent distribution.

Linac Particles per Slice: 64 – 512

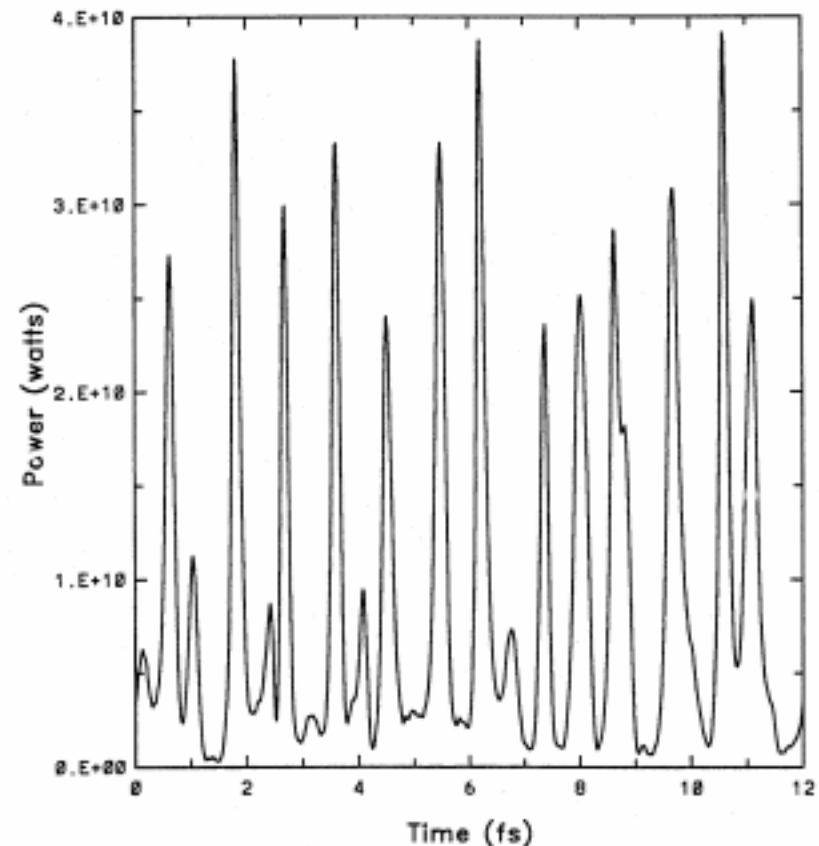
Slippage Lengths for Full Pulse:

160

Required Particles for Full Pulse:

1.3 M – 10 M

Output Field Power vs. Time



Large Periodicity Window ~ 5 % of FWHM LCLS Pulse

Computer Platforms

1980s and early 1990:

First Codes written for **Cray Supercomputers**

- Platform of Choice for Authors
- CPU-Time intensive codes
- Limited general accessibility

Mid 1990s:

Some codes migrated to or written for **Unix Workstation and VMS systems**

- To increase accessibility
- Optimized algorithms

Late 1990s

Migration towards **Personal Computers**

- High performance PCs
- Optimized algorithms
- Wider accessibility

Computer Bench Marks

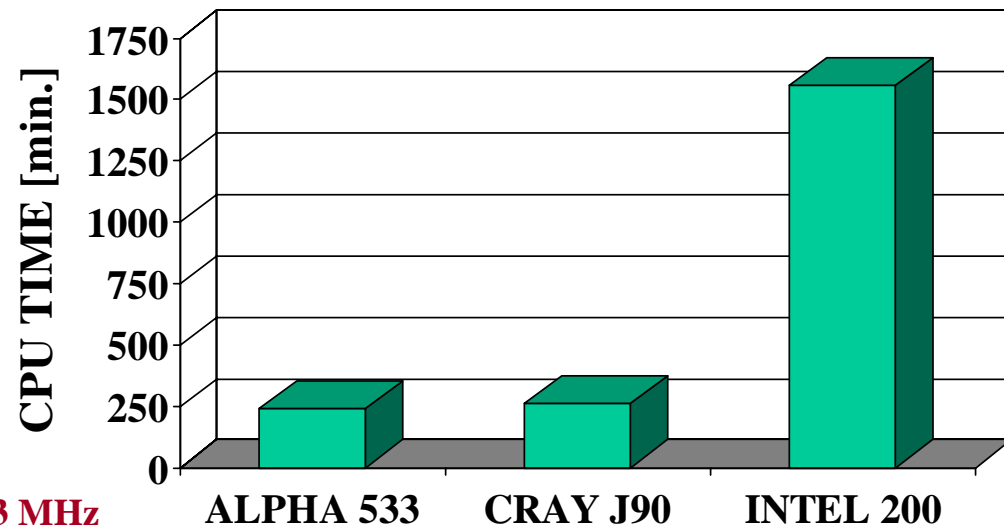
Test Case:

FEL CODE: **GINGER** CASE: **LCLS** WIGGLER LENGTH: **100 m**

SLICES: **768** PARTICLE / SLICE: **512**

MODE: **TIME DEPENDENT / POLYCHROMATIC**

PERIODIC BOUNDARY CONDITIONS



Computer Platforms:

ALPHA 533: ALPHA EV-5, VMS. 533 MHz

CRAY J90: CRAY J90SE. UNICOS 10.0 , 100 MHz

INTEL 200: INTEL Pentium Pro, Windows NT 4.0 , 200 MHz

X-Ray FEL Simulation Code Aspects A

- **Fully Time-Dependent Simulations**
FAST, FELEX, FS1T, GENESIS 1.3, GINGER
- **Full 3 Dimensional Description of Radiation Field and Particle Beam**
FAST, FELEX, FRED3D, GENESIS 1.3, MEDUSA, TDA3D
- **SASE Startup from Noise**
FAST, FELEX, FS1T, GENESIS 1.3, GINGER, RON
- **User Provided Particle Coordinates**
 - **Start-To-End Simulations**
 - **Analysis of Model Distributions****FAST, FELEX, FRED3D, GENESIS 1.3, MEDUSA, TDA3D**
- **Support for Statistical Analysis**
GENESIS 1.3 (for undulator errors)

X-Ray FEL Simulation Code Aspects B

- **Lumped Quadrupole Focusing**
GENESIS 1.3, GINGER*, MEDUSA, TDA3D
- **Support for Undulator Segmentation**
FRED3D, GENESIS 1.3, GINGER*, MEDUSA, RON, TDA3D
- **Magnetic Field Error Analysis**
FRED3D, GENESIS 1.3, MEDUSA, TDA3D, RON
- **Trajectory Control**
FRED3D, GENESIS 1.3, MEDUSA, TDA3D, RON

X-Ray FEL Simulation Code Aspects C

- **Harmonic Tracking**
MEDUSA, NUTMEG
- **Spontaneous Radiation**
 - Average Energy Loss
 - Emittance and Energy Spread Increase**GENESIS 1.3**
- **Wakefield Support**
GENESIS 1.3
- **Radiation Field Tracking between Undulator and Experiment**
FELEX ...

Draft List of LCLS Simulation Issues

- **Systematic Study of the Effects of β -Function Modulations**
- **Complete set of Construction and Alignment Tolerances**
- **Sensitivity to Initial Phase Space Distribution**
- **Effects of Spontaneous Radiation**
- **Effects of Coherent Radiation at Wavelength larger than BL.**
- **Effects of Wall Roughness and Resistive Wall Impedance**
- **Dependence of Error Tolerances on Position along Undulator**
- **Harmonic Tracking**
- **Radiation Field Tracking between Undulator and Experiment**

LCLS Project Codes

The LCLS project needs two FEL simulation codes with sufficient capabilities under full control of the project

Candidate LCLS Project Codes

GENESIS 1.3

GINGER

External contributions using other codes are welcome.

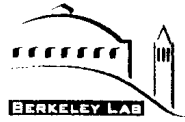
Conclusions

- **The initial basic design of the LCLS has been completed in the LCLS Design Study report.**
- **More detailed study will be done for the CDR.**
- **New experimental results expected starting in next 12 months.**
- **A number of FEL simulation codes exists. Not all necessary features are included.**
- **Code upgrade program is underway and will receive guidance from the workshop.**
- **Workshop will focus around the undulator, i.e., from the linac phase space distribution to the description of the radiation field out of the linac.**

WORKSHOP PRESENTATIONS III

Remarks on SASE Fluctuations and Undulator Errors

K.-J. Kim



Solution of 1-D FEL Theory

◆ Frequency domain:

$$\tilde{E}_\omega(z) = G_\omega(z) E_\omega(0)$$

$$\left(\rightarrow E(\xi, 0) = \sum_i \delta(\xi - \xi_i) \right)$$

$$E_\omega(0) = \sum_{i=1}^{Ne} e^{i2\pi\omega\xi_i} e^{i\theta_{i0}}$$

$$G_\omega(z) = e^{\sqrt{3}\rho k_u z} e^{-i\left(\frac{2}{3}\frac{\Delta\omega}{\omega_0} + \rho\right)k_u z} e^{-\frac{(\Delta\omega)^2}{4\sigma_\omega^2}\left(1 + \frac{i}{\sqrt{3}}\right)}$$

↑
amplification

$$\sigma_\omega \approx \omega_0 \sqrt{\frac{\rho}{(z/\lambda u)}} \rightarrow \text{gain narrowing}$$

$$P_\omega = \langle |E_\omega|^2 \rangle = |G_\omega(z)|^2 \left| \sum e^{i\theta_{i0}} \right|^2$$

\downarrow $e^{z/L_g S(\omega)}$ \downarrow Ne



Solution of 1-D FEL Theory ($\Delta\gamma=0$)

- ◆ Time Domain: Super position of randomly spaced wavetrains

$$E(z,t) = \frac{1}{\sqrt{z}} e^{\sqrt{3}\rho k_{\perp} u z} \sum_{i=1}^{N_e} e^{i\omega_0 \left[t - \frac{z}{c}(1-\rho\Delta\beta) + \xi_i^0 \right]}$$

↑ amplification
↑ reduction in phase velocity

\hookrightarrow random position of wave packet.

$$e^{-\frac{\left(t - \frac{z}{c} \left(1 + \frac{2}{3} \Delta\beta \right) + \xi_i^0 \right)^2}{4\sigma_{\tau}^2} - \frac{3}{4} \left(1 - \frac{i}{\sqrt{3}} \right) - i\omega_0 \xi_i^0}$$

↙ reduction in group velocity [slower than c by $\frac{2}{3}(c - v_{\parallel})$]

$$\Delta\beta = 1 - \beta_{\parallel} \qquad \sigma_{\tau} = \frac{1}{2\sigma_{\omega}} = \frac{1}{2\omega_0} \sqrt{\frac{z/\lambda u}{\rho}}$$

∴ Statistics of $\tilde{E}_\omega(z)$ is the same as that of

$$\tilde{E}_\omega(0) = \sum_{k=1}^{N_e} e^{i\omega t_k}$$

= sum of a large number of random phase

→ Invoke Central Limit Theorem

→ probability distribution of $E_\omega(0)$ is Gaussian:

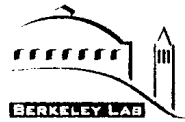
$$E_\omega = X + iY$$

$$P(X, Y) dx dy = e^{-\frac{X^2 + Y^2}{A}} dx dy$$

→ probability of $I_\omega = |E_\omega|^2 = X^2 + Y^2$ $dx dy = \frac{1}{2} d|E_\omega|^2 d\phi$

$$P(I_\omega) dI_\omega = e^{-\frac{I_\omega}{A}} dI_\omega$$

"Inverse exponential distribution"



Solution of 1-D FEL Theory

◆ Frequency domain:

$$\tilde{E}_\omega(z) = G_\omega(z) E_\omega(0)$$

$$\left(\rightarrow E(\xi, 0) = \sum_i \delta(\xi - \xi_i) \right)$$

$$E_\omega(0) = \sum_{i=1}^{Ne} e^{i2\pi\omega\zeta_i^0}$$

$$G_\omega(z) = e^{\sqrt{3}\rho k_u z} e^{-i\left(\frac{2}{3}\frac{\Delta\omega}{\omega_0} + \rho\right)k_u z} e^{-\frac{(\Delta\omega)^2}{4\sigma_\omega^2}\left(1 + \frac{i}{\sqrt{3}}\right)}$$

↑
amplification

$$\sigma_\omega \approx \omega_0 \sqrt{\frac{\rho}{(z/\lambda u)}} \rightarrow \text{gain narrowing}$$

$$P_\omega = \langle |E_\omega|^2 \rangle = |G_\omega(z)|^2 \underbrace{|\sum e^{i\theta_i}|^2}_{Ne}$$

\downarrow $e^{z/Lg} S(\omega)$

$$\bullet \quad \overline{I_\omega} = \int I_\omega P(I_\omega) dI_\omega = A$$

$$\overline{I_\omega^2} = \int I_\omega^2 \quad " \quad = 2 \overline{I_\omega}^2$$

\therefore Variance

$$\Delta I_\omega = \sqrt{\overline{I_\omega^2} - \overline{I_\omega}^2} = \overline{I_\omega}$$

= the same as average

\rightarrow 100% fluctuation

1-D

$$E_\omega(z) = \oint \frac{d\mu}{2\pi i} \frac{e^{-2i k_u z p \mu}}{D(\mu, \Delta\nu)} \left[E_\omega(0) + d \int d\eta \frac{\delta F(\omega, \eta; 0)}{\mu + \eta/p} \right]$$

$$\Delta\nu = \frac{\omega - \omega_0}{\omega_0} \quad \downarrow \quad \sum e^{i\theta_i}$$

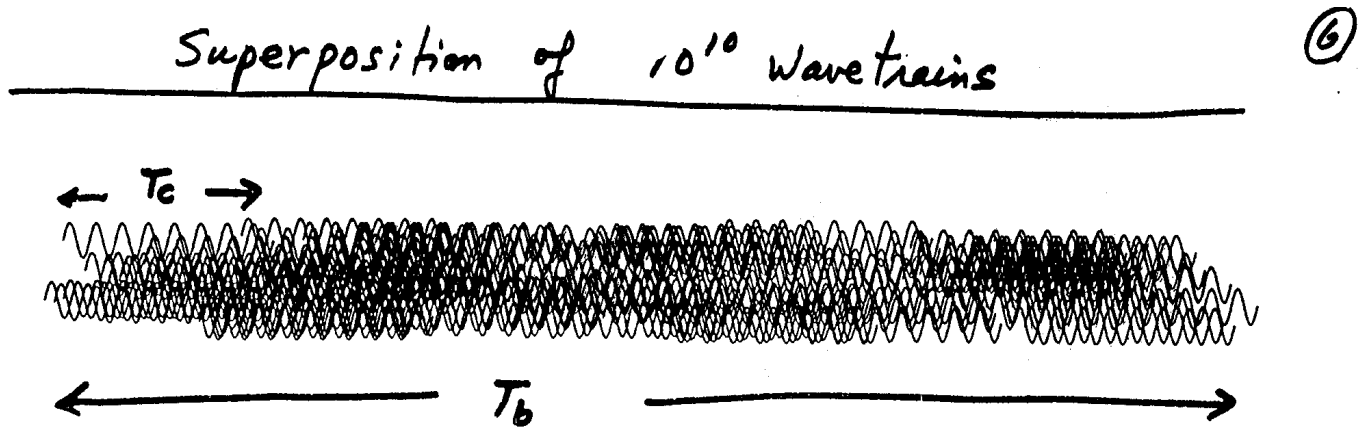
$$D(\mu, \Delta\nu) = \mu + \frac{\Delta\nu}{2\rho} + \int d\eta \frac{dV/d\eta}{\mu + \eta/p}$$

for $V = \delta(\eta)$ (ie $\frac{\Delta E}{E} \ll \rho$)

$$\boxed{D = \mu + \frac{\Delta\nu}{2\rho} + \frac{1}{\mu^2} = 0} \quad (\text{cubic eq.})$$

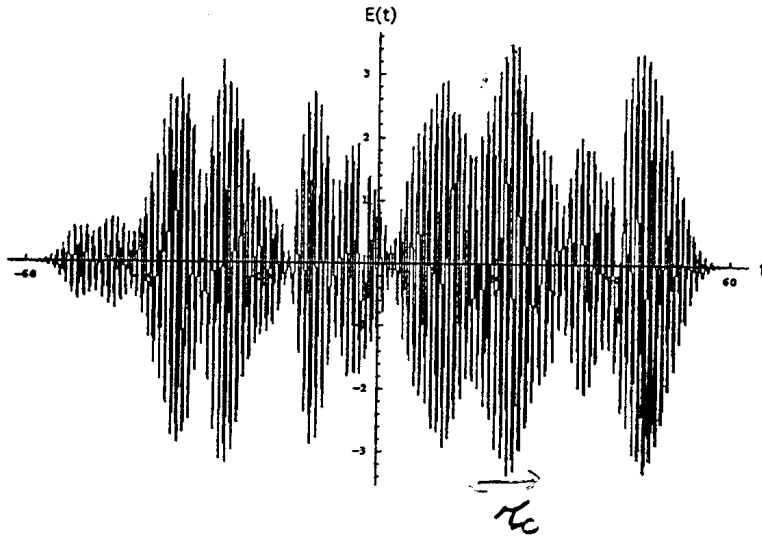
$$\rho = \left(\frac{e K^2 [JJ]^2 z_0 j}{32 \gamma_0^3 m c^2 k_u^2} \right)^{1/3} : \text{FEL scaling parameter}$$

$$P(\omega) \propto |E(\omega)|^2 \quad \left| \sum_i e^{i\theta_i} \right|^2 = N_c$$

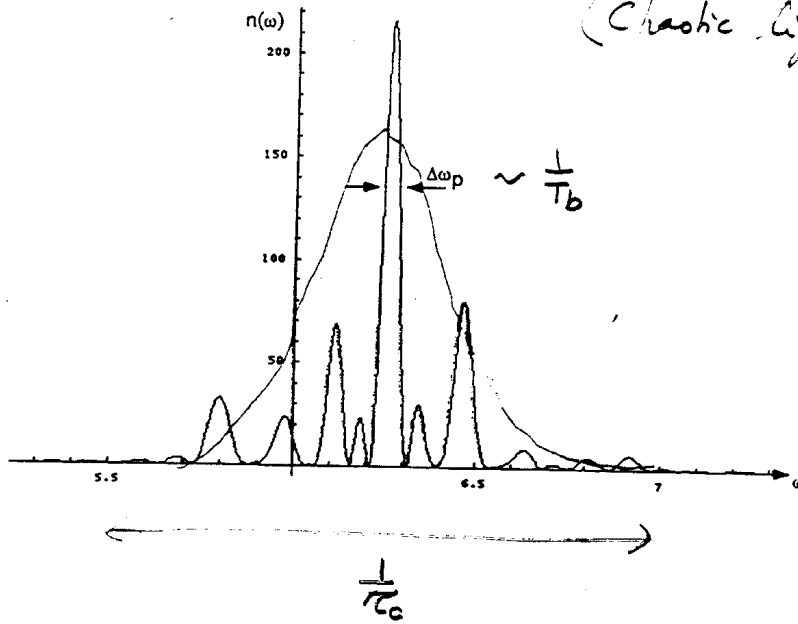


- How many modes ?
- # of photons ?

9



100% fluctuation
(Chaotic light)



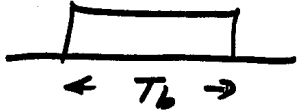
- So far we have considered the case where ω is precisely known \rightarrow Monochromator of infinite resolution.
(Also the case where t is well-defined)
- Now consider the statistics of ω -integrated intensity (look at the whole pulse)

$$W = \int d\omega I\omega$$

- There are $M \simeq \frac{\text{SASE bandwidth}}{\text{Spike bandwidth}} = \frac{\sigma_\omega}{(1/T_b)} = T_b \sigma_\omega$
"modes"

The fluctuation will be reduced by a factor \sqrt{M}

$$\Delta W = \overline{W} \times \frac{1}{\sqrt{M}}$$

- Precise calculation for "Top hat" bunch 

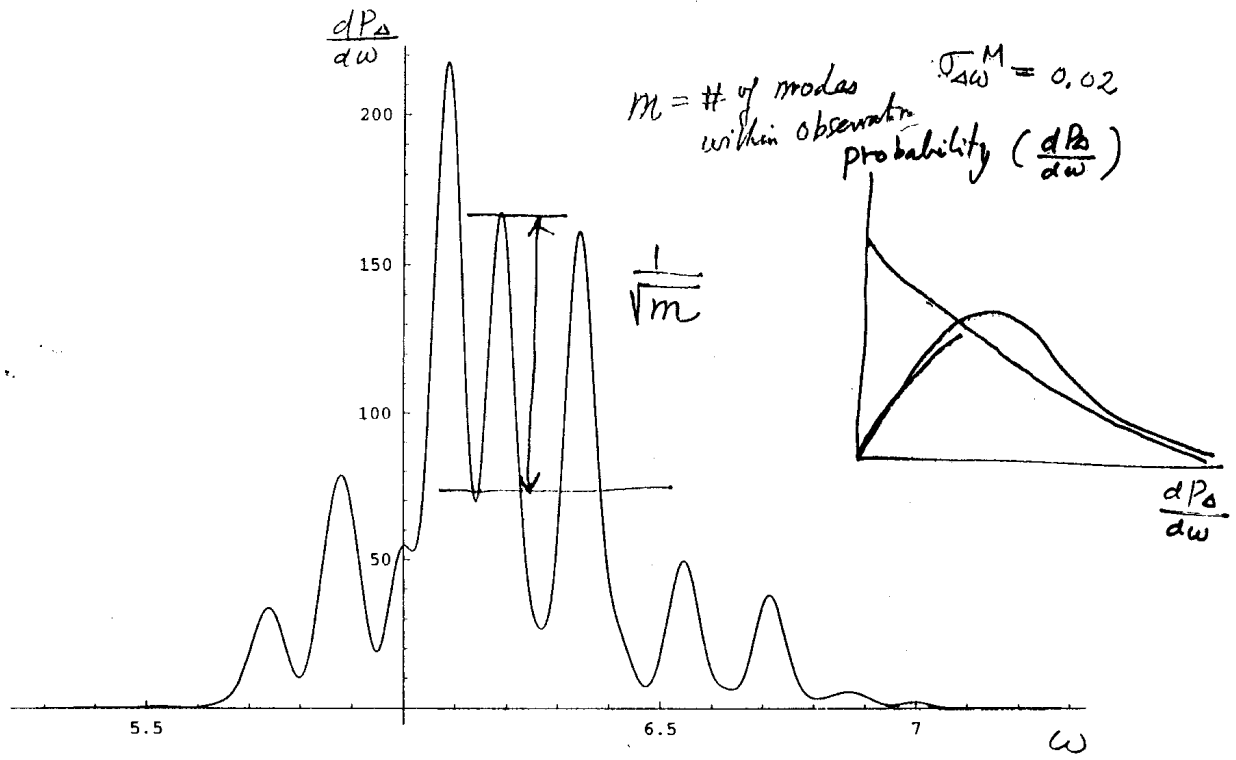
$$M = \frac{\sigma_w T}{\sqrt{\pi}} \quad (\text{Saldin, Schneidmiller \& Yurkov})$$

- Probability of W
 - \simeq probability of $W = I_1 + \dots + I_M$
 - I_i each given by inverse exponential
 - \rightarrow "Gamma" distribution

- Can generalize to partial filtering case.

⑧

random-test



- The same result can be obtained in t -domain:

$$M = \frac{\text{bunch length}}{\text{coherence length}} = \frac{l}{l_c} = \frac{T}{(1/\omega)} = \sigma \omega T$$

- Note that l_c is not "the cooperation length"!

- Quantum effect

$$(\Delta n)^2 = \frac{\bar{n}^2}{M} + \bar{n}$$

\hookrightarrow classical \hookrightarrow quantum (coherent state)

$$= \frac{\bar{n}^2}{M} \left(1 + \frac{1}{\delta} \right), \quad \delta = \frac{\bar{n}}{M}$$

$=$ # of photons/mode
 $=$ "degeneracy number"
 $\gg 1$ for SASE.

Transverse effect

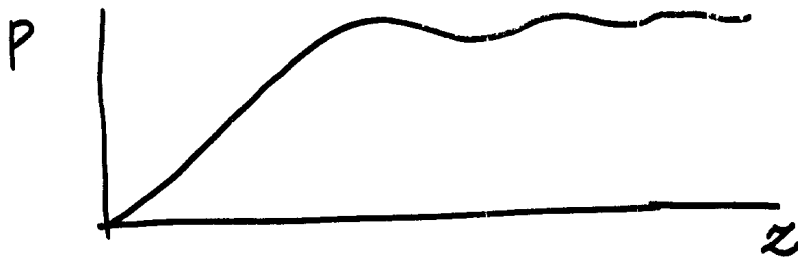
- If SASE is dominated by a single transverse mode then $M_{\text{trans}} = 1$.

(But, see Yu & Krinsky)

Two Undulators Scheme to reduce B.W.
(Feldhaus, Saldin, ...)



→ only works because U_2 operates well into the non-linear regime



Undulator Errors

- Trajectory error \rightarrow phase error $\delta\phi(\tau)$
$$\frac{d\delta\phi(\tau)}{d\tau} = \text{effective detuning}$$
- 1-D analysis with random effective detuning by
(YKGVZ)
- Reduction in intensity $e^{-\frac{2}{9}W\tau}$
$$W = \frac{1}{\tau} \langle (\delta\phi(\tau))^2 \rangle, \quad \tau = N/N_G$$
- Relate W to trajectory wander
 \rightarrow works well for long undulators with
periodic steering stations.

2. Effect of Wiggler Errors

(Yu, Krinsky, Gluckstern, van Zeijts
PRA, 45, 1163 (1992))



$$P = P_0 e^{-\left(\frac{x_{rms}}{x_{tol}}\right)^4}$$

$$x_{tol} = \begin{cases} \frac{L_s}{L_G} \times 0.145 \sqrt{\lambda_s L_G} \left(\frac{L_G}{\delta}\right)^{\frac{1}{4}} & (L_s \gg L_G) \\ \left(\frac{L_s}{L_G}\right)^{\frac{3}{4}} \times 0.266 \sqrt{\lambda_s L_G} \left(\frac{L_G}{\delta}\right)^{\frac{1}{4}} & (L_s \ll L_G) \end{cases}$$

L_s correction station spacing

δ wiggler distance

- For well-optimized undulators with slits, the rms phase error (rather than derivative) is kept under control

$$\sigma_\phi^2 = \frac{1}{L} \int \langle (\delta\phi(z))^2 \rangle dz$$

→ Reduction $e^{-\frac{\sigma_\phi^2}{\sqrt{3}} z}$

→ negligible for most cases

- True 3-D theory is not worked out yet.

WORKSHOP PRESENTATIONS IV

3D Analysis of Nonlinear Harmonic Generation

Z. Huang

Present at the X-ray FEL Theory and Simulation Workshop
SLAC, Stanford (Sep. 23-24, 1999)

3D Analysis of Nonlinear Harmonic Generation

Zhirong Huang
APS/ANL

in collaboration with Kwang-Je Kim

ADVANCED PHOTON SOURCE

Introduction

- Amplified harmonic emission in a planar wiggler (Colson)
SASE process is heavily in favor of the fundamental frequency
- A 1D model (Bonifacio *et al.*) and a 3D simulation (Freund *et al.*)
==> strong bunching at the fundamental can drive substantial
harmonic bunching and sizable harmonic power
- Nonlinear harmonic interaction: *
growth rate, transverse profile, bandwidth
- Third harmonic calculation with LCLS parameter:
power level ~ 0.7 % of the fundamental power

* Z. Huang, K.-J. Kim, to publish in FEL'99 proceedings

9/21/99

Zhirong Huang (zrh@aps.anl.gov)

1

ADVANCED PHOTON SOURCE

Harmonic Emission and Bunching

- In the electron comoving frame

$$8 \longrightarrow E \propto \sum_h a_h(\mathbf{r}, z) e^{ihk_1(z-ct)}$$

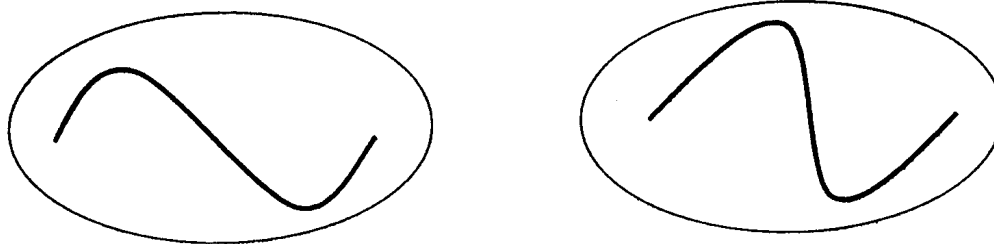
$h=1,3,5,\dots$ is the (odd) harmonic number

a_h is the scaled harmonic field ($a_{-h}=a_h^*$ to include c. c. terms)

- Before FEL saturation, we assume

$$\dots |a_h| < |a_{h-2}| < \dots < |a_3| < |a_1| < 1$$

- Harmonics are not independent, in the ponderomotive potential:



9/21/99

Zhirong Huang (zrh@aps.anl.gov)

2

ADVANCED PHOTON SOURCE

Harmonic Interaction

- Perturbation to the Vlasov equation to the h^{th} order \Rightarrow

$$\left(\frac{\partial}{\partial \bar{z}} + \frac{\nabla^2}{2ih} \right) a_h = \underbrace{a_h \text{ term}}_{\text{linear bunching}} + \underbrace{\sum_{h_1 + \dots + h_m = h} a_{h_1} \times \dots \times a_{h_m}}_{\text{nonlinear harmonic interaction}} \text{ term}$$

- In general

$$a_h = \underbrace{a_h^L}_{\text{SASE}} + \underbrace{a_h^{NL}}_{\text{Nonlinear Harmonic Generation}}$$

- Each a_h^L has a dominant mode with the largest growth rate λ_h
- SASE is predominantly the growth of the fundamental radiation
 $\text{Re}(\lambda_1) > \text{Re}(\lambda_3) > \text{Re}(\lambda_5) > \dots$
- At the fundamental, nonlinear term is much weaker until saturation
- At higher harmonics, nonlinear process may become dominant

ADVANCED PHOTON SOURCE

Nonlinear Harmonic Generation

- At the third, a_3^{NL} is dominated by a_1^3 term

$$a_3^{NL} \sim a_1^3 \sim \left(\frac{1}{\sqrt{N_c}} e^{\lambda_1 z} \right)^3 \quad \text{and} \quad a_3^L \sim \frac{1}{\sqrt{N_c}} e^{\lambda_3 z} \quad (N_c \text{ noise})$$

$\implies a_3^{NL} \gg a_3^L$ at some stage of the exponential gain regime

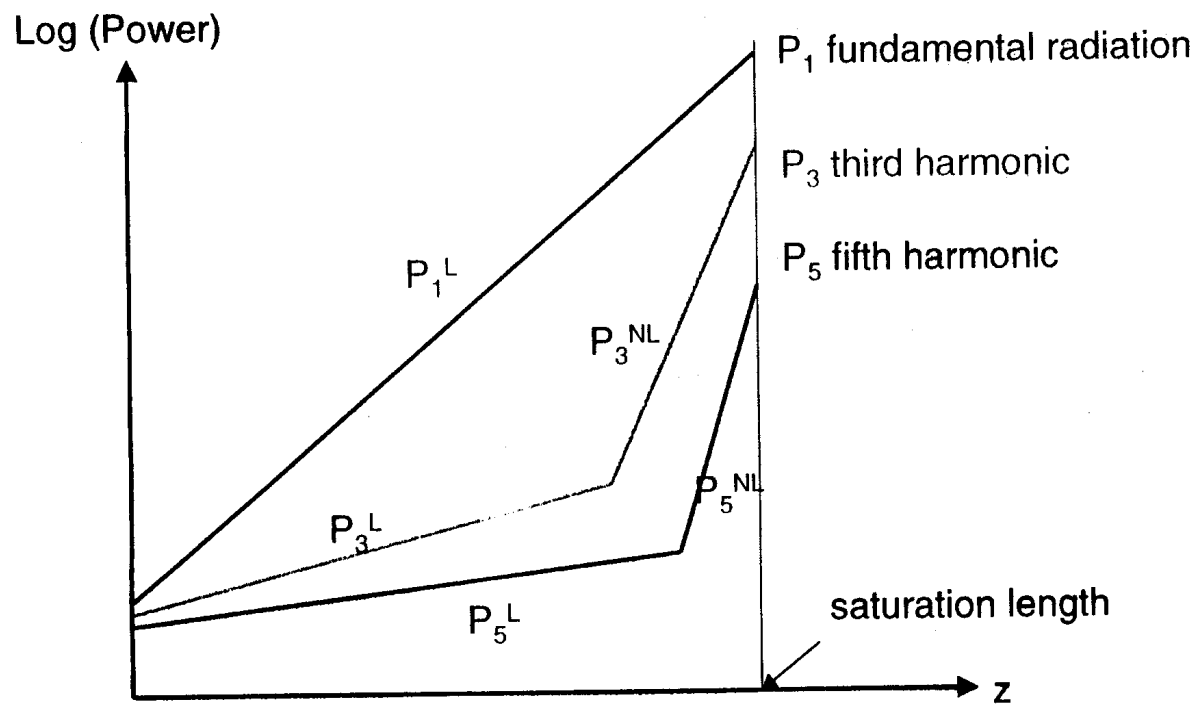
- At the fifth, a_5^{NL} is dominated by $a_1^2 a_3$ and a_1^5
 $\implies a_5^{NL} \sim a_1^5$ can be larger than a_5^L before saturation
- In general, $a_h^{NL} \sim a_1^h$, with a growth rate $h\lambda_1$ (Bonifacio..., Freund...)

- The transverse profiles of the nonlinear harmonics are completely determined by the fundamental radiation profile (mode)

- Bandwidth of $a_h^{NL} = \frac{1}{h} \times$ Bandwidth of a_1

- Coherent length of a_h^{NL} is the same as the fundamental

Evolution of Harmonic Radiation



9/21/99

Zhirong Huang (zrh@aps.anl.gov)

5

ADVANCED PHOTON SOURCE

Third Harmonic Radiation

$$\bullet \left(\frac{\partial}{\partial \bar{z}} + \frac{\nabla^2}{6i} \right) a_3^{NL} = \left(\frac{K_3}{K_1} \right)^2 \int d^2 \bar{p} \int d\eta \left[\int d\bar{s}_1 e^{i3\varphi\tau_1} a_3^{NL}(\mathbf{r}_1, s_1) \frac{\partial f_0}{\partial \eta} + \int d\bar{s}_1 e^{i\varphi\tau_1} a_1(\bar{\mathbf{r}}_1, \bar{s}_1) \frac{\partial}{\partial \eta} \int d\bar{s}_2 e^{i\varphi\tau_2} a_1(\bar{\mathbf{r}}_2, \bar{s}_2) \frac{\partial}{\partial \eta} \int d\bar{s}_3 e^{i\varphi\tau_3} a_1(\bar{\mathbf{r}}_3, \bar{s}_3) \frac{\partial f_0}{\partial \eta} \right]$$

$$\text{where } \varphi = \bar{\eta} - \frac{(\bar{p}^2 + k_\beta^2 r^2)}{2}$$

- Assume the initial coasting beam is Gaussian in transverse coordinates and in energy variables
- Assume a Gaussian mode for the transverse profile of the fundamental radiation
- Calculation takes into account all 3D effects such as emittance, energy spread, diffraction, and guiding

ADVANCED PHOTON SOURCE

Numerical Examples

- For APS LEUTL FEL at 530 nm, the third harmonic power

$$\frac{P_3^{NL}}{\rho P_{\text{beam}}} = 0.014 \left(\frac{P_1}{\rho P_{\text{beam}}} \right)^3 \quad (P_{\text{beam}} \text{ is the beam power})$$

==> right before saturation, $P_3 \sim 1\% P_1$

- Agrees well with MEDUSA simulation on the power level

- For LCLS (1.5 Å): power at the third harmonic (0.5 Å)

$$\frac{P_3^{NL}}{\rho P_{\text{beam}}} = 0.044 \left(\frac{P_1}{\rho P_{\text{beam}}} \right)^3$$

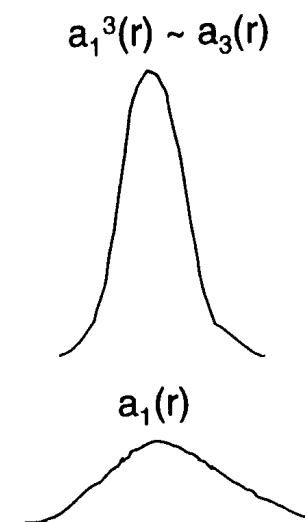
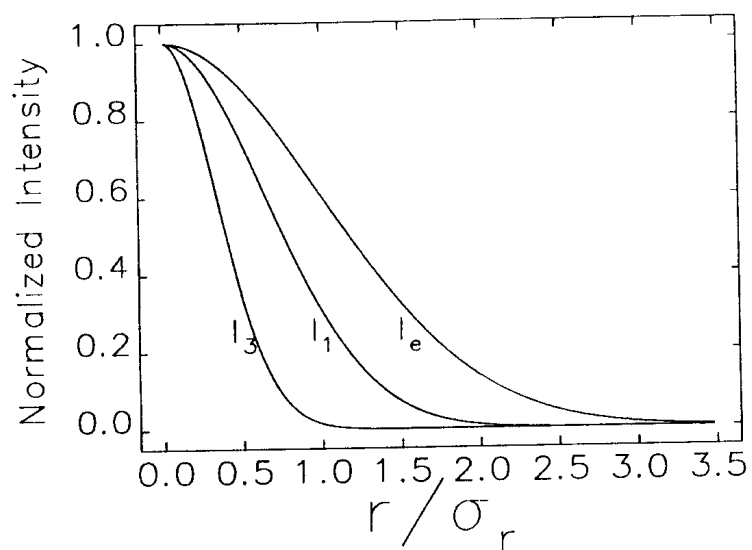
==> right before saturation, $P_3 \sim 0.7\% P_1$

- The brightness is at the third harmonic is 7% of the fundamental

ADVANCED PHOTON SOURCE

Transverse Profile

- Numerical calculation of the third harmonic intensity for LCLS



- The optical mode of the third harmonic is also guided, with a narrower waist than the fundamental due to the nonlinear mechanism

9/21/99

Zhirong Huang (zrh@aps.anl.gov)

8

ADVANCED PHOTON SOURCE

Conclusions

- Shorter coherent wavelength , significant power
- Nonlinear harmonic interaction exists in any high-gain FEL, not only in SASE FELs
- Plan to measure the third harmonic (at 1.7 μm) of the HGHG experiment (S. Biedron *et al.*) to verify the theoretical prediction
- In addition to other harmonic generation schemes (Bonifacio, Yu), the nonlinear harmonic interaction could be a promising mechanism to generate coherent radiation at short wavelengths

WORKSHOP PRESENTATIONS V

Exact and Variational Solutions of 3D Eigenmodes for High Gain FELs

M. Xie

Exact and Variational Solutions of 3D Eigenmodes in High Gain FELs

Ming Xie

Lawrence Berkeley National Laboratory, Berkeley, California 94720, USA

Abstract

Exact solution and variational approximation of eigenmodes in high gain FELs are presented. These eigenmodes specify transverse profiles and exponential growth rates of the laser field before saturation. They are self-consistent solutions of coupled Maxwell-Vlasov equations describing FEL interaction taking into account the effects due to energy spread, emittance and betatron oscillations of the electron beam, as well as diffraction and optical guiding of the laser field. A new formalism of scaling is introduced and based on which solutions in various limiting cases are discussed. In addition, a fitting formula is obtained from interpolating the variational solution for quick calculation of exponential growth rate of the fundamental mode.

Key words: 3D, High Gain FEL theory; Optical Guiding; SASE

1 Introduction

The main objective of this article is the determination of exponential growing modes (eigenmodes) in high gain FELs, taking into account the effects due to energy spread, emittance and betatron oscillations of the electron beam, as well as diffraction and optical guiding of the laser field. To deal with all these effects simultaneously, the most effective approach for analytical investigation is through coupled Maxwell-Vlasov equations. An equation satisfied by the modes of laser field was first derived by Kim [1], but without providing a solution. The first approximate solution of the equation was obtained by Yu et al. [2] for the fundamental mode, using a variational technique originally

¹ Work supported by the U.S. Department of Energy under contract No.DE-AC03-76SF00098.

² mailing address: Ming Xie, LBNL, MS.71-259, Berkeley, CA94720, USA; tel: 510-486-5616; fax: 510-486-6485; e-mail: mingxie@lbl.gov

introduced by Xie et al. [3]. The solution by Yu et al. assumes a waterbag model for unperturbed electron distribution in transverse phase space. Later, a special 2D case (sheet beam) of Gaussian model was considered by Hafizi et al. [4] for the fundamental mode, using also the variational technique. Taking a different approach from that of Kim [1] in handling the coupled Maxwell-Vlasov equations, Chin et al. [5] derived an equation satisfied by the mode of perturbed distribution function and obtained another approximate solution for the fundamental mode. However, this solution is known [5] to have a significant systematic error when approaching to the 1D limit.

In this article, we present the first exact solutions of 3D FEL eigenmodes, both fundamental and higher order. The unperturbed electron distribution is assumed to be of Gaussian shape in four dimensional transverse phase space and in energy variable, but uniform in longitudinal coordinate. For the fundamental mode, a variational solution is derived and from this solution a fitting formula is generated for the growth rate. A new formalism of scaling is introduced and based on which solutions are presented and discussed in various limiting cases.

2 Eigenmode Equation

The eigenmodes of laser field independent of initial condition can be determined by the following equation [1]

$$\left(\frac{\partial^2}{\partial \mathbf{x}^2} + \frac{ik_r}{L_{1d}}q\right)E(\mathbf{x}) = \frac{hk_r}{4L_{1d}^3} \int_{-\infty}^{\infty} d^2\mathbf{p} \int_{-\infty}^{\infty} d\eta \int_{-\infty}^0 ds s e^{\Phi} f_{\parallel}(\eta) f_{\perp}(\mathbf{x}^2 + \mathbf{p}^2/k_{\beta}^2) E[\mathbf{x} \cos(k_{\beta}s) + (\mathbf{p}/k_{\beta}) \sin(k_{\beta}s)], \quad (1)$$

where

$$\Phi = [q/2L_{1d} + i2k_w\eta - ik_w\Delta\nu - ik_r k_{\beta}^2(\mathbf{x}^2 + \mathbf{p}^2/k_{\beta}^2)/2]s,$$

$k_r = 2\gamma_0^2 k_w / (1 + a_w^2)$, $\eta = (\gamma - \gamma_0) / \gamma_0$, $\Delta\nu = (\omega - \omega_r) / \omega_r$ and $h = (2/\sqrt{3})^3$. The transverse profile of the slowly varying monochromatic laser field, $E(\mathbf{x})$, is defined by $\mathcal{E}(\mathbf{x}, z, t) = E(\mathbf{x}) \exp[qz/2L_{1d} + i(kz - \omega t)]$. To comply with a new scaling to be introduced later, here the complex exponential growth rate (eigenvalue), q , is scaled by the 1D power gain length, $L_{1d} = 1/2\sqrt{3}k_w\rho$, where $\rho = \sqrt[3]{\pi r_e n_0 a_w^2 f_B^2 / 4k_w^2 \gamma_0^3}$ is the Pierce parameter, $f_B = 1$ for helical wiggler and $f_B = J_0[a_w^2/2(1 + a_w^2)] - J_1[a_w^2/2(1 + a_w^2)]$ for planar wiggler, $a_w = 0.934\lambda_w[\text{cm}]B_{rms}[\text{T}]$, n_0 is the peak electron density on the axis, and r_e is the classical radius of electron. It is noted that the term proportional to \mathbf{x}^2 was

absent from the phase factor Φ in the original equation derived by Kim [1] and it was corrected later by Yu et al. [2].

The focusing system for the confinement of electron beam in a wiggler is assumed to have a transverse gradient invariant along the beam axis. It is characterized by a constant beta function β_f in both transverse planes. Thus betatron motion is governed by $\mathbf{p} = d\mathbf{x}/dz, d\mathbf{p}/dz = -k_\beta^2\mathbf{x}$. In particular for natural wiggler focusing, $k_\beta = k_w a_w / \sqrt{2}\gamma_0$. Respectively, the unperturbed longitudinal and transverse distribution functions are normalized according to $\int_{-\infty}^{\infty} d\eta f_{\parallel}(\eta) = 1$ and $u(\mathbf{x} = 0) = 1$, where $u(\mathbf{x}) = \int_{-\infty}^{\infty} d^2\mathbf{p} f_{\perp}(\mathbf{x}^2 + \mathbf{p}^2/k_\beta^2)$.

For convenience, Eq. (1) can be reduced to [2]

$$\left(\frac{\partial^2}{\partial \mathbf{x}^2} + \frac{ik_r}{L_{1d}} q \right) E(\mathbf{x}) = \int_{-\infty}^{\infty} d^2\mathbf{x}' \Gamma(\mathbf{x}, \mathbf{x}') E(\mathbf{x}'), \quad (2)$$

where

$$\Gamma(\mathbf{x}, \mathbf{x}') = \int_{-\infty}^0 ds \int_{-\infty}^{\infty} d\eta \frac{hk_r k_\beta^2 s}{4L_{1d}^3 \sin^2(k_\beta s)} e^{\Phi} f_{\parallel}(\eta) f_{\perp}(\chi),$$

$$\chi \equiv \mathbf{x}^2 + \mathbf{p}^2/k_\beta^2 = \frac{\mathbf{x}^2 + \mathbf{x}'^2 - 2\mathbf{x} \cdot \mathbf{x}' \cos(k_\beta s)}{\sin^2(k_\beta s)}.$$

3 Scaling and Limiting Cases

We now specify the unperturbed electron distribution as:

$$f_{\parallel}(\eta) = \frac{1}{\sqrt{2\pi}\sigma_\eta} e^{-\eta^2/2\sigma_\eta^2}, \quad (3)$$

$$f_{\perp}(\mathbf{x}^2 + \mathbf{p}^2/k_\beta^2) = \frac{1}{2\pi\sigma_x^2 k_\beta^2} e^{-(\mathbf{x}^2 + \mathbf{p}^2/k_\beta^2)/2\sigma_x^2}. \quad (4)$$

Here the transverse distribution is matched to the betatron focusing channel, giving rise to a constant beam size, σ_x . With Eqs.(3,4) and $\mathbf{X} = \mathbf{x}/\sigma_x, \tau = s/2L_{1d}$, Eq.(2) can be expressed in a scaled form

$$\left(2\eta_d \frac{\partial^2}{\partial \mathbf{X}^2} + iq \right) E(\mathbf{X}) = \int_{-\infty}^{\infty} d^2\mathbf{X}' \Pi(\mathbf{X}, \mathbf{X}') E(\mathbf{X}'), \quad (5)$$

where

$$\Pi(\mathbf{X}, \mathbf{X}') = \int_{-\infty}^0 \frac{\tau d\tau h}{2\pi \sin^2(2\sqrt{\eta_d \eta_\epsilon \tau})} e^\Psi,$$

$$\Psi = (q - i\eta_\omega)\tau - 2\eta_\gamma^2 \tau^2 - \frac{(1 + i\eta_\epsilon \tau)[\mathbf{X}^2 + \mathbf{X}'^2 - 2\mathbf{X} \cdot \mathbf{X}' \cos(2\sqrt{\eta_d \eta_\epsilon \tau})]}{2 \sin^2(2\sqrt{\eta_d \eta_\epsilon \tau})}.$$

There are four scaling parameters [6] in Eq.(5): $\eta_d = 1/F_d$ is a diffraction parameter, where $F_d = 2k_r \sigma_x^2 / L_{1d}$ is the Fresnel number of electron beam corresponding to a length scale of L_{1d} ; $\eta_\epsilon = 4\pi (L_{1d}/\lambda_\beta) k_r \epsilon$ and $\eta_\gamma = 4\pi (L_{1d}/\lambda_w) \sigma_\eta$ characterize the effective spread in longitudinal velocity due to emittance and betatron focusing and due to energy spread, respectively, where $\lambda_\beta = 2\pi \beta_f$, $\epsilon = k_\beta \sigma_x^2$ is rms beam emittance and σ_η is relative rms energy spread; finally, $\eta_\omega = 4\pi (L_{1d}/\lambda_w) \Delta\nu$ is a frequency detuning parameter. The Pierce parameter can now be expressed more conveniently as $\rho = \sqrt[3]{(I/I_A)(\lambda_w a_w f_B / 2\pi \sigma_x)^2 (1/2\gamma_0)^3}$, where I is the peak beam current and $I_A = 17.05$ kA is the Alfvén current.

It has been shown [2,7,8] that FEL equations can be scaled with a minimum number of scaling parameters and in different ways. The scaling formalism introduced here, termed L_{1d} scaling, differs from the previous ones in the following aspects. First, parameter η_ϵ is chosen to emphasize the combined effect of emittance and betatron focusing, rather than using $k_r \epsilon$ or $k_\beta/k_w \rho$ separately. Second, by employing the scaling with L_{1d} , rather than with ρ or D , the formulation is made more transparent and elegant, and its presentation and elucidation more convenient, as it will become evident later on.

In the 1D limit without diffraction, $\eta_d = 0$, all modes are degenerate with the same eigenvalue and Eq.(5) becomes

$$q + ih \int_{-\infty}^0 \frac{\tau d\tau e^{(q - i\eta_\omega)\tau - 2\eta_\gamma^2 \tau^2}}{1 + i\eta_\epsilon \tau} = 0. \quad (6)$$

Further, if $\eta_\epsilon = 0$ and $\eta_\gamma = 0$, then, $q(q - i\eta_\omega)^2 - ih = 0$. This is the well-known 1D cubic equation [8] which admits root with the highest growth rate, $q = 1 + i/\sqrt{3}$, at $\eta_\omega = 0$. From now on we will refer the origin, $\{0, 0, 0, 0\}$, in the scaled parameter space $\{\eta_d, \eta_\epsilon, \eta_\gamma, \eta_\omega\}$ as the 1D, ideal beam limit. In this limit, the scaled growth rate, $q_r \equiv L_{1d}/L_g$, reaches the absolute maximum of unity, where L_g is the power gain length by definition.

Another limiting case is known as the parallel beam limit, which can be obtained from Eq.(5) with $\eta_\epsilon = 0$

$$\left[2\eta_d \frac{\partial^2}{\partial \mathbf{X}^2} + iq - h e^{-\mathbf{X}^2/2} \int_{-\infty}^0 \tau d\tau e^{(q-i\eta_\omega)\tau - 2\eta_\gamma^2 \tau^2} \right] E(\mathbf{X}) = 0. \quad (7)$$

Further, if $\eta_\gamma = 0$, then for axially symmetric modes

$$\left[2\eta_d \frac{d}{RdR} \left(R \frac{d}{dR} \right) + iq + \frac{h}{(q-i\eta_\omega)^2} e^{-R^2/2} \right] E(R) = 0. \quad (8)$$

This is the same equation systematically studied earlier by Xie et al. [3,9–12], where both exact solutions for all modes and variational approximation for the fundamental mode were obtained.

4 Exact Solutions

In polar coordinate $\mathbf{X} = \{R, \phi\}$, Eq.(5) reads

$$\begin{aligned} & \left[2\eta_d \left[\frac{d}{RdR} \left(R \frac{d}{dR} \right) - \frac{m^2}{R^2} \right] + iq \right] E_m(R) \\ & = \int_0^\infty R' dR' G_m(R, R') E_m(R'), \end{aligned} \quad (9)$$

where m is the azimuthal mode index and

$$\begin{aligned} G_m(R, R') &= \int_{-\infty}^0 \frac{\tau d\tau i^{-m} h}{\sin^2(2\sqrt{\eta_d \eta_\epsilon \tau})} e^U J_m(V), \\ U &= (q - i\eta_\omega)\tau - 2\eta_\gamma^2 \tau^2 - \frac{(1 + i\eta_\epsilon \tau)(R^2 + R'^2)}{2 \sin^2(2\sqrt{\eta_d \eta_\epsilon \tau})}, \\ V &= \frac{i(1 + i\eta_\epsilon \tau) \cos(2\sqrt{\eta_d \eta_\epsilon \tau}) R R'}{\sin^2(2\sqrt{\eta_d \eta_\epsilon \tau})}. \end{aligned}$$

Applying Hankel transform pair

$$E_m(Q) = \int_0^\infty R dR J_m(QR) E_m(R),$$

$$E_m(R) = \int_0^\infty Q dQ J_m(QR) E_m(Q),$$

Eq.(9) can be converted into an integral equation

$$E_m(Q) = \int_0^\infty Q' dQ' T_m(Q, Q') E_m(Q'), \quad (10)$$

where

$$\begin{aligned} T_m(Q, Q') &= \frac{1}{iq - 2\eta_d Q^2} \int_0^\infty R dR \int_0^\infty R' dR' J_m(QR) J_m(Q'R') G_m(R, R') \\ &= \frac{i^{-m} h}{iq - 2\eta_d Q^2} \int_{-\infty}^0 \frac{\tau d\tau}{(1 + i\eta_\epsilon \tau)^2} e^{(q - i\eta_\omega)\tau - 2\eta_\gamma^2 \tau^2 - (Q^2 + Q'^2)/2(1 + i\eta_\epsilon \tau)} \\ &\quad J_m \left[\frac{i \cos(2\sqrt{\eta_d \eta_\epsilon \tau}) Q Q'}{1 + i\eta_\epsilon \tau} \right]. \end{aligned}$$

Upon discretization in Q space, the integral equation, Eq.(10), can be casted into a matrix form: $[\mathbf{T}_m(q) - \mathbf{I}]\mathbf{E}_m = 0$, where \mathbf{I} is a unit matrix. Then all the eigenvalues, q_{nm} , can be determined by solving equation: $\|\mathbf{T}_m(q) - \mathbf{I}\| = 0$. The corresponding eigenmode, \mathbf{E}_{nm} , can be calculated subsequently given the matrix $\mathbf{T}_m(q_{nm})$, where n is the radial mode index.

Consider LCLS nominal case as an example with the following parameters [13]: $\lambda_r = 1.5\text{\AA}$, $\gamma_0 = 28009$, $I = 3.4\text{kA}$, $\gamma_0\epsilon = 1.5\text{mm-mrad}$, $\sigma_\eta = 2 \times 10^{-4}$, $\beta_f = 18\text{m}$, a planar wiggler with $\lambda_w = 3\text{cm}$ and $\sqrt{2}a_w = 3.7$. The scaled parameters take the values: $\eta_d = 0.0367$, $\eta_\epsilon = 0.739$ and $\eta_\gamma = 0.248$. The intensity profiles of the three lowest order modes, E_{00} , E_{10} and E_{01} are shown in Fig.(1-3). Respectively, their eigenvalues and the corresponding optimal detunings are: $q_{00} = 0.4901 + i0.227$ ($\eta_\omega = -1.161$), $q_{10} = 0.125 - i0.0245$ ($\eta_\omega = -1.52$) and $q_{01} = 0.297 + i0.0662$ ($\eta_\omega = -1.40$).

5 Variational Approximation of Fundamental Mode

An approximate solution for the fundamental mode, E_{00} , is presented in this section. Similar solutions for the higher order modes, E_{10} and E_{01} , are given in another paper [14] in connection with the study of transverse coherence of SASE. The approximate solution derived here is, first of all, more efficient in calculation than the exact one. Secondly, it provides more physical insights,

in particular on the mode profile, in a simpler manner. The solution is based on an approximation technique introduced by Xie et al. [3]. There, standard variational method [15] was first extended to treat the eigenvalue problem in which the operator of the eigenmode equation, being neither Hermitian nor self-adjoint, has a nonlinear dependence on the complex eigenvalue. The generalized variational technique, acclaimed as one of the most flexible and general approximation method [16], has later been proven effective for a variety of 2D or 3D FEL eigenvalue problems [2,4,17]. According to the recipe [3], a variational functional may be constructed from Eq.(9) as follows:

$$\begin{aligned} & \int_0^{\infty} R dR E(R) \left[2\eta_d \frac{d}{R dR} \left(R \frac{d}{dR} \right) + iq \right] E(R) \\ & = \int_0^{\infty} R dR \int_0^{\infty} R' dR' E(R) G_0(R, R') E(R'). \end{aligned} \quad (11)$$

Substituting into Eq.(11) a trial function of the form, $E(R) = \exp(-\alpha R^2)$, where α is a complex variational parameter to be determined, and applying the variational condition, $\delta q / \delta \alpha = 0$, to the resulting equation, we obtain the following two equations from which the eigenvalue q and mode parameter α can be determined,

$$F_1(q, \alpha) \equiv \frac{iq}{4\alpha} - \eta_d - \int_{-\infty}^0 \tau d\tau h \frac{e^{f_1}}{f_2} = 0, \quad (12)$$

$$F_2(q, \alpha) \equiv \frac{\partial F_1}{\partial \alpha} = -\frac{iq}{4\alpha^2} + \int_{-\infty}^0 \tau d\tau h \frac{f_3 e^{f_1}}{f_2^2} = 0, \quad (13)$$

where

$$\begin{aligned} f_1 &= (q - i\eta_\omega)\tau - 2\eta_\gamma^2 \tau^2, \\ f_2 &= (1 + i\eta_\epsilon \tau)^2 + 4\alpha(1 + i\eta_\epsilon \tau) + 4\alpha^2 \sin^2(2\sqrt{\eta_d \eta_\epsilon} \tau), \\ f_3 &= 4(1 + i\eta_\epsilon \tau) + 8\alpha \sin^2(2\sqrt{\eta_d \eta_\epsilon} \tau). \end{aligned}$$

To take the 1D limit appropriately, a singularity is removed by introducing $\alpha = \alpha_s(\eta_d, \eta_\epsilon, \eta_\gamma, \eta_\omega) / \sqrt{\eta_d}$, where α_s is a well-behaved, smooth function of its arguments. Then by taking $\eta_d = 0$, Eqs.(12,13) lead to Eq.(6) for the eigenvalue and for the mode parameter

$$\alpha_s = \frac{1}{4} \sqrt{\frac{h \int_{-\infty}^0 \tau d\tau e^{f_1}}{\eta_\epsilon h \int_{-\infty}^0 \tau^3 d\tau e^{f_1} / (1 + i\eta_\epsilon \tau)^2 - 1}}. \quad (14)$$

Therefore in the 1D limit, variational solutions are the same as the exact ones. On the other hand, in the parallel beam limit with $\eta_\epsilon = 0$, and furthermore with $\eta_\gamma = 0$, Eqs.(12,13) become

$$iq\bar{q}^2 + \eta_d\bar{q}^2 - 2\sqrt{h\eta_d\bar{q}} + h = 0, \quad (15)$$

$$\alpha = \frac{1}{4} \left(\sqrt{\frac{h}{\eta_d\bar{q}^2}} - 1 \right), \quad (16)$$

where $\bar{q} = q - i\eta_\omega$. These are the same equations derived earlier by Xie et al. [3]. Equation (15) is a 3D extension of the usual 1D cubic equation.

Given parameter a , mode properties can be determined completely by comparing $E(R \equiv r/\sigma_x) = \exp(-\alpha R^2)$ with the usual Gaussian mode $E(r) = \exp(-r^2/w^2 + ik_r r^2/2R_c)$. Thus $w/2\sigma_x = \sqrt{1/4\alpha_r}$ and $R_c/L_{1d} = -F_d/4\alpha_i$, where w is the mode size and R_c the radius of phasefront curvature. Due to optical guiding, w remains constant along the wiggler and R_c is always positive (corresponds to a diverging phasefront) for the growing mode [3]. If such a mode is allowed to propagate in free space from a location such as the end of the wiggler, the mode will diverge with a Rayleigh length L_r , and have an apparent waist w_0 , located within the wiggler at a distance z_0 from the end of the wiggler, specifically: $L_r/L_{1d} = F_d/4\alpha_r[1 + (\alpha_i/\alpha_r)^2]$, $w_0/2\sigma_x = 1/\sqrt{4\alpha_r[1 + (\alpha_i/\alpha_r)^2]}$ and $z_0/L_{1d} = -F_d/4\alpha_i[1 + (\alpha_r/\alpha_i)^2]$. In addition, the far field divergence angle is $\theta_d \equiv w_0/L_r = \sqrt{\alpha_r[1 + (\alpha_i/\alpha_r)^2]}(\lambda_r/\pi\sigma_x)$. For the LCLS example, the variational method yields $q = 0.4902 + i0.2271$ and $\alpha_s = 0.099 - i0.11$, optimized at $\eta_\omega = -1.161$. The comparison of mode profiles is shown in Fig.(1). Detuning curves are given in Fig.(4).

Another approximate solution for Gaussian beam distribution was derived earlier by Chin et al. [5] using a truncated orthogonal expansion method. There, the resulting zeroth order dispersion relation for the eigenvalue, when expressed in terms the scaling introduced here, can be simply written as:

$$\int_{-\infty}^{\infty} \int_0^{\infty} \frac{dx dy y^3 e^{-x^2-y^2}}{(iq + \eta_\omega - 2\sqrt{2}\eta_\gamma x + \eta_\epsilon y^2)^2} \int_0^{\infty} \frac{dz z e^{-z^2}}{(iq - 2\eta_d z^2)} = \frac{\sqrt{\pi}}{2h}. \quad (17)$$

The solution of Eq.(17) is known to be more accurate for larger value of η_d . However, for the LCLS example, η_d is quite small and Eq.(17) yields $q = 0.313 + i0.138$ optimized at $\eta_\omega = -1.865$, showing a significant difference from the exact solution. In the 1D, ideal beam limit, Eq.(17) gives $q = (1/\sqrt[3]{2})q_{exact}$.

6 Fitting Formula for Gain Length

One of the most important FEL performance parameter is the gain length of the fundamental mode, L_g . To facilitate quick calculation of this quantity, a fitting formula is generated in a scaled form

$$\frac{L_{1d}}{L_g} \equiv q_r = \mathcal{F}(\eta_d, \eta_\epsilon, \eta_\gamma)|_{\eta_\omega^*}, \quad (18)$$

where at each point in the three dimensional parameter space $\{\eta_d, \eta_\epsilon, \eta_\gamma\}$ the scaled quantity L_{1d}/L_g is maximized at the optimal detuning η_ω^* .

The function \mathcal{F} is determined by interpolating the variational solutions with the following functional form

$$\frac{L_{1d}}{L_g} = \frac{1}{1 + \Lambda}, \quad (19)$$

where

$$\begin{aligned} \Lambda = & a_1 \eta_d^{a_2} + a_3 \eta_\epsilon^{a_4} + a_5 \eta_\gamma^{a_6} \\ & + a_7 \eta_\epsilon^{a_8} \eta_\gamma^{a_9} + a_{10} \eta_d^{a_{11}} \eta_\gamma^{a_{12}} + a_{13} \eta_d^{a_{14}} \eta_\epsilon^{a_{15}} \\ & + a_{16} \eta_d^{a_{17}} \eta_\epsilon^{a_{18}} \eta_\gamma^{a_{19}}, \end{aligned}$$

and the 19 fitting parameters are given in Table 1.

Table 1. Fitting parameters for gain length.

$a_1 = 0.45$	$a_2 = 0.57$	$a_3 = 0.55$	$a_4 = 1.6$
$a_5 = 3$	$a_6 = 2$	$a_7 = 0.35$	$a_8 = 2.9$
$a_9 = 2.4$	$a_{10} = 51$	$a_{11} = 0.95$	$a_{12} = 3$
$a_{13} = 5.4$	$a_{14} = 0.7$	$a_{15} = 1.9$	$a_{16} = 1140$
$a_{17} = 2.2$	$a_{18} = 2.9$	$a_{19} = 3.2$	

This is the same fitting formula published before without giving the derivation [6]. The accuracy of the fitting formula is shown in Fig.(5) for a typical case. In the special case with $\eta_d = 0$, the formula reproduces the exact solution from Eq.(6) practically with no discrepancy, as seen in Fig.(6).

7 Conclusions

A systematic approach is developed in three steps for the determination of 3D eigenmodes from Eq.(1). First and foremost, the exact solutions of both fundamental and higher order modes are obtained for the first time. Based on these solutions, complete information on the eigenmodes including eigenvalues and mode profiles can be extracted, examined, and used as a benchmark as well as an inspiration for approximate solutions. Secondly, a variational approximate solution of the fundamental mode is derived for the first time for Gaussian model. The solution is shown to be highly accurate in the parameter regime of interest to short wavelength FELs. It is also very efficient and robust in calculation, and as a result, the solution has been mapped out in the entire scaled parameter space. Finally, based on the wealth of information obtained with the variational solution, a transparent and elegant fitting formula for the gain length is generated. Apart from being compared with the variational solution, the formula has been found to be in good agreement with full-blown simulations [18]. Because of its convenience and accuracy, the formula has been widely used for design and optimization of high gain FEL systems [13]. A Chinese philosopher, Mao Tse-Tung, once said: let philosophy be liberated from the classrooms and books of philosophers, and turned into weapons in the hands of the masses. The three steps taken here is indeed a journey in that direction. The L_{1d} scaling introduced here has made that journey a pleasant trip in style.

References

- [1] K-J. Kim, Phys. Rev. Lett. 57 (1986) 1871.
- [2] L. Yu, S. Krinsky and R. Gluckstern, Phys. Rev. Lett. 64 (1990) 3011.
- [3] M. Xie and D. Deacon, Nucl. Instr. Meth. A 250 (1986) 426.
- [4] B. Hafizi and C. Roberson, Phys. Rev. Lett. 68 (1992) 3539.
- [5] Y. Chin, K-J. Kim and M. Xie, Phys. Rev. A 46 (1992) 6662.
- [6] M. Xie, IEEE Proc. for PAC95, No.95CH3584 (1996) 183.
- [7] G. Moore, Nucl. Instr. Meth. A 250 (1986) 381.
- [8] R. Bonifacio, C. Pellegrini and L. Narducci, Opt. Comm. 50 (1984) 373.
- [9] M. Xie, D. Deacon and J. Madey, Nucl. Instr. Meth. A 272 (1988) 528.
- [10] M. Xie, D. Deacon and J. Madey, Nucl. Instr. Meth. A 296 (1990) 672.
- [11] M. Xie, D. Deacon and J. Madey, Phys. Rev. A 41 (1990) 1662.

- [12] M. Xie, Theory of Optical Guiding in Free Electron Lasers, Ph.D. dissertation, Stanford University, (1988).
- [13] LCLS Design Study Report, SLAC-R-521, (1998).
- [14] M. Xie, 'Transverse Coherence of Self-Amplified Spontaneous Emission', These proceedings, also LBNL-44382, (1999).
- [15] P. Morse and H. Feshbach, Methods of Theoretical Physics, McGraw-Hill, New York, 1953, p.1108.
- [16] P. Luchini and H. Motz, Undulators and Free-Electron Lasers, Clarendon Press, Oxford, 1990, p.160.
- [17] P. Luchini and S. Solimeno, Nucl. Instr. Meth. A 272 (1988) 311.
- [18] H. Freund and P. O'Shea, Phys. Rev. Lett. 80 (1998) 520.

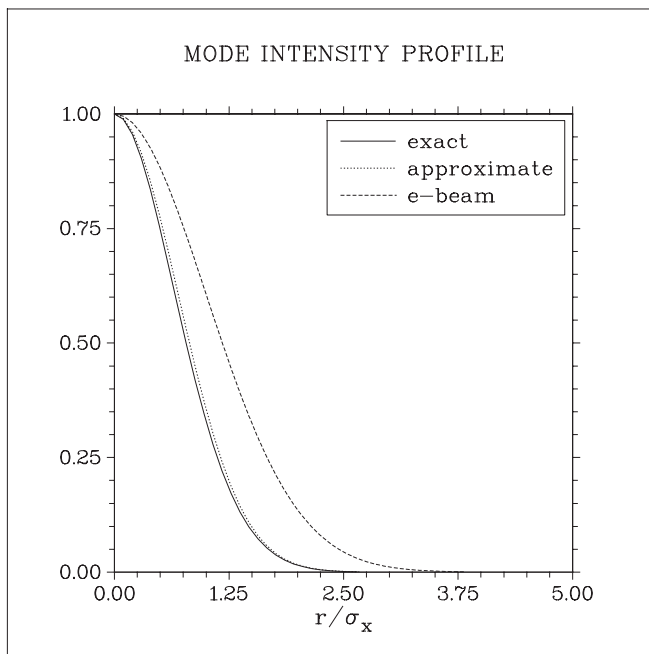


Fig. 1. Intensity profile of E_{00} mode from both the exact solution and variational approximation, superimposed with the electron density profile.

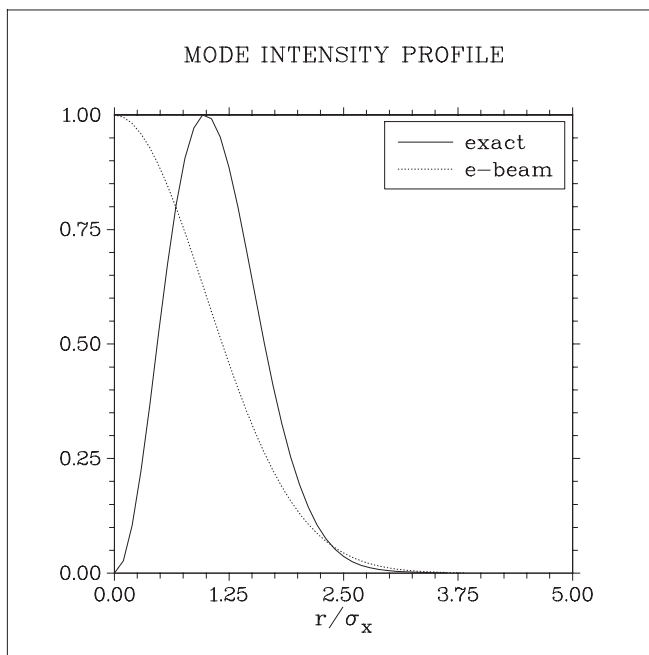


Fig. 2. Intensity profile of E_{10} mode from the exact solution, with the electron density profile.

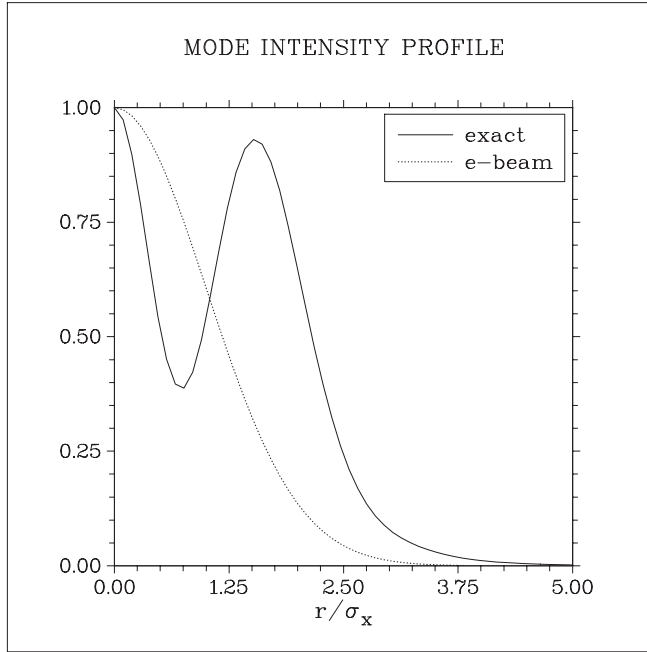


Fig. 3. Intensity profile of E_{01} mode from the exact solution, with the electron density profile.

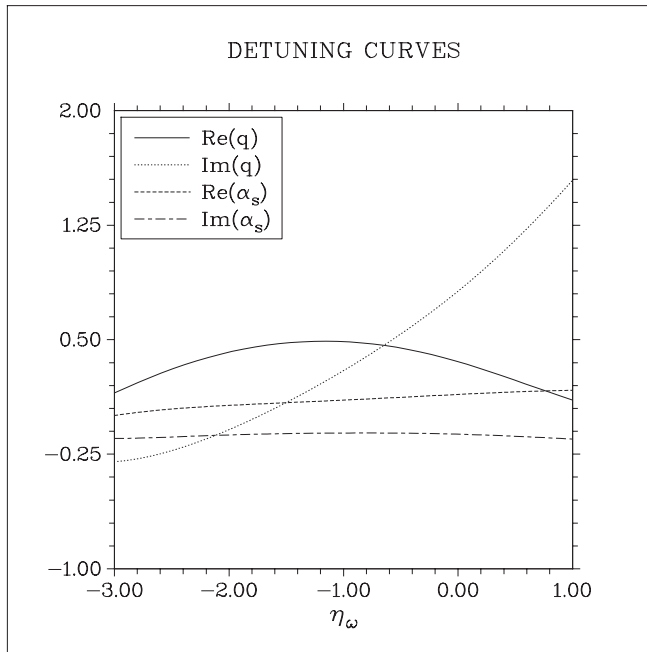


Fig. 4. Detuning curves from the variational solution.

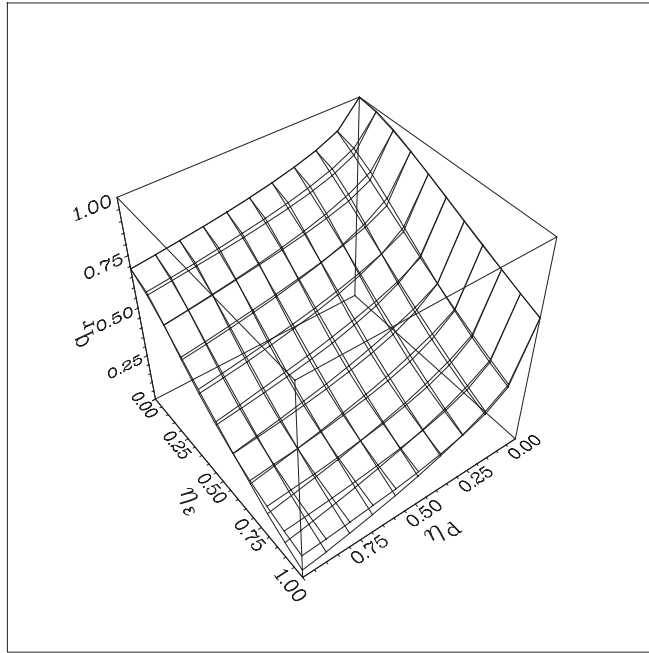


Fig. 5. Two surface plots showing $q_r = \mathcal{F}(\eta_d, \eta_\epsilon, \eta_\gamma = 0)$ are superimposed, one from the variational solution and another from the fitting formula.

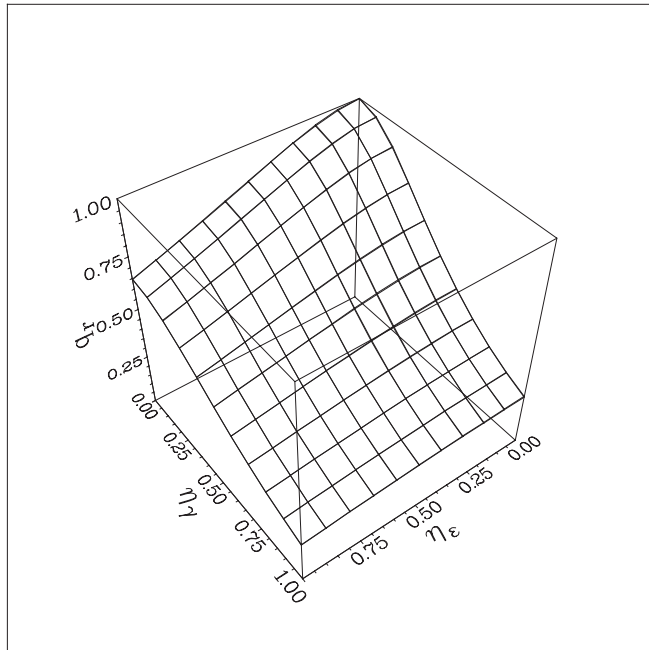
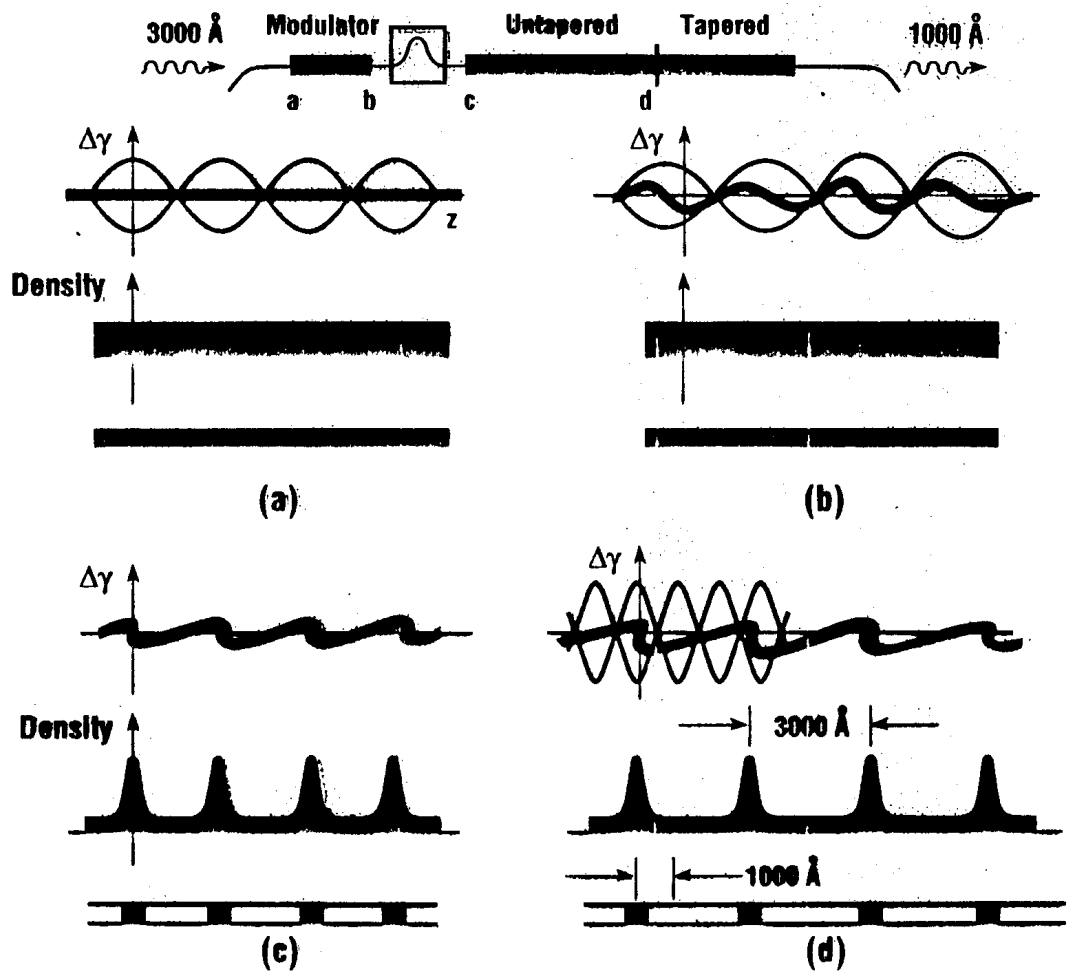


Fig. 6. Two surface plots showing $q_r = \mathcal{F}(\eta_d = 0, \eta_\epsilon, \eta_\gamma)$ are superimposed, one from the variational solution (same as the exact solution in this case) and another from the fitting formula. The difference between the two can hardly be seen in this case.

WORKSHOP PRESENTATIONS VI

High-Gain, Higher-Harmonic Theory

L.-H. Yu



UVFEL (100nm, BNL, 1990)

$$1. \quad P_{in} = 4 \text{ MW} \quad (300 \text{ nm})$$

$$P_{out} = 200 \text{ MW} \quad (100 \text{ nm})$$

$$L_g = 1.1 \text{ m}$$

$$\text{modulator} \quad 2 \text{ m}$$

$$\text{radiator} \quad 11 \text{ m}$$

2. Compare with SASE
saturation length

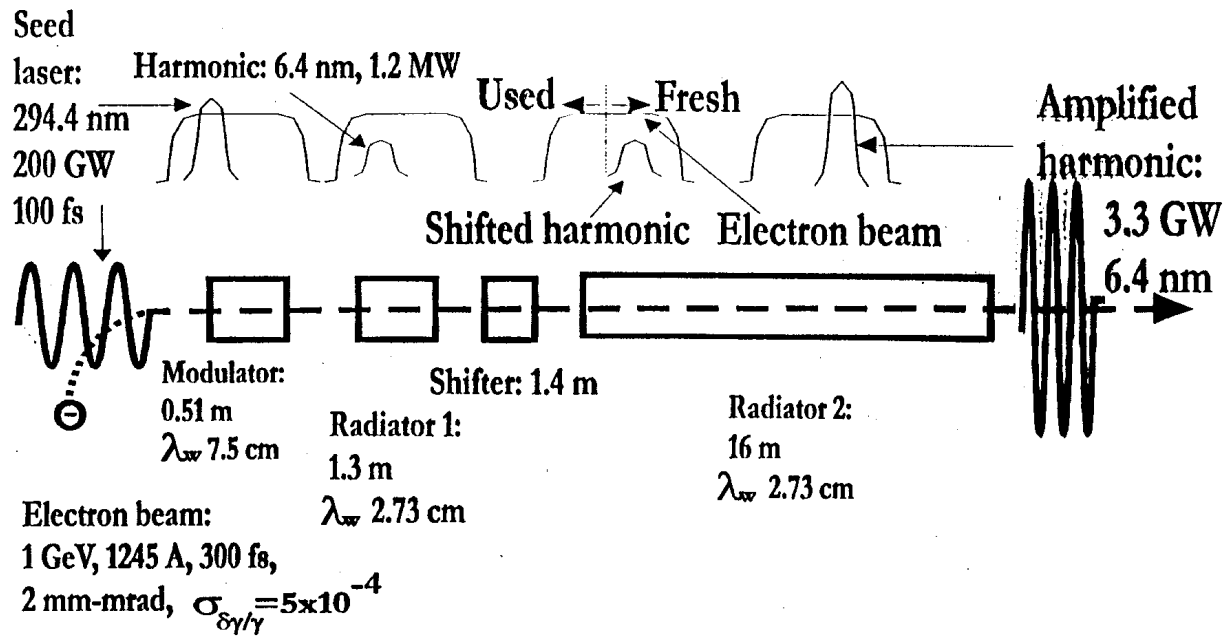
$$20 L_g = 22 \text{ m}$$

3. Chirped Pulse Amplification (CPA)

$$11 \text{ fs, } 264 \text{ nm} \rightarrow 4 \text{ ps, } 4.6 \text{ MW, } 4\% \text{ bandwidth}$$

$$\underline{\text{HG}} \rightarrow 4 \text{ ps, } 150 \text{ MW, } 3\% \text{ bandwidth, } 88 \text{ nm}$$

$$\rightarrow 5 \text{ fs, } 60 \text{ GW } 88 \text{ nm}$$



Fresh Bunch Scheme

Apply to hard X-rays:

key issues:

- Seed laser power \gg input noise
 - Equivalent input power of harmonic generation
 \gg noise power in radiator
 - When energy modulation \sim energy spread, use fresh bunch
-

Ultrafast Coherent UV and X-ray Sources

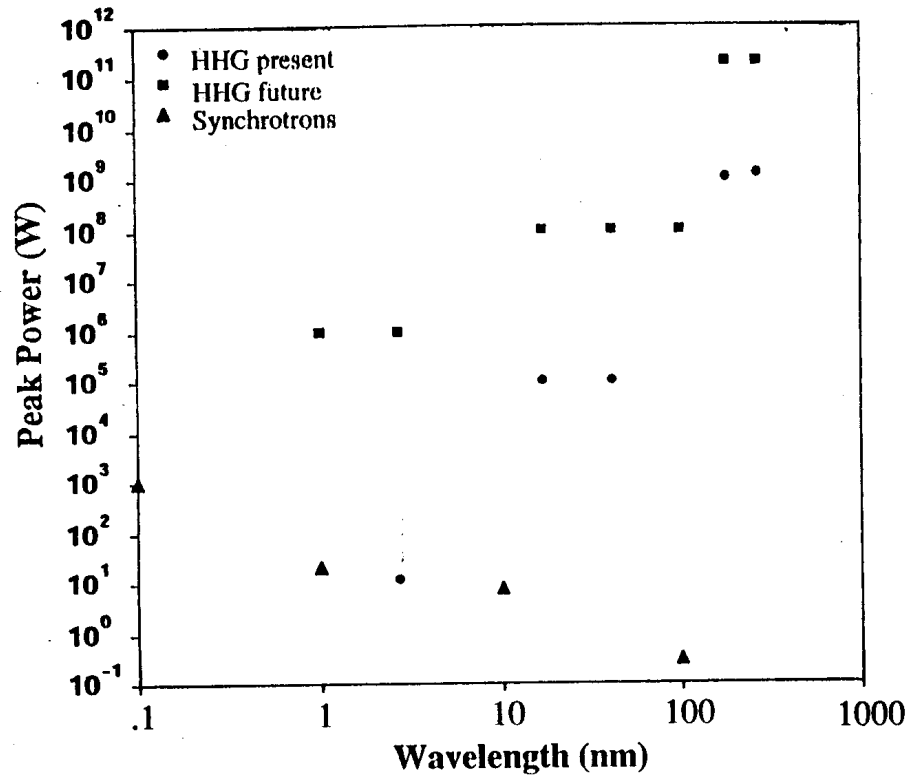
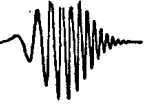
Prof. Henry C. Kapteyn
Prof. Margaret Murnane
Prof. Ivan Christov

Andy Rundquist, Charles Durfee, Sterling Backus, Zenghu
Chang, Haiwen Wang, Catherine Herne

University of Michigan

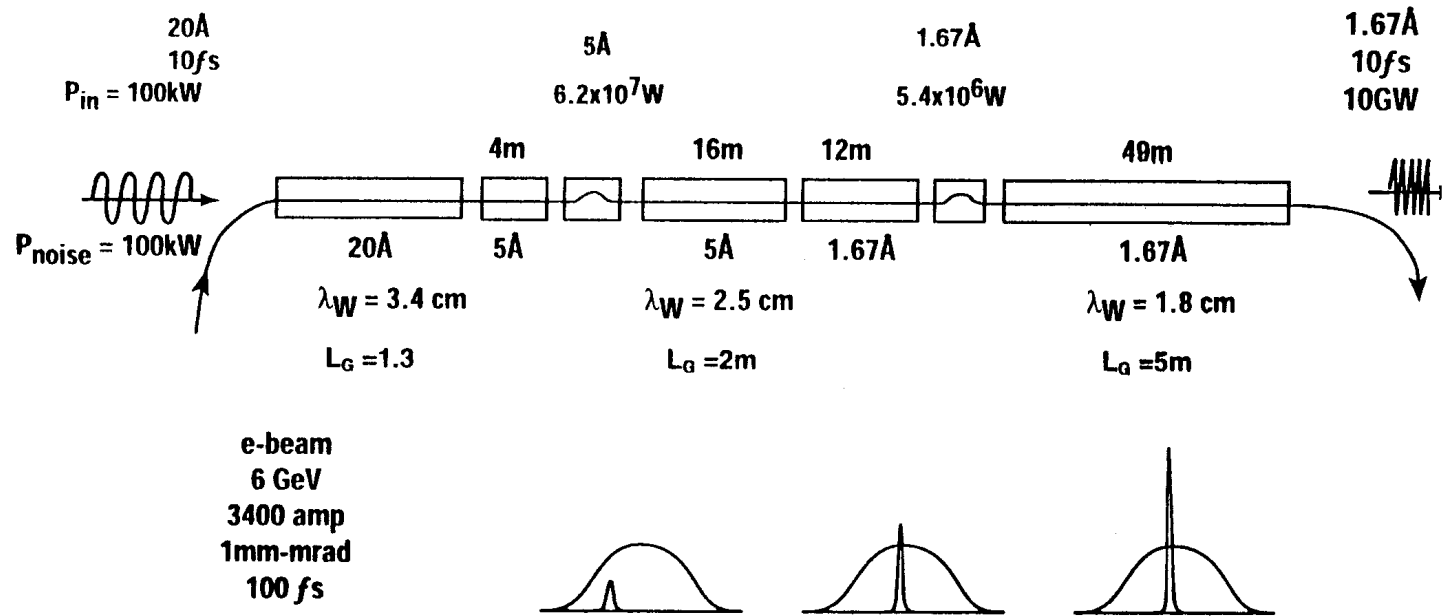


Peak power:



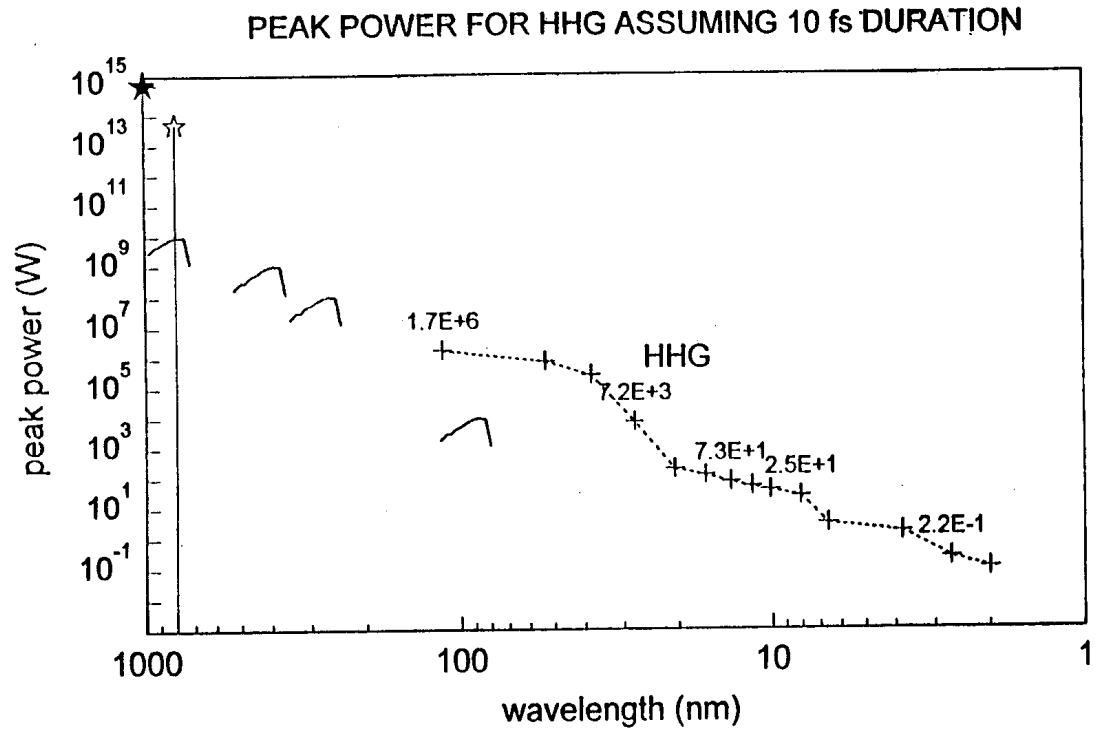
- **HHG radiation has diffraction-limited focusability**

Single Bunch Scheme



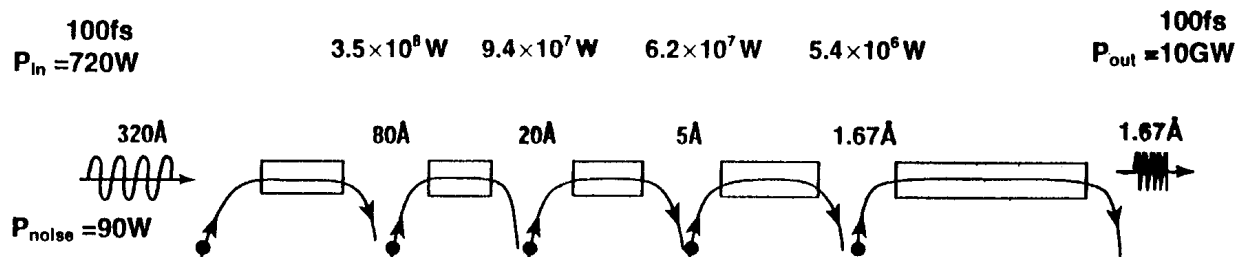
$L_{total} \approx 100m$

Assuming current fluctuate 10% p-p, fluctuation $\left(\frac{\Delta W}{W}\right)_{rms} = 5\%$. $\frac{\Delta\lambda}{\lambda} = \frac{1.67 \times 10^{-10}m}{3 \times 10^{-6}m} = 5 \times 10^{-5}$



Courtesy: L. DiMauro

5 Bunches Scheme



e-beam
 1.5 GeV 1.5 GeV 6 GeV 6 GeV 6 GeV
 2500 Amp 3400 Amp
 1 mm-mrad 1 mm-mrad
 300 fs 100 fs

λ (Å)	320	80	80	20	20	5	5	1.67	1.67
λ_c (cm)	3.6	2.6	2.6	1.8	3.4	2.5	2.5	1.8	1.8
L_w (m)	7	1	2.4	2	10	4	16	12	49
L_a (m)	0.4	0.5	0.5	0.75	1.3	2	2	5	5

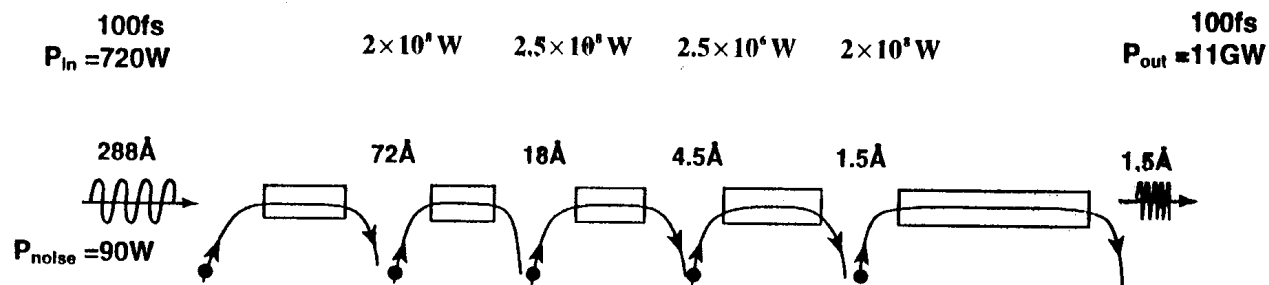
$L_{total} = 103m$

$$\frac{\Delta\lambda}{\lambda} = \frac{1.67 \times 10^{-19} m}{30 \times 10^{-6} m} = 5 \times 10^{-6}$$

Summary of the Estimate

	SASE	2-stage	HGHG single bunch	HGHG 5 bunch
pulse length (fs)	100	100	10	100
band width $\frac{\Delta\lambda}{\lambda}$	4×10^{-4}	5×10^{-5}	5×10^{-5}	5×10^{-6}
Fourier limit	5×10^{-6}	5×10^{-6}	5×10^{-5}	5×10^{-6}
pulse energy (mJ)	1	1	0.1	1
# photons	8×10^{11}	8×10^{11}	8×10^{10}	8×10^{11}
peak power (GW)	10	10	10	10
fluctuation	5%	10%-20%	5%	5%
Spon. power in fundamental (GW)	1	-	0.4	0.4
beam size			$\sim 30 \mu\text{m}$	
divergence			$\sim 0.5 \mu\text{rad}$	

LCLS HGHG Scheme



e-beam	2GeV	4GeV	14GeV	14GeV
1GeV	2500Amp	2500Amp	3400Amp	3400Amp
2500Amp	1mm-mrad	1mm-mrad	1.5mm-mrad	1.5mm-mrad
1mm-mrad	$\sigma_y = 5 \times 10^{-4}$	$\sigma_y = 5 \times 10^{-4}$	$\sigma_y = 2.1 \times 10^{-4}$	$\sigma_y = 2.1 \times 10^{-4}$
$\sigma_y = 1 \times 10^{-3}$	300fs	300fs	100fs	100fs
300fs				

λ (Å)	288	72	72	18	18	4.5	4.5	1.5	1.5
λ_w (cm)	3	2.1	3	2.1	3	2.1	3.9	3	3
L _w (m)	6.1	1	3.6	1.8	6.6	6	44	6	36.5
L _g (m)	0.3	0.4	0.56	0.86	1.2	2.6	3.65	6.6	6.6

L_{total} = 111m

L_{SASE} = 110m to reach 10GW

WORKSHOP PRESENTATIONS VII

Particle Transport

H. Freund

PARTICLE TRANSPORT

- Wiggler-Averaged (KMR) or Non-Wiggler-Averaged?
 - Run times
 - Accuracy
 - Ease of use/modification
 - End-to-End Models
- Undulator Transport
 - Injection to and ejection from the wiggler(s)
 - KMR not possible(?)
 - What is beam distribution in the wiggler?
 - End-to-End Models
 - Emittance growth
 - Effect on wave growth/guiding
 - Field Models
 - Wiggler Imperfections
 - Sinusoidal Wiggler models
 - Self-consistency(?)
 - Field Map
 - How to handle measured wiggler errors
 - Wiggler-Averaged or Non-Wiggler-Averaged
 - Is KMR possible?
 - Integrated Wiggler & Focusing Fields
 - Radiation startup
 - Radiation fields and transverse particle motion
- External Focusing
 - Quadrupoles (FODOs) and Dipoles
 - Wiggler-Averaged or Non-Wiggler-Averaged
- Error Tolerance Levels

WORKSHOP PRESENTATIONS VIII

Interfacing Multiple Simulation Codes

M. Borland

ADVANCED PHOTON SOURCE
<http://www.aps.anl.gov/asd/oag>

Operations Analysis Group
Michael Borland borland@aps.anl.gov

Interfacing Multiple Simulation Codes —FEL and Accelerator Codes—

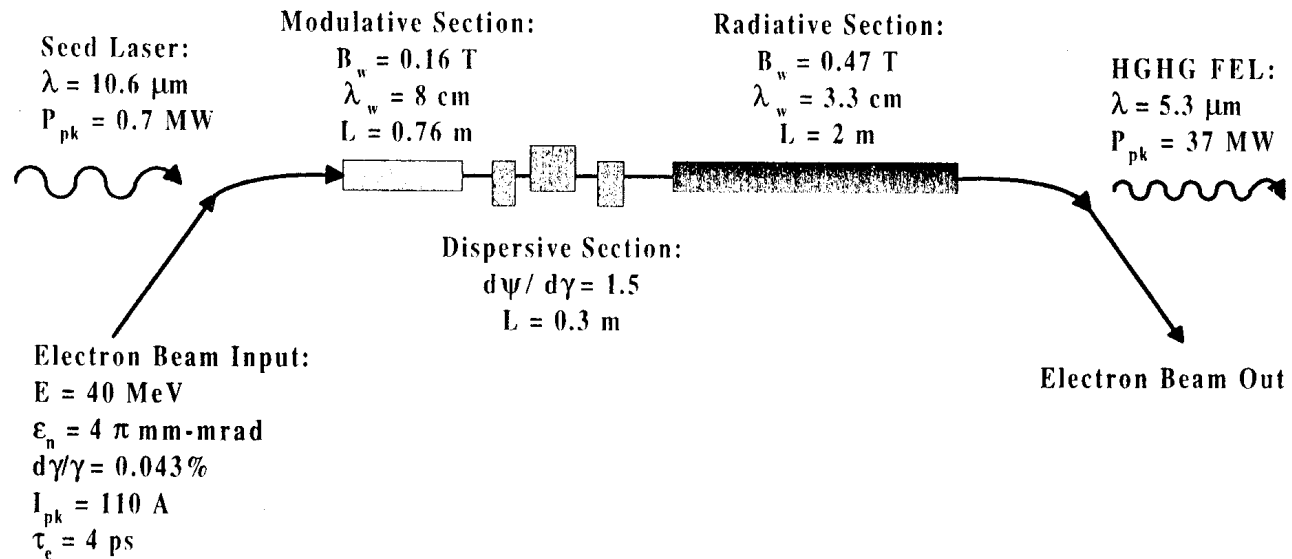
- Can we specify one or two *formats* in which FEL codes can or do accept data from accelerator codes?
- Can we build one or two standard adapter programs from accelerator codes to FEL codes?
- Is there interest in taking data from FEL codes to accelerator codes?
- Given a sufficiently clear specification, APS will write and maintain adapter codes based on SDDS files.

WORKSHOP PRESENTATIONS IX

The High-Gain Harmonic Generation Experiment

S. Biedron

THE HIGH-GAIN HARMONIC GENERATION EXPERIMENT

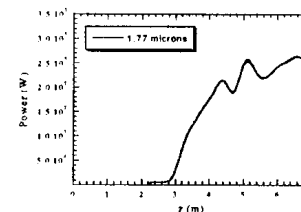
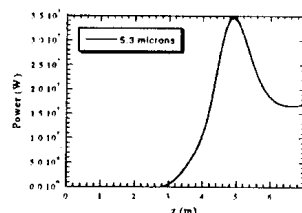


HGHG SIMULATIONS, continued

They were recently re-run with the higher harmonics of the radiative section included.*

- ◆ Since examination of the higher harmonic growth was desired, the third harmonic to the radiative section, 1.77 μm , which is the sixth harmonic to the fundamental seed laser, was also started with zero power.
- ◆ The dispersive section was scanned until the maximum growth for the second harmonic to the fundamental.
- ◆ 18 modes were simulated.
- ◆ Again, the “gain lengths” vary in inverse proportion to the harmonic number.
- ◆ The “fundamental” (5.3 μm) and third harmonic (1.77 μm) powers were compared with that found using the three-dimensional analytical model, for the case of a long, single-segmented radiative section tuned to the second harmonic.

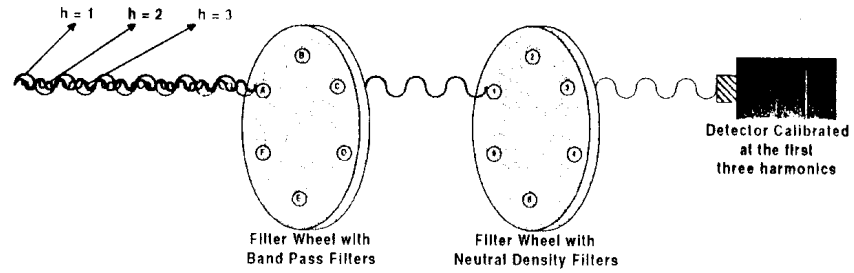
In the below two figures, the radiative section begins at 2.6 meters. With 35 MW in the fundamental, there is a resultant 0.25 MW in the third harmonic.



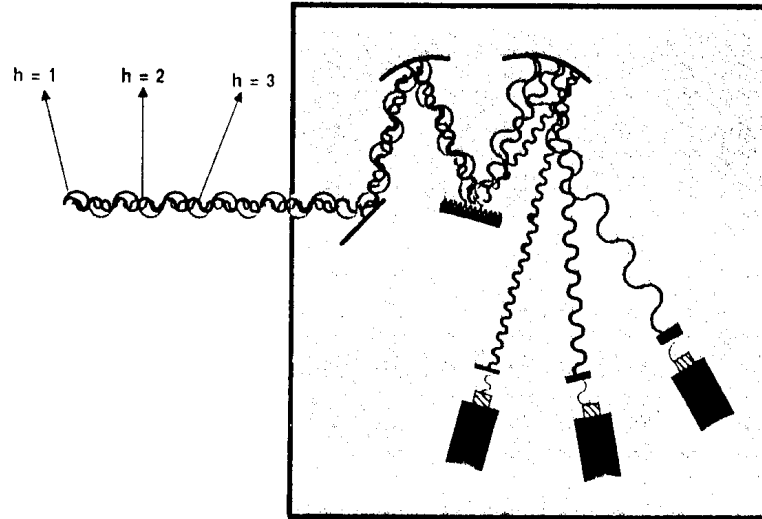
*S.G. Biedron et al., internal communication (to be published).

PLANNED EXPERIMENTAL VERIFICATION

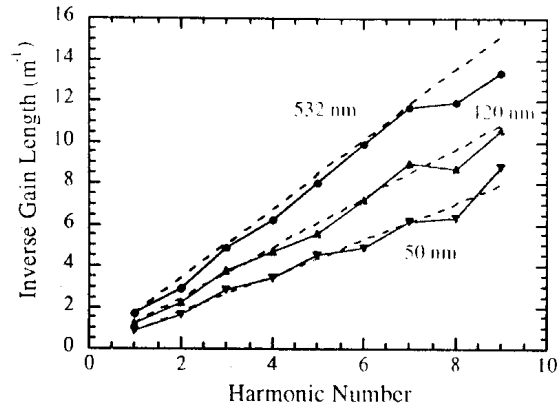
Multiple Shot Technique:



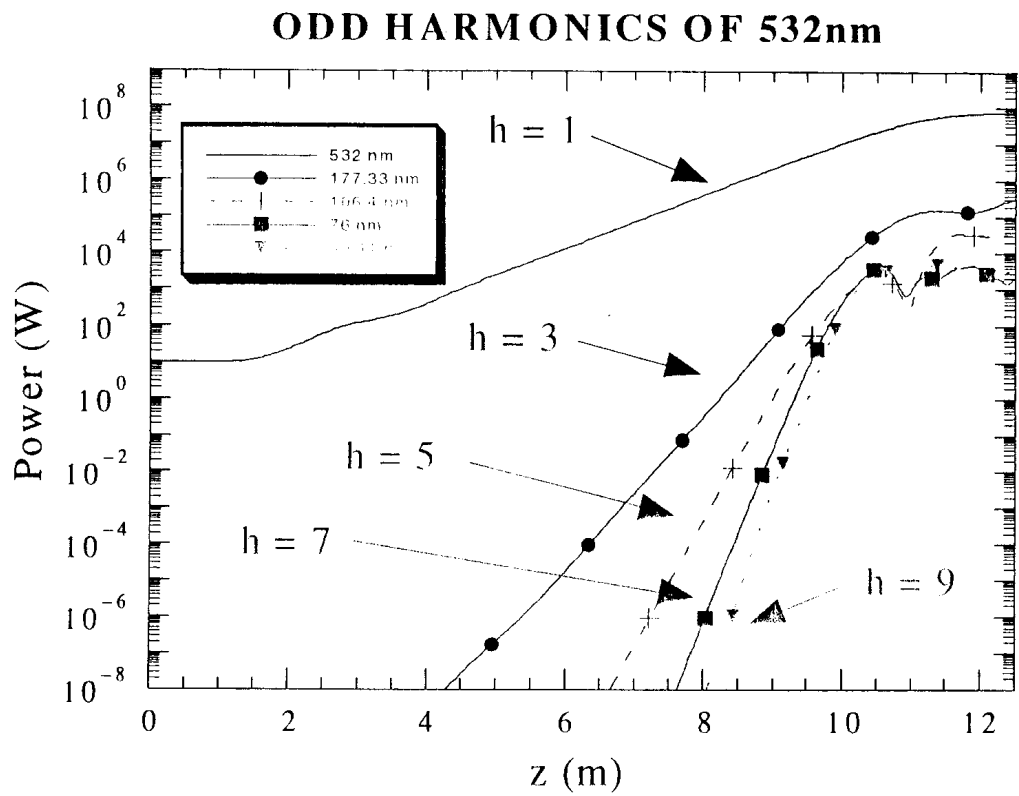
Single Shot Technique:



THE APS SASE FEL



Harmonic Number	Fundamental at 532 nm		Fundamental at 120 nm		Fundamental at 50 nm	
	L_G (m)	P_{sat}	L_G (m)	P_{sat}	L_G (m)	P_{sat}
1	0.5925	138.4 MW	1.039	402.2 MW	1.418	449.9 MW
2	0.3460	3.276 kW	0.5964	15.92 kW	0.6979	28.83 kW
3	0.2062	832.6 kW	0.4113	2.461 MW	0.4768	1.509 MW
4	0.1610	1.365 kW	0.2784	803.2 W	0.2639	10.39 kW
5	0.1248	42.04 kW	0.2643	724.2 kW	0.2690	1.489 MW
6	0.1015	381.8 W	0.1888	2.948 kW	0.2351	5.887 kW
7	0.0856	39.39 kW	0.1116	38.90 kW	0.2203	323.5 kW
8	0.0872	207.4	0.1112	973.6 W	0.1970	319.6 W
9	0.0670	39.99 kW	0.1324	13.98 kW	0.1614	49.13 kW



APPENDIX A. Synopses of several FEL Simulation Codes

The following pages give extended synopses of the FEL simulation codes MEDUSA, FELEX (both the original LANL version and the modified Boeing version), GENESIS, and GINGER. Each synopsis was written by the code author and/or principal user and additional details can be obtained from them.

MEDUSA Simulation Code, Version 2.0

H.P. Freund

Science Applications International Corp.

McLean, VA 22182

Contact: freund@mmace.nrl.navy.mil tel.: (202) 767-0034

Code Language: Fortran 77

Computer Platforms: Cray, Workstations, Macintosh, PC

Operating Systems: Unix, Mac OS, Windows

Inputs: Fortran Namelist

Outputs: Text files, no graphics capabilities (post-processing required)

Electron Beam/Magnetostatic Fields:

Particle trajectories are solved by integration of the complete 3-D Lorentz force equations for the magnetostatic and electromagnetic fields. No wiggler averaging is employed. Three magnetostatic field types are currently implemented:

1. Planar undulators: Three model forms for planar undulators are available. One is a parabolic-pole-face (PPF) model, the second is a flat-pole-face model, and the third is a more complex model with polynomial focusing in the wiggler plane. Each of these models is available in single- or multi-segment configurations. Adiabatic up- and down-tapers are available for describing the injection onto and ejection from the wiggler. Tapered amplitude undulators are supported.
2. Quadrupoles: The code employs a hard-edge quadrupole model.
3. Dipoles: The dipole model is also a hard-edge representation.

An arbitrary number of each of these field types can be selected, as are the field orientations, locations and axial extent of the different magnet segments. The Lorentz force equations are integrated by calculating the specific magnetic fields at the location of each particle.

A version of MEDUSA 1.0 exists in which the magnetostatic fields are specified by a field map that is read in at the start of the program. The field at each particle location is then found by interpolating from the field map to each particle location. Such a field map can incorporate the wiggler, quadrupole, and dipole fields into one model. Other types of field structure (such as a FODO lattice) can also be included. If there is sufficient interest, this field map/interpolator can be incorporated into MEDUSA 2.0 as well.

Wiggler errors are supported, and handled by allowing the wiggler amplitude to vary in arbitrary steps at intervals of some fraction of a wiggler period. The field amplitude at intermediate positions between the steps is determined by a uniform interpolation scheme. The amplitude errors can be generated using a random number generator, or they can be hardwired to model a specific set of wiggler errors.

Several electron beam models are available including Gaussian and/or Waterbag beam distributions, or flat-top beams with circular, elliptic, or sheet (rectangular) cross-sections. Since MEDUSA models beam injection into the wiggler, the parameters of these distributions must be chosen to correspond to the beam at the entrance to the wiggler (or at the exit of the accelerator/transport line). The beam distribution in the wiggler is then obtained in a self-consistent manner as the beam enters the wiggler.

The Radiation Field

The radiation field is fully polychromatic and is represented as a superposition of Gauss-Hermite modes in which the amplitude and phase are assumed to vary more slowly than the wavelength. Slow-time-scale equations for the evolution of the amplitudes and phases are then integrated simultaneously with the Lorentz force equations. A source-dependent expansion is also used to determine the evolution of the spot size and curvature of the Gauss-Hermite modes. This reduces the number of modes needed in the simulation, and dramatically reduces the run times.

MEDUSA includes multiple wavelengths under the assumption that each component occurs at a frequency that is a multiple of some reference frequency ω_0 . This spectral approach permits the treatments of either closely-spaced sidebands or harmonics. Thus, MEDUSA can treat the simultaneous growth of multiple harmonics or the startup from noise in a SASE FEL. However, the polychromatic feature requires the inclusion of a larger number of particles (than the monochromatic case) that results in longer run times.

Numerical Algorithm

A fourth order Runge-Kutta integration scheme is used to integrate the combined field and particle equations. The particles are loaded at the outset based upon the initial particle distributions using a Gaussian quadrature technique. This technique has the advantage that it implicitly describes a “quiet-start” load that minimizes both particle number and numerical noise.

Diagnostics

MEDUSA produces no graphical output, this is left up to the user. The principal output is a file that records header information on the beam wiggler/focussing magnets, and electromagnetic modes followed by a listing of the evolution of each mode with axial position. The modes are listed sequentially, and columns showing the axial position, power (W), spot size (cm), and curvature are given. In addition, the first mode also shows the rms

beam radius and number of particles in the simulation. A file is also written which shows the evolution of the beam centroid in x and y , the average width about the centroid in x and y , and the rms beam radius. The beam state (that is x , y , p_x , p_y , p_z , and the ponderomotive phase for each particle) can also be written to a file at selected axial positions. These text files are written in a form which is convenient for commercially available plotting packages (such as Kaleidagraph, Sigma Plot, Igor, etc.) to handle.

FELEX - LANL version

John C. Goldstein
Group XPA, MS B259
Los Alamos National Laboratory
Los Alamos, New Mexico 87545

Contact: jcg@lanl.gov tel.: 505-667-7281

FELEX (Free-Electron Laser Emulation eXperiment) is a 4-D (three spatial dimensions plus time for finite-duration optical and electron beam pulses) FEL simulation code written by B. D. McVey of LANL [1]. The original motivation (1984) for writing the code was to address problems of XUV FEL oscillators, but about one year after its beginning the work became sponsored by the SDI program at LANL. Over the next several years the code was expanded to treat many different specialized FEL problems [2,3], and, although the coding was primarily still composed by McVey, several other people made contributions to the code.

The code uses discrete, pointlike simulation "macro"-electrons (which have coordinates and velocities in 3-D) to represent an electron beam. Fields, magnetostatic (wiggler) and electromagnetic (optical), are computed on a 3-D grid composed of uniformly-spaced Cartesian coordinates. Within the wiggler region of an FEL, the simulation electrons interact with the wiggler and optical fields via classical Lorentz force equations which assume slow - compared to a wiggler wavelength - variations of the electrons' motion superimposed on the undulator-induced rapid transverse oscillations; the narrow-bandwidth optical field is represented by slowly-varying phase and amplitude functions which modulate the rapidly-varying sinusoidal phase function of a monochromatic carrier signal. All field and particle variables are allowed to vary in 3-D; transverse diffraction and refraction of the optical field are included. Together with slippage (the different axial velocities of the electron beam within the wiggler and the optical field) these assumptions follow the general FEL model introduced by Colson and Ride in 1979.

The code was constructed to primarily model FEL oscillators, therefore extensive models of optical components and resonators are included: these range from simple two-mirror stable resonators to multiple-mirror ring resonators with complex optical components like diffraction gratings. Mirror aberrations can be treated. The code uses the Huygens-Fresnel diffraction integral, evaluated by fast Fourier transforms, to propagate the optical field in spatial regions outside of the wiggler where free-space propagation alone occurs. The optical field generated by an FEL can be propagated through an optical system external to the laser itself. Misalignments of optical components can also be treated.

Various types of wiggler magnets can be used, including "self-designed" wigglers in which a pre-programmed "resonant particle" defines the nonuniform taper. Since the electrons' equations of motion do not follow trajectories within an individual wiggler wavelength, an instantaneous transverse deflection ("kick") is given to electrons every half period to model steering errors due to wiggler field errors. Various schemes of trajectory correction involving periodically-spaced localized external steering coils and (imperfect) beam position monitors have been extensively studied with FELEX. The code presently is set up to use only plane-polarized wigglers with either "natural" or two-plane focusing.

Electron shot noise is modeled for startup calculations. An auxiliary code was written to permit FELEX to input directly electron distributions calculated by the accelerator design/modeling code PARMELA. FELEX can be run with a single optical wavefront (CW single-frequency model), a temporally-finite pulse (which of course requires also a finite electron pulse), or with periodic boundary conditions on an optical "window" which typically is several slippage distances long - an approximation introduced by Colson. The optical field need not be at the fundamental FEL resonance frequency - any odd harmonic can be chosen, but multiple harmonic fields which are simultaneously present are not treated. Oscillator simulations require many passes through a wiggler with a recirculating optical pulse interacting with fresh electron pulses on each pass; single pass SASE FEL simulations are therefore much less consuming of computer time.

References

- [1] B. D. McVey, *Nucl. Instr. Meth. in Phys. Res.*, **A250**, pp. 449-455 (1985).
- [2] J. C. Goldstein, B. D. McVey, R. L. Tokar, C. J. Elliott, M. J. Schmitt, B. E. Carlsten, and L. E. Thode, *Proc. SPIE* vol. **1045**, pp. 28-35 (1989).
- [3] B. D. McVey, J. C. Goldstein, R. L. Tokar, C. J. Elliott, S. J. Gitomer, M. J. Schmitt, and L. E. Thode, *Nucl. Instr. Meth. in Phys. Res.*, **A285**, pp. 186-191 (1989).

FELEXN, Boeing simulation code, version B08

Claudio G. Parazzoli
Boeing, Phantom Works
P.O. Box 3999 MC 85-02
Seattle, WA 98124-2499

Contact: claudio.g.parazzoli@boeing.com tel.: 253-773-8299

FELEXN is a three-dimensional and time dependent computer code that computes the FEL performance from the phase space of the electron bunch, computed with the help of ARGUS, PARMELA and ABCI, at the entrance of a wiggler. This code has also been extensively modified from the original LANL version, written by B. McVey, to allow for the presence of Littrow-Gratings, hole coupling and the corrections of numerous coding errors. An interface between PARMELA and FELEXN has been created to transfer the phase space generated by PARMELA into FELEXN.

The code is currently being ported to Fortran90/95 to improve the CPU performance and runs on UNIX systems including Sun, HP and DEC workstations. The code integrates the FEL equations using the KMR (averaging) method and adopts the Slowly Varying Envelope Approximation (SVEA) to advance the optical field. Wiggler errors are included with the impulse being applied at mid pole.

FELEXN has the ability to operate in the amplifier or oscillator mode. The optical train for the amplifier or oscillator can include an arbitrary number of optical elements including mirrors, lenses, scrapers, apertures, out-couplers, etc. The optical field is propagated between optical elements via Fresnel integrals. The code operates in the single wave-front (*i.e.* monochromatic) mode when the temporal dependence of the pulse can be ignored and no information on the frequency spectrum is required. There is no restriction on the type of spatial optical modes that will be generated by the lasing process. A transverse Cartesian grid resolution of 64×64 or 128×128 pixels is usually adequate.

The optical radiation field is initiated either by shot noise or by a seed. The code can operate at different harmonics, but there is no coupling mechanism between harmonics. In time-dependent mode, the code can follow as many as 300 wave fronts, which usually provide a sufficient spectral resolution. Periodic boundary conditions are allowed. For oscillator simulations, laser cavity detuning is allowed and can be time-dependent.

An extensive post processing capability is available with many different types of two and three-dimensional plots being generated at the user request. Currently, MatLab is used to generate the plots and the pictures.

A number of improvements to the code are currently planned: the addition of the beam pipe effects on the optical field, wake-field effects within the wiggler, relaxation of the KMR assumption, porting to multi-processor machines, extension of the internal documentation, and the writing of a user manual.

GENESIS 1.3 Simulation Code

S. Reiche, DESY (contribution translated by H.-D. Nuhn, SSRL)

Contact: reiche@guinness.physics.ucla.edu

The Electron Beam

Transverse Motion: Analytical transport matrices are used for x , y , p_x , p_y . Input parameter is the instantaneous focusing strength, *i.e.*, the quadrupole field, g , and the natural focusing by the undulator field, a_w . The parameters g and a_w can be freely defined for each integration step (see below), A kick in p_x (and p_y for helical undulators) is used to simulate undulator errors or quadrupole misalignments. The kick due to field errors is calculated from the continuity condition between two undulator poles, if a phase advance of π per pole is assumed. Quadrupole misalignments are treated like dipole field errors. To increase the precision, the transverse motion is expanded into two steps, before and after the calculation of energy and phase.

Longitudinal Motion: The code uses a fourth order Runge-Kutta method. If a_w is zero for a given integration step, the coupling term between the electrons and the field is set to zero. This corresponds to a drift in phase and to a constant energy.

Additional Effects: The increase of energy spread and energy loss due to incoherent radiation is included. The formulae are based on a paper by Saldin, Schneidmiller and Yurkov. This feature has been added to the next version of GENESIS, which is still not official.

An arbitrary selectable energy loss per path length is included in the code. This feature allows to simulate wakefields. Further extensions to the code are conceivable.

The Radiation Field

The radiation field is defined on a uniform Cartesian grid. The field equations are solved with the ADI method (Alternating Direction Implicit). The electrostatic field is evaluated with a radially symmetric grid, that is centered around the electron bunch. The boundary condition corresponds to a Dirichlet condition. This is relatively inefficient and I hope that I will be able to replace it in the next version by a faster method (A multi-grid method is conceivable, because it would also be highly efficient for solving the radiation field equations.)

Diagnostics

Electron and radiation parameters such as energy, bunching factor, radiation power and instantaneous divergence of the radiation field are put out for every integration step. The output is in ASCII format. Additionally, the complete radiation field and all macro particle variables can be saved to disk for each simulation time step. The output of these data is in binary format.

Input

The Fortran Namelist feature is used for input of a good four dozen parameters. From these parameters, which are mostly global parameters, *i.e.*, independent of the longitudinal position within the bunch, the initial phase space distribution and the radiation field are generated. The bunch profile, *i.e.*, the local current amplitude, is either homogeneous or Gaussian. All other electron beam parameters are global. The initial radiation field is always a Hermite fundamental mode. The description of the magnetic field generates a FODO-Lattice, where focusing and defocusing quadrupoles can be described independently. An undulator module, whose length can be freely chosen, is padded with drift spaces before or after (freely selectable) the module to make the total length equal to an integer multiple of the FODO cell length. Quadrupole misalignment errors and field errors can be generated.

Additional input files, which extend the input capability:

Field: An arbitrary distribution on the Cartesian grid can be used instead of the internally generated Hermite distribution.

Magnetic Field: Undulator field strengths, quadrupole field strengths, kicks from field errors, quadrupole misalignments and kicks from corrector magnets can be specified in an input file for arbitrary sections.

Electron Beam: Electron beam parameters are specified in a lookup table. The first entry in the table is the longitudinal position, which is followed by electron parameters such as energy, emittance, local current amplitude and local energy loss. The latter allows the specification of wake potentials and thus the simulation of wakefields. When GENESIS generates the electron slices it interpolates between values from this table. With this, any profile including a coherent energy spread can be simulated.

Time Dependent Simulation: GENESIS starts at the end of the bunch. It takes a slice and lets the radiation field pass through. The radiation field is stored. After the slice has passed through the entire undulator, the next slice is loaded and the previously stored radiation field is reused.

Shot noise is added through a small variation in the phase of the macro particles (based on a report by Pennman), where each particle is combined with its three mirror particles, so that it is corrected for every arbitrary position within the electron slice.

Additional Options

GENESIS allows to scan over certain parameters, *i.e.* it allows for variation of the resonant wavelength or independent distribution of magnetic field errors.

The amount of data produced is large and a post processor is recommended. At DESY, we use the IDL code XGENESIS. It is conceivable to use macros for EXCEL, Kaleidograph or others.

Description of the time-dependent GINGER FEL Simulation Code

William Fawley, MS 71-J
LBNL, 1 Cyclotron Road
Berkeley, CA 94720

Contact: fawley@lbl.gov tel.: 510-486-6229

Overview

GINGER is a direct, time-dependent (polychromatic) extension of the original LLNL 2-D FEL code FRED. GINGER has been extensively rewritten in Fortran90 and has been successfully compiled and run on platforms ranging from CRAYs (C90, J90- serial and parallel SMP mode, T3E - serial mode) to workstations (Sun, SGI, Mac/LinuxPPC, Dec Alpha/Windows NT). The postprocessor, also written in Fortran90, at present requires NCAR graphics. Typical run times in single slice monochromatic (FRED) mode is of order a minute or less on a 250-Mhz class workstation. Long LCLS-class, time-dependent SASE runs are of order 1-2 CPU hours on a CRAY J90 SV1 processor. The GINGER executable (and postprocessor XPLOTGIN) are available from public storage space at the DOE NERSC.

Time-dependent Formulation

Within the code, the field and the particle beams are resolved into discrete, equally spaced transverse slices whose individual duration in time is λ_s / c but whose temporal separations can be many times λ_s / c . All field quantities are presumed to be the product of a slow dependence $E(r, z, t)$ multiplied by a fast dependence modulation term $e^{i(kzz - \omega t)}$. Within GINGER itself, only the slow temporal modulation of the field is followed. Decomposition into separate frequency components around the central angular frequency ω_0 is done by the postprocessor, which uses FFT's. Either periodic boundary conditions in time may be used or not, the former appropriate to long pulses, the latter to short pulses for which slippage plays a major role. For the latter, a time-dependent current may be used (parabolic or Gaussian profile) but, at present, no other beam parameters may vary in time.

GINGER approximates slippage in the following way: A given optical slice interacts with a single electron beam slice for a discrete distance $\Delta z_{\text{interact}}$. At the end of this distance, the given electron beam slice "falls back" in time (here time is measured back from the head of the optical pulse) to interact with the next field slice. For drift sections, the slippage rate is reduced to that equivalent to the difference between the group velocity of the wave and the forward (perpendicular momentum-free) velocity, v_z , of the electron beam

The code actually follows a given slice of macroparticles all the way through the wiggler, slipping them back, in time, relative to the slices of the EM field at appropriate discrete positions in z . With this choice, it was possible to structure the code such that only one set of macroparticles need be in memory at any given instant, whereas all field slices

remain in memory at all times. In SMP parallel mode, each processor works with one particular electron slice and some particle-to-disk IO occurs through the simulation.

Interaction Equations, Radiation Field Description, Gridding and Spatial BC

GINGER uses the wiggler-averaged Kroll-Morton-Rosenbluth (KMR) interaction equations together with a Gear-scheme (predictor-corrector) method to advance both the “slowly” varying electromagnetic field, E , and the longitudinal macroparticle quantities, (γ, θ) . For numerical reasons, E is represented as a complex quantity rather than by the equivalent amplitude and phase. Step-size and error control in the predictor-corrector is done locally for each slice (although output z -locations are identical for all slices). The initial field radial profile is normally a simple Gaussian but combinations of more complicated radial Hermite modes may also be input. The input field can be monochromatic at the central frequency or at an offset frequency. It may also include a flat or random amplitude input spectrum over a partial subset or over the maximum possible frequency band (set by the Nyquist criterion, determined by the temporal separation of e-beam/field slices) centered on the central frequency.

For non-waveguide geometries, GINGER uses a z -independent, non-linear, expanding radial grid that near the axis is nearly linear in r^2 and then exponentially expands for large r . The number of grid points, the outer boundary radius, and region over which the grid is linear is controlled by user input. A Dirichlet condition exists at the outer boundary, which can lead to (possibly unphysical) reflections if this boundary is too close.

Macroparticle Loading and Particle Mover

GINGER uses a moderate number of macroparticles (typically 512-8192) per electron beam slice. The default macroparticle load is a uniformly filled ellipsoid in 4-D phase space with alternatives of Gaussians or “super-Gaussians”. One may specify the e-beam size by giving either (a) its radius (b) normalized MKS emittance, or (c) the central beam brightness (given the input current). Alternatively, one may input the Twiss parameters α, β (for both the x and y planes) or radial mismatch factors to load an electron beam out of equilibrium with the initial focusing. Yet another possibility is to read macroparticle phase space coordinates (γ, x, y, x', y') directly from a separate input file.

The default beam energy distribution is a delta function centered the e-beam Lorentz factor, γ , specified in the input input, or, alternatively, the beam energy in MeV. One may also specify non-zero energy spread with either a waterbag or Gaussian profile. By default, the particles are loaded in phase space with a bit-reversed quiet start such that each particle at $\{x, x', y, y', \gamma, \theta\}$ will have 7 mirror particles at whose longitudinal phase differ by integral multiples of $2\pi/8$. If diagnosing third harmonic bunching is unimportant, the number of mirror particles can be reduced to 3. When shot noise fluctuations are desired for SASE and related studies, a random $\delta\theta$ from a Poisson distribution is added to each particle at the beginning of the run.

The fully relativistic Cartesian particle mover in GINGER is essentially identical to that of FRED and employs a 4th-order Runge-Kutta algorithm. The mover follows the particle betatron motion; the wiggle motion is averaged-out following the KMR approximation. Forces from radial electric and azimuthal magnetic fields are presumed to cancel exactly.

Wiggler and Focusing Description

GINGER can model either a helically or linearly polarized wiggler. In time-dependent mode, the wiggler strength can be either constant with z or variable with z with the variation in a_w being read from a separate wiggler file. Natural wiggler focusing exists for both helical and linear wigglers. Multiple external focusing options exist: a) z -independent, quadrupole focusing, b) quadrupole focusing whose strength is directly proportional to the wiggler strength ratio (this is appropriate for "curved pole tip" focusing), c) FODO-style AG quadrupole focusing with constant but separate values for the F and D quadrupole gradients, d) z -independent strong focusing (*e.g.* as from a ion channel). At each z -step in the Gear integrator, a local value of wiggler and focusing strengths is used. At present, no wiggler error fields or quadrupole misalignments are modeled in GINGER (this capability exists in the monochromatic FRED3D code). Recently, the capability to model wigglers with periodic drift spaces has been added. Discrete optical klystron sections can also be modeled.

Additional Capabilities

GINGER can simulate propagation in waveguides and oscillator configurations in both monochromatic and polychromatic mode. GINGER in a single execution run has the capability to vary one input parameter (*e.g.* current, energy) over a linear or logarithmic range and record the output. This process is the equivalent of doing multiple FRED-mode runs. In SMP parallel mode, this can be done very efficiently. The postprocessor recognizes this type of scan and will plot many output parameters (*e.g.* power, bunching) versus the varying input parameter.

Input/Output

GINGER uses a standard Fortran90 *namelist* formulation for input. A tapered wiggler profile can be input via a separate file. Power, bunching (both at the fundamental and third harmonic), and radially resolved electric field information is output for each temporal slice at multiple z -locations into an ASCII file which is then used for post-processing. In monochromatic FRED mode, particle phase space dumps at discrete z -locations can also be written into a binary file.

The postprocessor normally creates extensive color graphics, either direct to the user via X11 windows, or to NCAR CGM or Postscript disc files. Certain quantities can also be output as simple ASCII files or in HDF format for additional processing with other

visualization tools. Via a preferences file, the user has a fair amount of control as to what quantities are plotted or written to disc files.

Possible Future Upgrades

Irrespective of other changes, GINGER will be further modularized to cleanly separate different physics sections from each other. Eventually, it is hoped that individual users will be able to “plug in” their own special sections (e.g. external focusing) without interfering with the remaining code body. Currently a port is in progress to permit GINGER to run in parallel on MPP architectures (i.e. T3E) via MPI message passing. Additional upgrading of the external focusing package to model actual configurations more exactly will occur, nearly certainly, in FY2000.

A major question exists as to whether it is worthwhile to give GINGER true 3D (*i.e.*, r - θ - z) capability to model non-axisymmetric effects such as wiggler errors, quadrupole misalignments, elliptical e-beam profile, *etc.* It is not clear whether understanding the role of such effects require a time-dependent code as compared with a code such as FRED3D. In any event, S. Reiche's GENESIS already has this capability. Likewise, it is not obvious that giving GINGER the ability to model true harmonic gain is worthwhile given the existence of other codes such as a NUTMEG and MEDUSA.

APPENDIX B: List of Attendees**Ilan Ben-Zvi**

BNL / NSLS
P.O. Box 5000, MS 725C
Upton, NY 11973
Phone: +1-516-344-5143
Fax: +1-516-344-3029
E-Mail: ilan@bnl.gov
USA

Vinod Kumar Bharadwaj

SLAC / AD
2757 Sand Hill Rd, MS 18
Menlo Park, CA 94025
Phone: +1-650-926-4596
Fax: +1-650-926-8533
E-Mail: vinod@slac.stanford.edu
USA

Sandra Gail Biedron

ANL / APS
9700 S. Cass Avenue, MS B2164
Argonne, IL 60464
Phone: +1-630-252-1162
Fax: +1-630-252-5703
E-Mail: biedron@aps.anl.gov
USA

Richard M. Bionta

LLNL
7000 East Ave., MS L-050
Livermore, CA 94550-9234
Phone: +1-925-423-4846
Fax: +1-925-423-3371
E-Mail: bionta1@llnl.gov
USA

Michael Borland

ANL / APS
9700 S. Cass Avenue
Argonne, IL 60439
Phone: +1-630-252-4205
Fax: +1-630-252-5703
E-Mail: borland@aps.anl.gov
USA

Bruce E. Carlsten

LANL / LANSCE-9

Los Alamos, NM 87545
Phone: +1-505-667-5657
Fax: +1-505-665-8207
E-Mail: bcarlsten@lanl.gov
USA

Jym E. Clendenin

SLAC / AD
2575 Sand Hill Rd, MS 18
Menlo Park, CA 94025
Phone: +1-650-926-2962
Fax: +1-650-854-7268
E-Mail: clen@slac.stanford.edu
USA

William B. Colson

Naval Postgraduate School / Physics Department
833 Dyer Road
Monterey, CA 93943
Phone: +1-831-656-2765
Fax: +1-831-656-2834
E-Mail: colson@physics.nps.navy.mil
USA

Massimo Cornacchia

SLAC / SSRL
2575 Sand Hill Rd, MS 69
Menlo Park, CA 94025
Phone: +1-650-926-3906
Fax: +1-650-926-4100
E-Mail: cornacchia@slac.stanford.edu
USA

Roger J. Dejus

ANL / APS, Bld 401
9700 S. Cass Avenue
Argonne, IL 60439
Phone: +1-630-252-9163
Fax: +1-630-252-9303
E-Mail: dejus@aps.anl.gov
USA

Paul J. Emma

SLAC / NLC
2575 Sand Hill Rd, MS 66
Meno Park, CA 94025
Phone: +1-650-926-2458
Fax: +1-650-926-2407
E-Mail: emma@slac.stanford.edu
USA

William M. Fawley

LBNL / Accelerator Fusion Research
1 Cyclon Road, MS 71J
Berkeley, CA 94720
Phone: +1-510-486-6229
Fax: +1-510-486-2323
E-Mail: Fawley@lbl.gov
USA

Massimo Ferrario

INFN-LNF / Ricerca
Via Enrico Fermi 40, CP-13
Frascati (ROMA), I-00044
Phone: +39-6-94032216
Fax: +39-6-94032565
E-Mail: ferrario@lnf.infn.it
Italy

Henry P. Freund

SAIC
1710 Goodridge Dr.
McLean, VA 22102
Phone: +1-202-767-0034
Fax: +1-202-767-1280
E-Mail: freund@mmace.nrl.navy.mil
USA

John C. Goldstein

LANL / Group XPA
P.O. Box 1163, MS B259
Los Alamos, NM 87545
Phone: +1-505-667-7281
Fax: +1-505-665-7725
E-Mail: jcg@lanl.gov
USA

Zhirong Huang

ANL / ASD-PHY
9700 S. Cass Avenue
Argonne, IL 60439
Phone: +1-630-252-6023
Fax: +1-630-252-5703
E-Mail: zrh@aps.anl.gov
USA

Hai Jiang

UCLA / Physics
404 Hilgard Ave.
Los Angeles, CA 90095-1547
Phone: +1-310-390-2291
Fax:
E-Mail: haijiang@physics.ucla.edu
USA

Kwan-Je Kim

ANL / ASD
9700 S. Cass Avenue, MS 401
Argonne, IL 60439
Phone: +1-630-252-4647
Fax: +1-630-252-7369
E-Mail: kwangje@aps.anl.gov
USA

Lowell Klaisner

SLAC / TD
2575 Sand Hill Rd, MS 24
Menlo Park, CA 94025
Phone: +1-650-926-2726
Fax: +1-650-926-8657
E-Mail: klaisner@slac.stanford.edu
USA

Patrick Krejcik

SLAC / AD
2575 Sandhill Rd, MS 18
Menlo Park, CA 94025
Phone: +1-650-926-2790
Fax:
E-Mail: pkr@slac.stanford.edu
USA

Heinz-Dieter Nuhn

SLAC / SSRL
1685 Stevens Place, MS 69
Menlo Park, CA 94025
Phone: +1-650-926-2275
Fax: +1-650-926-4100
E-Mail: nuhn@slac.stanford.edu
USA

Claudio G. Parazzoli

Boeing / Engineering Technology
P.O. Box 3999, MS 8502
Seattle, WA 98124-2499
Phone: +1-253-773-2899
Fax: +1-253-773-4685
E-Mail: claudio.g.parazzoli@boeing.com
USA

Claudio Pellegrini

UCLA / Physics Department
405 Hilgard Ave.
Los Angeles, CA 90095-1547
Phone: +1-310-206-1677
Fax: +1-310-206-5251
E-Mail: pellegrini@physics.ucla.edu
USA

Carl B. Schroeder

University of California at Berkely / Physics
1 Cyclotron Road, Bld 71, MS 259
Berkeley, CA 94720
Phone: +1-510-486-6465
Fax:
E-Mail: carl@physics.berkeley.edu
USA

Roman O. Tatchyn

SLAC / SSRL
2575 Sand Hill Rd, MS 69
Menlo Park, CA 94025
Phone: +1-650-926-2731
Fax: +1-650-926-4100
E-Mail: tatchyn@slac.stanford.edu
USA

Li Hua Yu

BNL / Physics Department
P.O. Box 5000
Upton, NY 11973-5000
Phone: +1-516-344-5012
Fax: +1-516-344-3029
E-Mail: lhyu@bnl.gov
USA

Ming Xie

LBNL / Accelerator Fusion Research
1 Cyclon Road, MS 71B
Berkeley, CA 94720
Phone: +1-510-486-5616
Fax: +1-510-486-6485
E-Mail: mingxie@lbl.gov
USA